THE
PHYSICAL REVIEW
A journal of experimental and theoretical physics established by E. L. Nichols in 1893

SECOND SERIES, VOL. 68, NOS. 1 AND 2 JULY 1 AND 15, 1945

The Excitation of Heavy Nuclei

MARCELLUS L. WIEDENBECK
Department of Physics, University of Notre Dame, Notre Dame, Indiana
(Received March 20, 1945)

A new metastable isomer of gold was found. The energy level system of gold has been studied in the region from the threshold to 3.3 Mev. The energy of the metastable state was found to be approximately 250 kev and higher activation levels which combine with the metastable state are found at 1.22±0.03, 1.68, 2.15, 2.56, and 2.97 Mev, respectively. This excitation has also been produced by fast neutrons by the Au-*n*-*n* reaction and the threshold for this process has been determined. The previously known 43-minute period of mercury has been produced by direct x-ray irradiation as well as a 42-day period in columbium. The strontium activity, known previously from neutron excitation, of 2.7 hours half-life has been produced by both x-ray and electron bombardment of this element.

INTRODUCTION

ALTHOUGH activity may be produced in stable nuclei by means of the ordinary reactions such as γ-n, n-$2n$, n-γ, n-α, p-n, etc., the most direct proof of the existence of a metastable state in such stable nuclei lies in the production of this activity by the direct irradiation of the element by x-rays or electrons below the threshold for photo-disintegration of the given nucleus. At these energies the only activity which can be produced is that which is excited in one of the isotopes originally present and, therefore, can be attributed to a metastable state of a stable nucleus. If the metastable state belongs to a relatively abundant isotope, one can produce sufficient activity, even at low energies, and thus obtain an excitation curve[1] from which may be obtained much valuable information concerning the nuclear energy level system of that nucleus.[2]

The Van de Graaff-Herb electrostatic generator furnishes a convenient and suitable source of x-rays and electrons for the study of these excitation curves. In a quantitative determination of the energies of the various activation levels which combine with the metastable state, the x-ray excitation curve is the more accurate of the two. When the energy of the monokinetic electron beam, which produces the x-rays, reaches a higher activation level, the curve shows a sharp increase in slope. The intersection of the two linear portions of the curve, each obtained from numerous experimental points, clearly defines the energy of this activation level. It is not possible to produce excitation by a natural source of γ-rays since the process is one of line absorption, the natural width of the line being of the order of millivolts while the total width, including the Doppler effect, is of the order of a few volts.

EXPERIMENTAL

A. Mercury

An activity with a half-life of 43 minutes has been observed and chemically identified as mer-

[1] B. Waldman, G. B. Collins, and E. M. Stubblefeld, Phys. Rev. **A55**, 1129 (1939); M. L. Wiedenbeck, Phys. Rev. **67**, 92 (1945).
[2] E. Guth, Phys. Rev. **59**, 325 (1941).

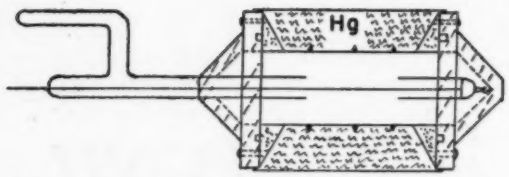

FIG. 1. Thin walled aluminum counter. The bombarded mercury was contained between the outer cylinder and the counter wall.

cury by Heyn,[3] and others[4,5] when mercury is irradiated with fast neutrons in the process Hg-n-$2n$. This activity was also produced by Krishnan and Nahum[6] by the Hg-d-p reaction. It was not clear whether this activity was to be ascribed to a metastable state of a stable mercury nucleus or to an unstable nucleus which decays to Au by K-capture.[6]

We have now produced the activity with this period by bombarding mercury with x-rays of maximum energy of 2.6 Mev. The metallic mercury was irradiated for thirty minutes with the x-rays produced when an electron beam current of 150 microamperes struck a thick gold target. The mercury was then poured around a thin walled aluminum counter (Fig. 1). The decay curve shown in Fig. 2 clearly indicates the presence of the 43-minute period which can, therefore, definitely be attributed to Hg*. The relatively small activity prohibits the obtaining of a complete excitation curve at the present time and indicates that the isotope possessing the metastable state is relatively low in abundance.

B. Strontium

The isotope Sr^{87} has been shown to possess a metastable level 0.38 Mev above the ground state. This has been excited by the Sr^{87}-n-n[7,8] reaction as well as having been grown in the processes: Rb-p-n,[9] Sr-n-γ,[8,9] Zr-n-α,[10] and from Y^{87} by K decay.[7] This 2.7-hour activity has now also been produced by the direct x-ray bombardment of strontium in the reaction: $Sr^{87}+\gamma \rightarrow Sr^{87*}$ and by the electron bombardment of strontium chloride in the reaction:

$$Sr^{87}+e_{\nu 1} \rightarrow Sr^{87*}+e_{\nu 2}.$$

C. Columbium

A radioactive isomer of stable Cb^{93} has been produced in the beta-decay of Zr^{93}.[10–13] Sagane, *et al.*[10] have reported a half-life of the order of 55 days. Pool and Edwards[13] have more recently reported a decay period of 38.7 days for this activity. After eighteen hours of bombardment with x-rays produced by a beam of 150 microamperes of 2.6-Mev electrons stopped on a gold target, a small columbium sample showed an initial activity of 2000 counts per hour when the sample was placed before a thin windowed (1.5-mil Al) counter. This activity was found to decay with a half-life of approximately 42 days.

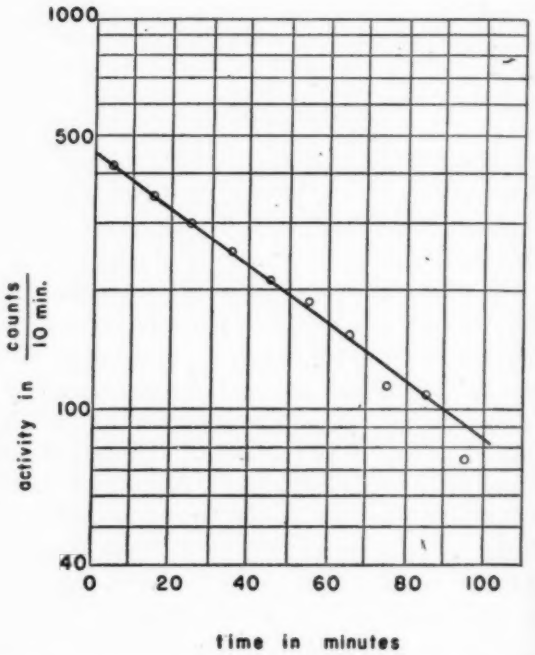

FIG. 2. Decay curve for Hg*. The half-life of mercury in the transition: $Hg^* \rightarrow Hg+\gamma$ is 43 minutes.

[3] F. Heyn, Nature **139**, 842 (1937).
[4] E. McMillan, M. Kamen, and S. Ruben, Phys. Rev. **52**, 375 (1932).
[5] M. L. Pool, J. M. Cork, and R. L. Thornton, Phys. Rev. **52**, 239 (1937).
[6] R. S. Krishnan and E. A. Nahum, Proc. Camb. Phil. Soc. **36**, 490 (1940).
[7] L. A. Dubridge and J. Marshall, Phys. Rev. **57**, 348 (1940).
[8] H. Reddemann, Naturwiss. **28**, 110 (1940).
[9] L. A. Dubridge and J. Marshall, Phys. Rev. **56**, 706 (1939).
[10] R. Sagane, S. Kojima, G. Miyamoto, and M. Ikawa, Phys. Rev. **57**, 1180 (1940).
[11] O. Hahn and F. Strassmann, Zeits. f. Physik **121**, 729 (1943).
[12] W. N. Moquin and M. L. Pool, Phys. Rev. **65**, 60 (1944).
[13] M. L. Pool and J. E. Edwards, Phys. Rev. **67**, 60 (1945).

D. Gold

We have previously reported[14] an activity of half-life 7.5±0.5 seconds which was produced by the bombardment of gold with an x-ray beam. Since there is but one stable isotope of gold, this activity must be attributed to a metastable state in Au^{197}.

In the ground state gold has a spin of 3/2 which, therefore, would imply a spin of 9/2 or 11/2 for the metastable state. Gold is the first known isotope in which the spin in the ground state is other than 1/2 or 9/2 and is thus an exception to the empirical rule set forth by Mattauch[15] that stable isotopes possessing such metastable states will have spins of 1/2 or $\geqslant 9/2$.

This activity has been determined as a function of the accelerating potential from the threshold to 3.3 Mev and is shown in Fig. 3. The activity is given as the number of counts during the first minute starting five seconds after the sample had been bombarded for thirty seconds with x-rays produced by an electron beam of 100 microamperes. The sample which was used in these measurements was a gold cylinder which formed the cathode of a self-quenching argon-ether counter. Several of such cylinders had been tried including a copper cylinder plated on the inside with ½ mil of gold. However, a pure gold cylinder was found to be most satisfactory and was used in obtaining all measurements.

As in the previous cases, it is seen that the excitation curve is composed of a series of straight line segments, the intersection of which gives the positions of the higher activation levels which combine with the metastable state. These breaks are found at 1.22±0.03 Mev, 1.68, 2.15, 2.56 and 2.97 Mev, respectively.

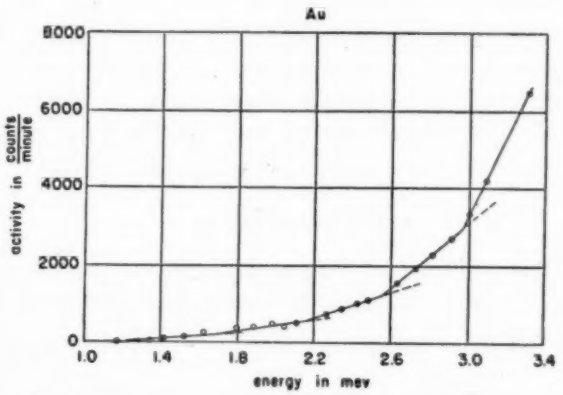

FIG. 3. X-ray excitation curve for gold. The intersection of the straight line segments gives the energy of the activated levels which combine with the metastable state.

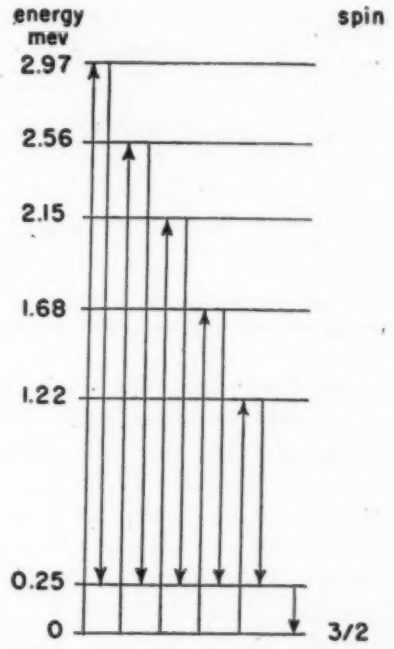

FIG. 4. Nuclear energy level diagram for gold showing the various transitions which occur.

The energy of the metastable level was obtained by measuring the energy of the conversion electrons emitted in the transition: $Au^{197*} \rightarrow Au^{197} + \gamma$. A thick gold disk was placed before the thin window of a counter with a brass cylinder, and the sample was irradiated at a fixed accelerating potential and with a constant beam current. Aluminum foils were interposed between the counter and the gold, and thus the activity was determined as a function of the thickness of aluminum. From this data, one obtains a value of approximately 250 kev for the energy of this level.

A nuclear energy level diagram showing the various levels which combine with the metastable level and the transition involved is shown in Fig. 4.

Activities due to metastable states of stable nuclei have been produced in several instances[7,16] by the inelastic collision of fast neutrons with the

[14] M. L. Wiedenbeck, Phys. Rev. **67**, 53 (1945).
[15] J. Mattauch, Zeits. f. Physik **117**, 246 (1941).
[16] M. Goldhaber, R. D. Hill, and L. Szilard, Phys. Rev. **55**, 47 (1939); Nature **142**, 521 (1938).

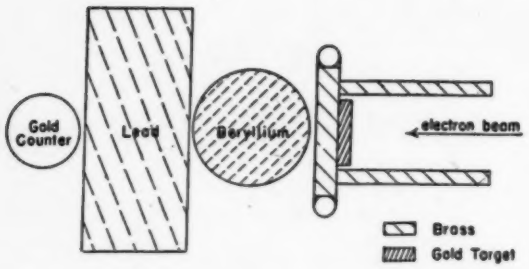

FIG. 5. Target arrangement for the excitation of gold with neutrons produced from the Be-γ-n reaction.

stable nucleus. Up to this time no quantitative data have been obtained concerning the energy of the neutrons required to produce this excitation. One should expect, of course, that the neutron threshold is practically identical with the x-ray threshold, but a direct proof is of interest. The electrostatic generator furnishes a convenient source of neutrons of known energy which can be produced by the Be-γ-n reaction. The distribution of energies of the neutrons is continuous as is the x-ray spectrum which produces them.

The intensity of any neutron line is linear[17] (in this energy region) with the applied accelerating potential above its threshold. The maximum energy of the neutrons so obtained is: $V_n=8/9(V-1.63)$, where V is the applied electron accelerating voltage.

Since the threshold for the gold excitation was found to be 1.22 Mev with x-rays, it seemed possible that this activity could also be produced with the neutron spectrum described above. Gold has the additional advantage over any other known metastable isomer since it exhibits no other short period neutron capture reactions.

An arrangement was set up as shown in Fig. 5. The x-rays were allowed to strike one-half pound of powdered beryllium placed directly in front of the target. Lead of four-inch thickness was placed between the beryllium and the self-quenching counter containing the gold cathode. The lead served as a shield to protect the counter from the x-rays.

With the apparatus set up in this manner, the activity produced by the x-rays was determined by bombardment without having the beryllium in position. Next, the beryllium was placed in position. No increase in activity beyond the small residual x-ray activity was found until the maximum energy of the neutrons exceeded 1.22 Mev. With maximum neutron energies in the range from 1.22 to 1.3 Mev, a considerable excess counting rate was obtained which increased linearly with energy as in the case of x-ray excitation. This indicates that the threshold for the process, $Au^{197}+n_{\nu 1}\rightarrow Au^{197*}+n_{\nu 2}$, is identical with that of x-rays.

DISCUSSION

Again, as in the case of silver, cadmium, and indium, the energy levels of gold were found to start in the region of 1.2 Mev, and successive higher levels are approximately equally spaced with a difference of 0.4 Mev between them. No convergence of the levels is indicated at these energies.

These experiments check the theory and show that the excitation processes in the cases of x-rays, electrons, and neutrons are similar. As one increases the energy of the x-rays or electrons producing the excitation, one eventually reaches a limit when this energy is equal to the binding energy of a neutron in the nucleus and thus produces the photo- or electro-disintegration of that nucleus. The similarity with the neutron process indicates that when the energy of the incident neutrons reaches the binding energy of a nuclear neutron, the n-$2n$ process can occur.[18] This process may be looked upon as one of neutro-disintegration, differing from that of photo-disintegration, however, due to the required momentum consideration of the incident neutron.

ACKNOWLEDGMENT

The author takes great pleasure in thanking Dr. Eugene Guth for his assistance with these problems.

[17] M. L. Wiedenbeck and Rev. C. J. Marhoefer, Phys. Rev. 67, 54 (1945).

[18] V. F. Weisskopf and D. H. Ewing, Phys. Rev. 57, 47 (1940).

The Determination of Refractive Indices of Colloidal Particles by Means of a New Mixture Rule or from Measurements of Light Scattering

WILFRIED HELLER
Chemistry Department, University of Chicago, Chicago, Illinois
(Received January 2, 1945)

A new theoretical mixture rule is developed for determining the refractive index of colloidal particles from differential refractometric measurements. The new rule gives better results for colloidal solutions than the mixture rules of Newton, Lorenz-Lorentz, or Wiener if the difference between the refractive indices of the colloidal particles and of the medium is small. If the difference is large, but not in excess of 0.7, the refractive index of the particles can still be obtained with an accuracy in the third or fourth decimal by using an empirical correction equation. If colloidal solutions are very opaque, the refractive index of the particles can be calculated from light scattering. Application of the respective equation requires that the refractive index of the medium and the size of the particles are known. The gravimetric and volumetric measurements involved in the determination of density of colloidal particles can be replaced in part or entirely by measurements of light scattering and refractivity.

I. A NEW MIXTURE RULE FOR DETERMINING THE REFRACTIVE INDEX OF COLLOIDAL CRYSTALS OR MOLECULES

A. The Classical Mixture Rules

A SERIES of mixture rules has been proposed for determining the refractive index of a dispersed substance, n_p, indirectly, from measurements of the refractive index of the total dispersed system, n_t, and of the refractive index of the medium of dispersion, n_m. Except for a few rules of minor significance, they are:

Newton, theoretical:

$$n_t^2 = \varphi_m n_m^2 + \varphi_p n_p^2, \tag{1}$$

Lorenz-Lorentz, theoretical:

$$\frac{n_t^2-1}{n_t^2+2} = \varphi_m \frac{n_m^2-1}{n_m^2+2} + \varphi_p \frac{n_p^2-1}{n_p^2+2}, \tag{2}$$

Wiener, theoretical:

$$\frac{n_t^2-n_m^2}{n_t^2+u} = \varphi_p \frac{n_p^2-n_m^2}{n_p^2+u}, \tag{3}$$

Lichtenecker, empirical:

$$\log n_t = \varphi_m \log n_m + \varphi_p \log n_p, \tag{4}$$

Avogadro-Biot-Beer-Landolt-Christiansen-Wintgen, empirical:

$$n_t = \varphi_m n_m + \varphi_p n_p. \tag{5}$$

φ_m and φ_p are the respective volume fractions. The term u in Eq. (3) is a function of the shape of the particles. $u = 2n_m^2$, if the particles are spherical. Equation (3) is then identical with Eq. (2).

A large series of experiments by various authors has shown that the "refractive increment" $(n_t - n_m)/c$—in which c is the weight concentration of the particles—is practically independent of c in dilute colloidal solutions. *A priori*, the empirical Eq. (5) appears therefore to be most suited for colloidal systems. All equations are tested in Table I in which n_p is calculated for colloidal sulphur.[1]

In addition to being empirical, Eq. (5) has a second disadvantage, which is shared also by the other mixture rules: both n_t and n_m must be known. If they are determined in two separate experiments, small temperature differences will play a role, because they affect the values of n_t, n_m, and φ.

TABLE I. Refractive indices of S at room temperature.

Experimental values (Mean) (From *International Critical Tables*)	Values calculated for infinite dilution from mixture rules (Assumed density: 2.000)				
	Eq. (1)	Eqs. (2, 3)	Eq. (4)	Eq. (5)	Eq. (9)
2.085	1.885	2.267	2.184	2.008	1.992

[1] Since sulphur is only slightly lyophilic, the medium of dispersion should have little effect upon n_p, i.e., it should be expected that $n_{p\,exp} = n_{p\,calc}$.

It appeared desirable, therefore, to develop a new mixture rule which has a theoretical foundation and which allows the direct use of differential refractometric data.

B. The New Mixture Rule

A mixture rule which meets the two requirements can be derived easily on the basis of the two principal theories developed on light-scattering. There is, on the one hand, the well-known theory of Rayleigh[2] and Mie,[3] in which light scattering is considered as an effect due to material units. As a consequence, n_p enters into the equations developed, in addition to n_m. On the other hand, there is the theory of Smoluchowski[4] and Einstein[5] in which light scattering is considered as an effect due to fluctuations, fluctuations in density in liquids and fluctuations in concentration in liquid mixtures. More complete equations for liquid mixtures and solutions have been derived by Raman[6] who takes into account in these systems both fluctuations in density and in concentration. Light scattering due to fluctuations in density is negligible compared to light scattering due to fluctuations in concentration, if the solutions are colloidal. This special case has been considered recently by Debye.[7] In the equation at which Debye arrives, the refractive index of the particles obviously does not enter, but n_t enters in addition to n_m.

A mixture rule can therefore be obtained by combining the equation of Rayleigh and the equation of Debye. This can be achieved by a simple transformation of the former equation. The classical formulation of the Rayleigh equation is

$$R=\frac{24\pi^3}{\lambda^4}\left(\frac{a^2-1}{a^2+2}\right)^2 \nu v^2 I_0, \qquad (6)$$

where R is the Tyndall radiation, I_0 the intensity of the incident primary beam, $a=n_p/n_m$, ν the number of the light scattering particles per cm³, v the volume of these particles, and λ the wave-length in the medium. The quantities R and I_0 which are inconvenient for the present purpose can be replaced by considering rather the decrease in intensity of the primary beam during its passage through the light scattering system. Since the light intensity can be defined as the energy incident upon the unit surface area per unit time, the absolute loss in intensity (I_0-I) has the dimension erg$\times$cm$^{-3}\times$sec.$^{-1}$=g$\times$cm^{-1} $\times$sec.$^{-3}$. Since the light radiation has the dimension, erg$\times$sec.$^{-1}$, it follows that the Tyndall radiation, which is proportional to the volume illuminated, has also the dimension g$\times$cm^{-1} $\times$sec.$^{-3}$. Consequently, the absolute loss in intensity $(I_0-I)=R$ (whenever the decrease in intensity of the primary beam is due exclusively to coherent light scattering), and the fractional decrease in intensity over unit distance:

$$\tau=\frac{I_0-I}{I_0}=\frac{24\pi^3}{\lambda^4}\left(\frac{a^2-1}{a^2+2}\right)^2 \nu v^2. \qquad (6a)$$

After substituting the wave-length in vacuum, λ_0, for λ and after replacing the ratio, a, by differences of the refractive indices involved, the transformed equation:

$$\tau=\frac{24\pi^3}{\lambda_0^4}\frac{n_m^4(n_p^2-n_m^2)^2}{(n_p^2+2n_m^2)^2}\varphi v, \qquad (6b)$$

is obtained, which is suitable for the present purpose. Debye's equation, on the other hand, is:

$$\tau=\frac{32\pi^3}{3\lambda_0^4}n_m^2(n_t-n_m)^2\frac{1}{\nu}. \qquad (7)$$

Upon combining (6b) and (7) the mixture rule

$$n_{p(s)}^2=\frac{n_m^3+2bn_m^2(n_t-n_m)}{n_m-b(n_t-n_m)} \qquad (8)$$

is obtained where

$$b=2/3\varphi.$$

Compared to Eq. (5), the measurement of n_t is replaced by a differential measurement (n_t-n_m) under elimination of temperature errors. The advantage of the differential measurement may be expected to be particularly pronounced in very dilute solutions where (n_t-n_m) is very small. Such solutions are not likely to give reliable results unless differential measurements are carried out.

[2] Lord Rayleigh, Phil. Mag. **41**, 107, 274, 447 (1871); **44**, 28 (1897); **47**, 375 (1899).
[3] G. Mie, Ann. d. Physik **25**, 377 (1908); P. Debye, Thesis, Munich (1908).
[4] M. v. Smoluchowski, Ann. d. Physik **25**, 205 (1908).
[5] A. Einstein, Ann. d. Physik **33**, 1275 (1910).
[6] C. V. Raman and K. R. Ramanathan, Phil. Mag. **45**, 213 (1923); see also R. Gans, Zeits. f. Physik **17**, 371 (1923).
[7] P. Debye, J. App. Phys. **15**, 338 (1944).

TABLE II. Magnitude of error in calculations of refractive indices from Eq. (8).

$n_{p(8)}-n_m$	$n_{p(8)}$ if $n_m=1.333000$	Errors occur in the
0.00235–0.00775	1.33535–1.34075	6th decimal
0.00775–0.0245	1.34075–1.3575	5th decimal
0.0245 –0.082	1.3575 –1.415	4th decimal
0.082 –0.225	1.415 –1.588	3rd decimal
0.225 –0.750	1.588 –2.083	2nd decimal
0.750 –2.18	2.083 –3.51	1st decimal

C. The Limits of Validity of the New Mixture Rule

The theory of Rayleigh-Mie has been verified repeatedly,[8] i.e., particle sizes determined on the basis of the equation developed by Mie, of which the Rayleigh Eq. (6) is a special case, were found to be in quantitative agreement with the actual particle sizes. Similarly, the equation of Debye has been verified.[9] There can therefore be no doubt that the new mixture rule is valid for systems which satisfy the assumptions involved in the two theories on light scattering: Eq. (6) is based on the assumption that the difference (n_p-n_m) is very small; Eq. (7) is based on the assumption that fluctuations in density are negligible compared to fluctuations in concentration. Equation (8) should, therefore, be valid, if (n_p-n_m) is very small and if the dispersed particles (crystals or molecules) are large enough to scatter considerably more light than the molecules of the medium. The former condition can be fulfilled by choosing the right medium. The latter condition is fulfilled in colloidal solutions. It is not fulfilled in liquid mixtures nor in solutions of small molecules or ions.

Both Eqs. (6) and (7) presuppose that the dispersed systems are dilute and that the light scattering particles are small as compared to the wave-length used, that they are spherical and isotropic. However, identical correction factors would have to be introduced into either equation in order to make them applicable to systems of moderate concentration and to large or non-spherical or intrinsically anisotropic particles. Consequently, these partly unknown correction factors are cancelled out in the combination of Eqs. (6) and (7) to Eq. (8). No influence of the size or shape of colloidal particles upon $n_{p(8)}$ should therefore be expected unless the refractive index actually varies with the size and shape of the particles, an experimentally unknown effect which might be found, however, in a spectral region near an absorption band.[10] Neither should the colloid concentration have any effect on $n_{p(8)}$ as long as the concentration is small enough so as not to affect the refractive indices themselves. The probable error involved in calculations of $n_{p(8)}$ and as due to the finite value of (n_p-n_m) is compiled in Table II. (The error is obtained by a procedure discussed below.) The error occurs in the fifth or fourth decimal, if $(n_{p(8)}-n_m)$ has a value not in excess of 0.025 and 0.082, respectively.

D. Another Formulation of the New Mixture Rule

Upon reviewing the present paper, Professor Debye drew the author's attention to another simple possibility of deriving the result expressed by Eq. (8). The same result can be obtained by calculating (Clausius-Mosotti) what the dielectric constant is of a medium in which a sufficiently small number of spheres of different dielectric constant is dispersed.

According to Debye, the result expressed by the new mixture rule can be formulated as follows:

$$\alpha=\Delta/(1+\tfrac{1}{3}\Delta), \tag{8a}$$

or

$$\Delta=\alpha/(1-\tfrac{1}{3}\alpha). \tag{8b}$$

The quantity

$$\Delta=\frac{n_p^2-n_m^2}{n_m^2},$$

and the quantity

$$\alpha=2\frac{(n_i-n_m)/n_m}{\varphi}.$$

It is assumed, as in the case of Eqs. (6) and (7) that the dielectric constant $\epsilon=n^2$. Equations (8a) and (8b) check, of course, with Eq. (8).

E. Application of the New Mixture Rule Outside of the (n_p-n_m) Range of Satisfactory Validity

It is sometimes not possible to select the medium in which (n_p-n_m) is sufficiently small in

[8] E.g., Niels Pihlblad, Thesis; Uppsala (1918).
[9] W. Heller and H. B. Klevens, Phys. Rev. 67, 61 (1945).
[10] W. Heller, Comptes rendus 205, 971 (1937).

TABLE III. Refractive indices in hydrosols.

Dispersed substance	$\varphi \times 10^3$	n_l	n_m	$n_{p(b)}$	$n_{p(g)}$	$n_{p(r)}$	$(n_{p(b)}-n_{p(r)})\times 10^3$	$(n_{p(g)}-n_{p(r)})\times 10^3$
SiO_2	3.075	1.33705	1.3325	1.4837	1.4805	1.4803	3.4	0.2
SiO_2	0.5815	1.33353	1.3325	1.5144	1.5097	1.5099	4.5	−0.2
Egg albumin	3.10	1.33946	1.3325	1.5651	1.5571	1.5571	8.0	0.0
Gelatin	3.10	1.34110	1.3332	1.5988	1.5882	1.5881	10.7	0.1
Hg-sulfosalicylic acid	2.323	1.34388	1.3330	1.8457	1.8014	1.8015	44.2	−0.1
AlOOH	1.047	1.33789	1.3325	1.9035	1.8472	1.8471	56.4	0.1
ThO_2	1.609	1.34302	1.3325	2.0893	1.9834	1.9863	103.0	−2.9
S	3.805	1.35917	1.33408	2.0985	1.9901	1.9934	105.1	−3.3
S	0.395	1.33592	1.33329	2.1070	1.9956	2.0000	107.0	−4.4
TiO_2	0.373	1.33657	1.3325	2.8599	2.3518	2.4236	436.5	−71.8
TiO_2	7.577	1.41991	1.3325	3.0080	2.3878	2.4861	521.9	−98.3

TABLE IV. Refractive indices at various sol concentrations. I. SiO_2−sol.

$\varphi \times 10^3$	n_l	n_m	$n_{p(b)}$	$n_{p(g)}$	$n_{p(r)}$	$(n_{p(b)}-n_{p(r)})\times 10^3$	$(n_{p(g)}-n_{p(r)})\times 10^3$
0.5815	1.33353	1.3325	1.5144	1.5097	1.5099	4.5	−0.2
0.8626	1.33394	1.3325	1.5037	1.4995	1.4990	4.7	0.5
1.0213	1.33421	1.3325	1.5042	1.5000	1.5000	4.2	0.0
1.3155	1.33469	1.3325	1.5032	1.4991	1.4990	4.2	0.1
1.6076	1.33514	1.3325	1.5008	1.4968	1.4966	4.2	0.2
1.9460	1.33561	1.3325	1.4962	1.4924	1.4923	3.9	0.1
2.5815	1.33634	1.3325	1.4846	1.4813	1.4813	3.3	0.0
3.0751	1.33705	1.3325	1.4837	1.4805	1.4803	3.4	0.2

TABLE V. Refractive indices at various sol concentrations. II. S−sol.

g S/100 cc	n_l	n_m	$n_{p(b)}$	$n_{p(g)}$	$n_{p(r)}$	$(n_{p(b)}-n_{p(r)})\times 10^3$	$(n_{p(g)}-n_{p(r)})\times 10^3$
0.79	1.33592	1.33329	2.1070	1.9956	2.0000	107.0	−4.4
1.59	1.33871	1.33338	2.1136	2.0001	2.0038	109.8	−3.7
2.72	1.34256	1.33347	2.1108	1.9982	2.0022	108.6	−4.0
3.81	1.34612	1.33364	2.0921	1.9856	1.9890	103.1	−3.4
4.23	1.34755	1.33370	2.0918	1.9854	1.9887	103.1	−3.3
4.76	1.34933	1.33375	2.0915	1.9852	1.9882	103.3	−3.0
5.44	1.35171	1.33384	2.0949	1.9875	1.9908	104.1	−3.3
6.34	1.35473	1.33394	2.0933	1.9865	1.9899	103.4	−3.4
7.61	1.35917	1.33408	2.0985	1.9901	1.9934	105.1	−3.3

TABLE VI. Refractive indices in methyl-ethylketon-sols.

Dispersed substance	$\varphi \times 10^3$	n_l	n_m	$n_{p(b)}$	$n_{p(g)}$	$n_{p(r)}$	$(n_{p(b)}-n_{p(r)})\times 10^3$	$(n_{p(g)}-n_{p(r)})\times 10^3$
Acetylcellulose	1.047	1.37899	1.3778	1.4933	1.4914	1.4919	1.4	−0.5
Acetylcellulose	7.277	1.38711	1.3778	1.5080	1.5056	1.5057	2.3	−0.1
Nitrocellulose	2.746	1.37841	1.3741	1.5346	1.5309	1.5310	3.6	−0.1

order to make the probable error negligible. This is particularly true in the case of colloids which are stable only in one medium, e.g., in an aqueous medium. A selection of the medium is excluded also in those cases where the value of n_p shall be used for obtaining information on the approximate degree of solvation (hydration) of the particles in a particular medium. The probable error will then often not be negligible. For example, if water is the medium, the error will most often be in the fourth or third decimal if the dispersed substance is a liquid or a solid respectively.

A survey on the variation of the error with (n_p-n_m) is given in Table III for aqueous colloidal systems. Experimental data on n_p and n_m

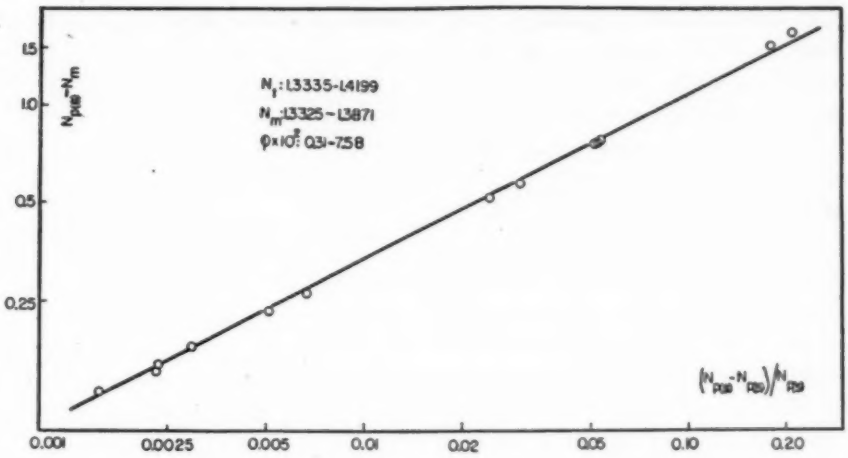

FIG. 1. (Wherever N appears in the figure n should be substituted.)

as obtained by Freundlich and Rogowski[11] and by Odén[12] are used. It is assumed that the n_p-values obtained by means of Eq. (5), $n_{p(5)}$, are correct in a first approximation and that consequently the difference $(n_{p(8)}-n_{p(5)})$ can be taken as an approximate criterion on the error committed in applying Eq. (8) in the case of large (n_p-n_m) values.

An inspection of Table III shows that the log of the fractional discrepancy $(n_{p(8)}-n_{p(5)})/n_{p(5)}$ is a linear function of the log of $(n_{p(8)}-n_m)$. This relationship is plotted in Fig. 1 which contains data of the Tables IV and V. From Fig. 1 the empirical function

$$n_{p(9)}=\frac{n_{p(8)}}{0.093(n_{p(8)}-n_m)^{1.99}+1} \qquad (9)$$

is obtained. The use of this correction equation reduces the discrepancy considerably if $(n_{p(8)}-n_m)$ assumes large values. For small $(n_{p(8)}-n_m)$ values, on the other hand, the use of the correction equation is not advisable.

F. Influence of the Colloid Concentration

The influence of the colloid concentration is tested in Tables IV and V, the latter referring to a case where $(n_{p(8)}-n_m)$ is far too large to give reliable results by means of Eq. (8) alone. In either of the two systems, the calculated n_p increases somewhat with decreasing colloid concentration. The increase is the same whether Eq. (8) or the equation combination (9) or Eq. (5) are used. It is therefore advisable to calculate n_p for infinite dilution. Differential measurements of (n_l-n_m) as directly used in Eq. (8) are the only procedure which will allow one to obtain the most accurate n_p for $\varphi \to 0$.

G. The Influence of the Absolute n_m-Values

Careful refractometric measurements on non-aqueous colloidal solutions are scarce. A few data of Freundlich and Rogowski are used in Table VI. The comparison of these data with those of Table III seems to indicate that the absolute value of n_m has no influence upon the validity of Eq. (8). No influence was to be expected.

II. DETERMINATION OF REFRACTIVE INDICES FROM "ABSORPTION" MEASUREMENTS

Equation (6b) can be transformed to

$$n_p^2=n_m^2\frac{n_m^2+2f}{n_m^2-f}, \qquad (10)$$

where

$$f=\frac{\lambda_0^2}{2}\left(\frac{\tau}{6\pi^2 v\varphi}\right)^{\frac{1}{2}}=\frac{\lambda_0^2 p}{2m}\left(\frac{\tau}{6\pi^2\nu}\right)^{\frac{1}{2}}=\frac{\lambda_0^2 p}{2}\left(\frac{\tau}{6\pi^2 mc}\right)^{\frac{1}{2}}$$

(m: the mass of a particle, p its density, c the concentration, in g cm^{-3}). Since

$$I/I_0=\tau-1,$$

the refractive index n_p can be determined from

[11] H. Freundlich and F. Rogowski, Kolloid Beih. **37**, 215 (1933).
[12] S. Odén, Zeits. f. physik. Chemie **80**, 735 (1912).

measurements of the apparent (conservative) absorption without any refractometric measurement being necessary, in the case of known n_m, provided only that the particle weight (molecular weight), the density and the concentration of the particles are known. Since data on the two latter quantities must be known also if any of the preceding mixture rules are to be applied, the practical difference of Eq. (10) compared to the earlier ones is that the n_t or (n_t-n_m) measurement is replaced by an absorption measurement. This practical difference defines the cases where the use of Eq. (10) is of particular practical interest (very turbid systems or very opaque particles).

This alternate principle of n_p determinations is restricted, of course, to application under the well-known conditions (particle size, particle shape, colloid concentration, and value of (n_p-n_m)) for which the Rayleigh equation is valid. If all conditions are met except the condition of spherical shape and of isotropy, Eq. (10) may still be applied, however, by introducing the Cabannes factor.[13] This means that τ must be replaced by

$$\frac{1-(7/6)\delta}{1+0.5\delta},$$

where the depolarization factor $\delta=i_{\parallel}/i_{\perp}$ ($i_{\perp}$ is the intensity of the "Rayleigh component" which vibrates perpendicular to the plane of observation and $i_{\parallel}$ is the intensity of the orthogonal component).

APPENDIX—OPTICAL DETERMINATION OF DENSITIES

The density of colloidal particles is generally determined by pyknometric methods or by methods of floating. In some instances, it may be of advantage to substitute optical methods for these methods. There are several possibilities which are implied in equations given in preceding sections of this paper.

The transformation of Eq. (5) leads to

$$\rho_p=\rho_m\frac{w_p}{w_m}\frac{n_p-n_t}{n_t-n_m}=\rho_t\frac{w_p}{w_t}\frac{n_p-n_m}{n_t-n_m}, \qquad (11)$$

where w is the weight in g. The use of this equation differs from the use of the conventional Eq. (12) (case of exclusive pyknometric determinations of ρ_p)

$$\rho_p=\frac{w_p}{w_t/\rho_t-w_m/\rho_m} \qquad (12)$$

by the substitution of two gravimetric-volumetric data, e.g., of w_m and ρ_m by two refractometric data (n_t-n_m) and n_p. Both Eqs. (11) and (12) should be valid on the assumption of additivity and of negligible volume contraction.

More interesting appears the relation

$$\rho_p=\frac{3}{2}c\frac{n_m(n_p^2-n_m^2)}{(n_t-n_m)(n_p^2+2n_m^2)}, \qquad (13)$$

which is obtained by transformation of Eq. (8). This equation makes it possible to determine densities exclusively from refractometric data, provided, of course, that the concentration is known. The application of Eq. (13) is subject to the restrictions imposed on the use of Eq. (8).

If the particle weight (molecular weight) and the light scattering power of the dispersed substance is known, then part of the refractometric data may be replaced by data on turbidity (absorption). This is possible by transforming Eq. (6b) to:

$$\rho_p=\frac{24\pi^3}{\lambda_0^4}\frac{n_m^4(n_p^2-n_m^2)^2}{(n_p^2+2n_m^2)^2}\frac{m}{\tau}\varphi, \qquad (14)$$

or

$$\rho_p=\frac{2}{\lambda_0^2}n_m^2\frac{n_p^2-n_m^2}{n_p^2+2n_m^2}\left(\frac{6\pi^3cm}{\tau}\right)^{\frac{1}{2}}. \qquad (14a)$$

Equations (13) and (14) have the disadvantage of requiring that n_p is known. This will often be a deterrent to using them in the place of Eq. (12).

This disadvantage can be avoided by using rather a transformation of Eq. (7)

$$\rho_p=\frac{3\lambda_0^4}{32\pi^3}\frac{\tau}{n_m^2(n_t-n_m)^2}\frac{c}{v}, \qquad (15)$$

which requires that the volume of the particles (molecules) is known.

[13] J. Cabannes, Ann. de physique **15**, 5 (1921); *La diffusion moléculaire de la lumière* (Paris, 1929). See also P. Debye, reference 7.

PHYSICAL REVIEW VOLUME 68, NUMBERS 1 AND 2 JULY 1 AND 15, 1945

High Frequency Vibrations of Thin Crystal Plates

H. EKSTEIN
Armour Research Foundation, Chicago, Illinois

(Received May 4, 1945)

The boundary conditions of free vibration can be satisfied on the major surfaces of a plane-parallel plate if the displacement components are assumed to be products of trigonometric functions. In addition, the boundary conditions can be approximately satisfied on the minor surfaces when the plate is thin. The theory leads to a frequency equation

$$\nu = \tfrac{1}{2}(c/\rho)^{\frac{1}{2}}[(n/2b)^2 + k(m/2a)^2]^{\frac{1}{2}}$$

which has been found empirically to satisfy observations. The theoretical values of the constant k are 3.7 and 1.8 for the AT and BT quartz plates, respectively, while the observed values are 3.9 and 1.7, respectively.

INTRODUCTION

FREE elastic vibrations of anisotropic plates were treated extensively by W. Voigt[1] who developed a general theory. Voigt's theory is limited to the case where the wave-length is large as compared with the thickness and it must fail when the wave-length is of the order of magnitude or smaller than the thickness. This latter case was not interesting to Voigt; because of their high frequency it was impractical to excite these vibrations. By piezoelectric excitation, it has been possible to excite vibrations of high frequency in thin plates. I. Koga[2] treated them theoretically by assuming the plate to be infinitely extended and gave a rigorous solution for this case. Experiments[3,4] showed, however, that while one resonant frequency and the calculated mode of motion were in good agreement, numerous other frequencies could be detected which were not foreseen by the theory of the infinite plate. The purpose of the present paper is to explain these deviations by presenting a theory of the thin plate whose lateral extension is large but not infinite.

The consideration will be limited to the case where the elastic constants c_{15}, c_{16}, c_{25}, c_{26}, c_{35}, c_{36}, c_{45}, and c_{46} are zero or negligibly small. According to Voigt,[1] the former is the case when the x-axis of the reference system (which we assume parallel to one long edge) coincides with a twofold axis of symmetry. This case includes those quartz plates whose one major edge is parallel to the crystallographic x-axis. Most of the experimental work was done on this type of quartz plate.

Standing sine-waves along one major edge will be first considered so that the boundary conditions on the major surface can be met rigorously. With these solutions, the boundary conditions on the smaller lateral surfaces can be satisfied approximately.

Standing Sine-Waves along the X-Direction

We consider a rectangular plane-parallel plate of edges $2a$, $2b$, and $2c$ where $2b$ is the thickness. The origin of coordinates is in the center and the x-, y-, and z-directions are parallel to the edges $2a$, $2b$, and $2c$, respectively. If, as we assume,

$$c_{15}=c_{16}=c_{25}=c_{26}=c_{35}=c_{36}=c_{45}=c_{46}=0,$$

the stress-strain relations are:*

$$\begin{aligned}
-X_x &= c_{11}x_x + c_{12}y_y + c_{13}z_z + c_{14}y_z \\
-Y_y &= c_{12}x_x + c_{22}y_y + c_{23}z_z + c_{24}y_z \\
-Z_z &= c_{13}x_x + c_{23}y_y + c_{33}z_z + c_{34}y_z \\
-Y_z &= c_{14}x_x + c_{24}y_y + c_{34}z_z + c_{44}y_z \\
-X_z &= c_{55}x_z + c_{56}x_y \\
-X_y &= c_{56}x_z + c_{66}x_y.
\end{aligned} \tag{1}$$

The boundary conditions for the free body are:

$$\begin{aligned}
X_x\cos(n,x) + X_y\cos(n,y) + X_z\cos(n,z) &= 0, \\
X_y\cos(n,x) + Y_y\cos(n,y) + Y_z\cos(n,z) &= 0, \\
X_z\cos(n,x) + Y_z\cos(n,y) + Z_z\cos(n,z) &= 0,
\end{aligned} \tag{2}$$

[1] W. Voigt, *Lehrbuch der Kristallphysik* (B. G. Teubner, Leipzig, 1928).
[2] I. Koga, Physics **3**, 70 (1932).
[3] J. V. Atanasoff and P. J. Hart, Phys. Rev. **59**, 85 (1941).
[4] W. P. Mason, Bell Sys. Tech. J. **19**, 74 (1940).

* Voigt's notations are used, so that compressional stresses are positive.

which should be satisfied on all six faces. The dynamic equations are:

$$\rho\omega^2 u=\frac{\partial X_x}{\partial x}+\frac{\partial X_y}{\partial y}+\frac{\partial X_z}{\partial z},$$
$$\rho\omega^2 v=\frac{\partial X_y}{\partial x}+\frac{\partial Y_y}{\partial y}+\frac{\partial Y_z}{\partial z}, \tag{3}$$
$$\rho\omega^2 w=\frac{\partial X_z}{\partial x}+\frac{\partial Y_z}{\partial y}+\frac{\partial Z_z}{\partial z},$$

where $\omega=2\pi\nu$ is the angular frequency and u, v, and w are the components of the displacement vector.

We desire at first to satisfy Eqs. (3) in the whole body and Eqs. (2) on the major surfaces $y=\pm b$ only. Furthermore, the displacement components will be assumed to be independent of z. Tentatively, the solution will be written as a linear combination of plane waves of the form

$$u=U\exp[i(\alpha x+py)],$$
$$v=V\exp[i(\alpha x+py)], \tag{4}$$
$$w=W\exp[i(\alpha x+py)],$$

where U, V, and W are constants.

If the strains are calculated in the usual way from Eqs. (4) and substituted into Eqs. (1), we obtain:

$$\begin{aligned}
-X_x&=i(c_{11}\alpha U+c_{12}pV+c_{14}pW)\\
&\quad\times\exp[i(\alpha x+py)],\\
-Y_y&=i(c_{12}\alpha U+c_{22}pV+c_{24}pW)\\
&\quad\times\exp[i(\alpha x+py)],\\
-Z_z&=i(c_{13}\alpha U+c_{23}pV+c_{34}pW)\\
&\quad\times\exp[i(\alpha x+py)],\\
-Y_z&=i(c_{14}\alpha U+c_{24}pV+c_{44}pW)\\
&\quad\times\exp[i(\alpha x+py)],\\
-X_z&=i(c_{55}\alpha W+c_{56}pU+c_{56}\alpha V)\\
&\quad\times\exp[i(\alpha x+py)],\\
-X_y&=i(c_{56}\alpha W+c_{66}pU+c_{66}\alpha V)\\
&\quad\times\exp[i(\alpha x+py)].
\end{aligned} \tag{5}$$

Substituting into Eqs. (3), we get:

$$\begin{aligned}
&U(-\rho\omega^2+c_{66}p^2+c_{11}\alpha^2)+V\alpha p(c_{12}+c_{66})\\
&\qquad+W\alpha p(c_{14}+c_{56})=0,\\
&U\alpha p(c_{12}+c_{66})+V(-\rho\omega^2+c_{66}\alpha^2+c_{22}p^2)\\
&\qquad+W(c_{56}\alpha^2+c_{24}p^2)=0,\\
&U\alpha p(c_{14}+c_{56})+V(c_{56}\alpha^2+c_{24}p^2)\\
&\qquad+W(-\rho\omega^2+c_{55}\alpha^2+c_{44}p^2)=0.
\end{aligned} \tag{6}$$

The compatability of Eqs. (6) requires that

$$\begin{vmatrix}
c_{66}p^2+c_{11}\alpha^2-\rho\omega^2 & \alpha p(c_{12}+c_{66}) & \alpha p(c_{14}+c_{56})\\
\alpha p(c_{12}+c_{66}) & c_{22}p^2+c_{66}\alpha^2-\rho\omega^2 & c_{56}\alpha^2+c_{24}p^2\\
\alpha p(c_{14}+c_{56}) & c_{56}\alpha^2+c_{24}p^2 & c_{44}p^2+c_{55}\alpha^2-\rho\omega^2
\end{vmatrix}=0. \tag{7}$$

Solving Eqs. (7) for p^2, we obtain three roots p_1^2, p_2^2, p_3^2, and from Eqs. (6) the corresponding ratios $U_1:V_1:W_1$; $U_2:V_2:W_2$ and $U_3:V_3:W_3$, where the p_i^2s and the ratios $U_i:V_i:W_i$ are functions of $\rho\omega^2$ and α^2.

The form of this function can be seen if we substitute $p/\alpha=q$ and divide each row of the determinant (7) by α^2:

$$\begin{vmatrix}
c_{66}q^2+c_{11}+\rho\omega^2/\alpha^2 & q(c_{12}+c_{66}) & q(c_{14}+c_{56})\\
q(c_{12}+c_{66}) & c_{22}q^2+c_{66}-\rho\omega^2/\alpha^2 & c_{56}+c_{24}q^2\\
q(c_{14}+c_{56}) & c_{56}+c_{24}q^2 & c_{44}q^2+c_{55}-\rho\omega^2/\alpha^2
\end{vmatrix}=0. \tag{8}$$

From this, we see that the roots p_i^2 will have the form

$$p_i^2=\alpha^2 f_i(\rho\omega^2/\alpha^2), \tag{9}$$

and the ratios $U_i:V_i:W_i$ are only functions of $\rho\omega^2/\alpha^2$. To each value p_i^2 belong two complex waves:

$$u=U_i\exp[i(\alpha x+p_i y)]$$
. . . . . .

and

$$u=U_i\exp[i(\alpha x-p_i y)].$$
. . . . . .

We form real linear combinations of these complex waves:

$$u = U_i \cos \alpha x \sin p_i y,$$
$$v = V_i \sin \alpha x \cos p_i y, \qquad (10A)$$
$$w = W_i \sin \alpha x \cos p_i y;$$

or

$$u = U_i \cos \alpha x \cos p_i y,$$
$$v = V_i \sin \alpha x \sin p_i y, \qquad (10B)$$
$$w = W_i \sin \alpha x \sin p_i y;$$

and the final solution will be a linear combination of the three functions (10A) or (10B):

$$u = \cos \alpha x \cdot \sum L_i U_i \sin p_i y,$$
$$v = \sin \alpha x \cdot \sum L_i V_i \cos p_i y, \qquad (11A)$$
$$w = \sin \alpha x \cdot \sum L_i W_i \cos p_i y;$$

or

$$u = \cos \alpha x \cdot \sum L_i U_i \cos p_i y,$$
$$v = \sin \alpha x \cdot \sum L_i V_i \sin p_i y, \qquad (11B)$$
$$w = \sin \alpha x \cdot \sum L_i W_i \sin p_i y;$$

where the $U_i \cdots$ and p_i are known functions of $\rho\omega^2$ and α^2, while the L_i are to be determined by the boundary conditions. The strains are now:

$$x_x = -\alpha \sin \alpha x \cdot \sum L_i U_i \sin p_i y,$$
$$y_y = -\sin \alpha x \cdot \sum p_i L_i V_i \sin p_i y,$$
$$z_y = -\sin \alpha x \cdot \sum p_i L_i W_i \sin p_i y, \qquad (12A)$$
$$z_x = \alpha \cos \alpha x \cdot \sum L_i W_i \cos p_i y,$$
$$x_y = \cos \alpha x \cdot \sum L_i (U_i p_i + \alpha V_i) \cos p_i y,$$

for case A; or

$$x_x = -\alpha \sin \alpha x \cdot \sum L_i U_i \cos p_i y,$$
$$y_y = \sin \alpha x \cdot \sum p_i L_i V_i \cos p_i y,$$
$$z_y = \sin \alpha x \cdot \sum p_i L_i W_i \cos p_i y, \qquad (12B)$$
$$z_z = \alpha \cos \alpha x \cdot \sum L_i W_i \sin p_i y,$$
$$x_y = \cos \alpha x \cdot \sum L_i (\alpha V_i - p_i U_i) \sin p_i y,$$

for case B.

The boundary conditions require that the stresses

$$Y_y = Y_z = X_y = 0 \quad \text{at} \quad y = \pm b.$$

Substituting the strains, Eqs. (12), into Eqs. (1), we obtain

$$\sum L_i (c_{12}\alpha U_i + c_{22} p_i V_i + c_{24} p_i W_i) \sin p_i b = 0,$$
$$\sum L_i (c_{14}\alpha U_i + c_{24} p_i V_i + c_{44} p_i W_i) \sin p_i b = 0, \qquad (13A)$$
$$\sum L_i (c_{66} p_i U_i + c_{66}\alpha V_i + c_{56}\alpha W_i) \cos p_i b = 0,$$

for case A; or

$$\sum L_i (-c_{12}\alpha U_i + c_{22} p_i V_i + c_{24} p_i W_i) \cos p_i b = 0,$$
$$\sum L_i (-c_{14}\alpha U_i + c_{24} p_i V_i + c_{44} p_i W_i) \cos p_i b = 0, \qquad (13B)$$
$$\sum L_i (-c_{66} p_i U_i + c_{66}\alpha V_i + c_{56}\alpha W_i) \sin p_i b = 0,$$

for case B.

The compatibility of Eqs. (13) demands that the corresponding determinant vanish.

In view of Eq. (9), we can divide each Eq. (13) by α and we then have only functions of $\rho\omega^2/\alpha^2$ in the parentheses. The transcendental functions $\sin p_i b$ and $\cos p_i b$ will have the form

$$\sin \alpha b f_i^{\lambda}(\rho\omega^2/\alpha^2), \quad \cos \alpha b f_i^{\lambda}(\rho\omega^2/\alpha^2).$$

Consequently, the determinant of Eqs. (13) will yield a transcendental equation which relates $\rho\omega^2/\alpha^2$ to αb. Solution of this equation yields the frequency as a function of the wave-length $1/\alpha$ and of the product αb under the form

$$\rho\omega^2 = \alpha^2 g(\alpha b).$$

When this is done, Eqs. (8) yield the ratio $L_1 : L_2 : L_3$ and the displacement components are known from Eqs. (11).

While this formal solution is impractical for numerical results, a numerical solution can be carried out by assuming some numerical value for $\rho\omega^2/\alpha^2$ and calculating the roots, q_i, of Eq. (8) and the corresponding ratios $U_i : V_i : W_i$.

Then Eqs. (13) yield a transcendental equation for αb, the only unknown in (13). Thus the whole frequency spectrum can be determined.

It is shown in Appendix I that Eqs. (7) and (13) include as a special case Timoshenko's theory of flexural vibrations in an isotropic plate.

Thickness Vibrations

We shall discuss Eqs. (7) and (13) for the case where α is very small, i.e., the displacement is a very slowly variable function of x. Physically, this can be expected to be true in a plate whose thickness is very small as compared to its lateral dimensions. If the displacement is independent of x as can be assumed in an infinitely extended

plate, $\alpha=0$ and Eq. (7) becomes

$$\begin{vmatrix} c_{66}p^2-\rho\omega^2 & 0 & 0 \\ 0 & c_{22}p^2-\rho\omega^2 & c_{24}p^2 \\ 0 & c_{24}p^2 & c_{44}p^2-\rho\omega^2 \end{vmatrix}=0. \quad (14)$$

This determinant has the characteristic values

$$p_{01}^2=\rho\omega^2/c_{66}, \quad p_{02}^2=\rho\omega^2/c_2', \quad p_{03}^2=\rho\omega^2/c_3', \quad (15)$$

where

$$c_{2,3}'=\tfrac{1}{2}(c_{22}+c_{44}\pm[(c_{22}-c_{44})^2+4c_{24}^2]^{\frac{1}{2}}). \quad (16)$$

I. Koga[2] has shown that the boundary conditions on the surface of an infinitely extended plane-parallel plate are satisfied when

$$p_{0i}=n\pi/2b\equiv\beta \quad \begin{pmatrix} i=1,2,3 \\ n=1,2,3\cdots \end{pmatrix}. \quad (17)$$

This must also be a solution of Eqs. (13A) or (13B). Indeed, if

$$p_{01}=(\rho\omega^2/c_{66})^{\frac{1}{2}}=n\pi/2b \quad (n \text{ odd}), \quad (18)$$

then we use the functions (11A). From the determinant (14), it is evident that the corresponding ratio is

$$U_1:V_1:W_1=1:0:0.$$

Because of Eq. (18)

$$\cos p_{01}b=0.$$

Therefore, the Eqs. (13A) are satisfied by

$$L_1:L_2:L_3=1:0:0.$$

If, on the other hand,

$$p_{02}=n\pi/2b \quad \text{or} \quad p_{03}=n\pi/2b \quad (n \text{ odd}),$$

then we use the functions (10B). From Eqs. (6) and (14), it can be seen that in both cases

$$U_2=U_3=0.$$

Again,

$$\cos p_{02}b=0,$$

or

$$\cos p_{03}b=0;$$

and (13B) is satisfied with

$$L_1=L_3=0,$$

or

$$L_1=L_2=0,$$

respectively. Similar considerations show that for n even, Koga's solution satisfies Eqs. (13A or B) if $\alpha=0$.

We return to the case where α is not zero, but small. Equations (6) can be written as

$$(A+\alpha/pB+\alpha^2/p^2C)\mathbf{U}=\rho\omega^2/p^2\mathbf{U}, \quad (19)$$

where

$$A=\begin{pmatrix} c_{66} & 0 & 0 \\ 0 & c_{22} & c_{24} \\ 0 & c_{24} & c_{44} \end{pmatrix},$$

$$B=\begin{pmatrix} 0 & c_{12}+c_{66} & c_{14}+c_{56} \\ c_{12}+c_{66} & 0 & 0 \\ c_{14}+c_{56} & 0 & 0 \end{pmatrix}, \quad (20)$$

$$C=\begin{pmatrix} c_{11} & 0 & 0 \\ 0 & c_{66} & c_{56} \\ 0 & c_{56} & c_{55} \end{pmatrix}.$$

Putting

$$1/pB+\alpha/p^2C=D, \quad (21)$$

Eq. (19) becomes

$$(A+\alpha D)\mathbf{U}=\rho\omega^2/p^2\mathbf{U}. \quad (22)$$

Disregarding for the moment the fact that D still contains α and p, we obtain from perturbation theory the second-order solution of Eq. (22):

$$\mathbf{U}_k=\mathbf{U}_{0k}+\alpha\sum_l{}'\frac{D_{kl}\mathbf{U}_{0l}}{\rho\omega^2/p_{0k}^2-\rho\omega^2/p_{0l}^2}, \quad (23)$$

$$\frac{\rho\omega^2}{p_k^2}=\frac{\rho\omega^2}{p_{0k}^2}+\alpha D_{kk}+\alpha^2\sum_l{}'\frac{D_{kl}^2}{\rho\omega^2/p_{0k}^2-\rho\omega^2/p_{0l}^2}, \quad (24)$$

where

$$\begin{aligned} D_{kl}&=(D\mathbf{U}_{0k}\cdot\mathbf{U}_{0l})=(\mathbf{U}_{0k}\cdot\{1/PB+\alpha/p^2C\}\mathbf{U}_{0l}) \\ &=1/p(\mathbf{U}_{0k}\cdot B\mathbf{U}_{0l})+\alpha/p^2(\mathbf{U}_{0k}\cdot C\mathbf{U}_{0l}) \\ &=1/pB_{kl}+\alpha/p^2C_{kl}. \end{aligned} \quad (25)$$

In Eq. (25), $\mathbf{U}_{0k}$ are the normalized eigenvectors of the secular equation (14) which satisfy the following relations:

$$\begin{aligned} &c_{22}V_{02}+c_{24}W_{02}=c_2'V_{02}, \\ &c_{24}V_{02}+c_{44}W_{02}=c_2'W_{02}; \end{aligned} \quad (26a)$$

$$\begin{aligned} &c_{22}V_{03}+c_{24}W_{03}=c_3'V_{03}=-c_3'W_{02}, \\ &c_{24}V_{03}+c_{44}W_{03}=c_3'W_{03}=c_3'V_{02}. \end{aligned} \quad (26b)$$

The third member of Eqs. (26b) follow from the orthogonality of the eigenvectors. Further,

$$\begin{aligned} &\mathbf{U}_{01}=(1,0,0), \quad \mathbf{U}_{02}=(0,V_{02},W_{02}), \\ &\mathbf{U}_{03}=(0,-W_{02},V_{02}), \end{aligned} \quad (27)$$

with

$$V_{02}=\left[1+\left(\frac{c_{22}-c_2'}{c_{24}}\right)^2\right]^{-\frac{1}{2}}=W_{03},$$
$$W_{02}=-\frac{(c_{22}-c_2')}{c_{24}}\left[1+\left(\frac{c_{22}-c_2'}{c_{24}}\right)^2\right]^{-\frac{1}{2}}=-V_{03}; \tag{28}$$

and, of course,

$$V_{02}^2+W_{02}^2=V_{03}^2+W_{03}^2=1. \tag{29}$$

The expansions (23) and (24) will fail if the matrix A is accidentally degenerate or quasi-degenerate, i.e., if two of the values

$$c_{66},\quad c_2',\quad c_3'$$

are equal or nearly equal. In this case, the degeneracy should be first removed by the conventional methods.

It can be seen that $B_{kk}=(\mathbf{U}_{0k}\cdot B\mathbf{U}_{0k})$ vanishes. Indeed, the vectors $\mathbf{U}_{0k}$ have either no y- and z-components or no x-component. Application of the matrix B to these vectors produces a new vector which has no x-component or no y- and z-components, respectively, so that the scalar product of vector and transformed vector vanishes in either case. Therefore, by Eq. (25):

$$D_{kk}=\alpha/p^2(C\mathbf{U}_{0k}\cdot\mathbf{U}_{0k})=\alpha/p^2C_{kk}. \tag{30}$$

According to Eq. (25):

$$D_{kl}^2=1/p^2(\mathbf{U}_{0k}\cdot B\mathbf{U}_{0l})^2+\cdots=1/p^2B_{kl}^2 \qquad (k\neq l), \tag{31}$$

where the dots stand for terms of higher order. Equations (23) and (24) become

$$\mathbf{U}_k=\mathbf{U}_{0k}+\alpha/p_{0k}\sum{}'\frac{B_{kl}\mathbf{U}_{0l}}{\rho\omega^2/p_{0k}^2-\rho\omega^2/p_{0l}^2}, \tag{32}$$

$$\rho\omega^2/p_k^2=\rho\omega^2/p_{0k}^2+\alpha^2/p_{0k}^2\kappa_k \tag{33}$$

where

$$\kappa_k=C_{kk}+\sum{}'\frac{B_{kl}^2}{\rho\omega^2/p_{0k}^2-\rho\omega^2/p_{0l}^2}.$$

In Eqs. (32) and (33) we have, on the right-hand side, replaced p_k^2 by p_{0k}^2 because a correction would only add terms of higher order. As shown above, if $\alpha=0$,

$$\rho\omega^2/\beta^2=\begin{cases}c_{66}\\ c_2'\\ c_3'.\end{cases}$$

If α is small, the expansion

$$\rho\omega^2/\beta^2=(1+\epsilon)\begin{cases}c_{66}\\ c_2'\\ c_3'\end{cases} \tag{34}$$

can be assumed. ϵ must be determined as a function of α. Combining Eqs. (33), (34), and (15), we get

$$p_k^2=\frac{\rho\omega^2}{c+\alpha^2\kappa_k/p_{0k}^2}=\frac{\beta^2(1+\epsilon)c}{c+\alpha^2c\kappa_k/\rho\omega^2}$$
$$\cong\frac{\beta^2(1+\epsilon)c}{c+\alpha^2\kappa_k/\beta^2(1+\epsilon)}\cong\beta^2(1+\epsilon-r^2\kappa_k/c), \tag{35}$$

where c stands for either one of the three values given in Eq. (34), and the notation

$$\alpha/\beta=r, \tag{36}$$

is used.

In the following, *we shall treat explicitly the shear vibration whose zero-order approximation is given by Eq. (18)*. If

$$\rho\omega^2/\beta^2=(1+\epsilon)c_{66}, \tag{37}$$

then by Eq. (35)

$$p_1^2=\beta^2(1+\epsilon-r^2\kappa_1/c_{66}). \tag{38}$$

κ_1 is given by Eq. (33). In appendix II it is shown that explicitly

$$\kappa_1=c_{11}+\frac{2(c_{14}+c_{56})c_{24}(c_{12}+c_{66})-(c_{14}+c_{56})^2(c_{22}-c_{66})-(c_{12}+c_{66})^2(c_{44}-c_{66})}{(c_{22}-c_{66})(c_{44}-c_{66})-c_{24}^2}. \tag{39}$$

Substituting the expansions (32) and (33) with (27) and (17) into (13A), we have

$$L_1c_{66}(p_{01}+\cdots)\cos p_1b+L_2\alpha\left(c_{66}\frac{B_{12}}{c_2'-c_{66}}+c_{66}V_{02}+c_{56}W_{02}+\cdots\right)\cos(p_{02}b+\cdots)$$
$$+L_3\alpha\left(c_{66}\frac{B_{13}}{c_3'-c_{66}}+c_{66}V_{03}+c_{56}W_{03}+\cdots\right)\cos(p_{03}b+\cdots)=0,$$

$$L_1\alpha\left(c_{14}+c_{24}\sum_{2,3}\frac{B_{1l}V_{0l}}{c_{66}-c_l'}+c_{44}\sum_{2,3}\frac{B_{1l}W_{0l}}{c_{66}-c_l'}\right)\sin p_{01}b+L_2(c_{24}V_{02}+c_{44}W_{02}+\cdots) \tag{40}$$
$$\times(p_{02}+\cdots)\sin(p_{02}b+\cdots)+L_3(c_{24}V_{03}+c_{44}W_{03})(p_{03}+\cdots)\sin(p_{03}b+\cdots)=0,$$
$$L_1\alpha\left(c_{12}+c_{22}\sum_{2,3}\frac{B_{1l}V_{0l}}{c_{66}-c_l'}+c_{24}\sum_{2,3}\frac{B_{1l}W_{0l}}{c_{66}-c_l'}\right)\sin p_1b+L_2(c_{22}V_{02}+c_{24}W_{02}+\cdots)$$
$$\times(p_{02}+\cdots)\sin(p_{02}b+\cdots)+L_3(c_{22}V_{03}+c_{24}W_{03}+\cdots)(p_{03}+\cdots)\sin(p_{03}b+\cdots)=0.$$

The dots stand for terms of higher order which can be omitted.

The terms of Eqs. (40) will be simplified one by one: By Eq. (38)

$$p_1\cong\beta(1+\tfrac{1}{2}[\epsilon-r^2\kappa_1/c_{66}]), \tag{41}$$

$$\cos p_1b=\cos\frac{n\pi}{2}(1+\tfrac{1}{2}[\epsilon-r^2\kappa_1/c_{66}])\cong\mp\frac{\pi n}{4}(\epsilon-r^2\kappa_1/c_{66}). \tag{42}$$

The upper sign refers to $n=1, 5, 9\cdots$ and the lower to $n=3, 7, 11\cdots$. The factors $\sin p_1b$ which appear with the first terms of the second and third Eqs. (40) are

$$\sin p_1b\cong\sin n\pi/2=\pm1. \tag{43}$$

The two signs refer again to the two cases mentioned above. Smaller terms are omitted here as they are in addition to unity. By Eqs. (20) and (27)

$$\begin{aligned}B_{12}&=(\mathbf{U}_{01}\cdot B\mathbf{U}_{02})=(c_{12}+c_{66})V_{02}+(c_{14}+c_{56})W_{02},\\ B_{13}&=(\mathbf{U}_{01}\cdot B\mathbf{U}_{03})=-(c_{12}+c_{66})W_{02}+(c_{14}+c_{56})V_{02};\end{aligned} \tag{44}$$

$$c_{66}\frac{B_{12}}{c_2'-c_{66}}+c_{66}V_{02}+c_{56}W_{02}=V_{02}\left(\frac{c_{66}(c_{12}+c_{66})}{c_2'-c_{66}}+c_{66}\right)+W_{02}\left(\frac{c_{66}(c_{14}+c_{56})}{c_2'-c_{66}}+c_{56}\right)$$
$$=\frac{1}{c_2'-c_{66}}[V_{02}c_{66}(c_{12}+c_2')+W_{02}(c_{14}c_{66}+c_2'c_{56})]; \tag{45}$$

$$c_{66}\frac{B_{13}}{c_3'-c_{66}}+c_{66}V_{03}+c_{56}W_{03}=c_{66}\frac{B_{13}}{c_3'-c_{66}}-c_{66}W_{02}+c_{56}V_{02}$$
$$=\frac{1}{c_3'-c_{66}}[V_{02}(c_{66}c_{14}+c_3'c_{56})-W_{02}c_{66}(c_{12}+c_3')]. \tag{46}$$

In view of Eqs. (26a) and (26b):

$$c_{14}+c_{24}\left(\frac{B_{12}V_{02}}{c_{66}-c_2'}+\frac{B_{13}V_{03}}{c_{66}-c_3'}\right)+c_{44}\left(\frac{B_{12}W_{02}}{c_{66}-c_2'}+\frac{B_{13}W_{03}}{c_{66}-c_3'}\right)=\frac{c_2'B_{12}W_{02}}{c_{66}-c_2'}+\frac{c_3'B_{13}W_{03}}{c_{66}-c_3'}+c_{14}. \tag{47}$$

The second and third terms of the second Eq. (40) become in view of (26a) and (26b)

$$L_2c_2'p_{02}W_{02}\sin p_{02}b+L_3c_3'p_{03}V_{02}\sin p_{03}b. \tag{48}$$

Also,

$$c_{12}+c_{22}\left(\frac{B_{12}V_{02}}{c_{66}-c_2'}+\frac{B_{13}V_{03}}{c_{66}-c_3'}\right)+c_{24}\left(\frac{B_{12}W_{02}}{c_{66}-c_2'}+\frac{B_{13}W_{03}}{c_{66}-c_3'}\right)=c_{12}+\frac{c_2'B_{12}V_{02}}{c_{66}-c_2'}+\frac{c_3'B_{13}V_{03}}{c_{66}-c_3'}. \tag{49}$$

The second and third terms of the third Eq. (40) become in view of (26a) and (26b):

$$L_2c_2'p_{02}\sin p_{02}b-L_3c_3'W_{02}p_{03}\sin p_{03}b.$$

According to Eqs. (15) and (18):

$$p_{01}=\beta,\quad p_{02}=\beta(c_{66}/c_2')^{\frac{1}{2}},\quad p_{03}=\beta(c_{66}/c_3')^{\frac{1}{2}}.$$

Equations (40) read now:

$$\mp L_1 c_{66}\beta\frac{n\pi}{4}(\epsilon-r^2\kappa/c_{66})+L_2\frac{\alpha}{c_2'-c_{66}}[V_{02}c_{66}(c_{12}+c_2')+W_{02}(c_{14}c_{66}+c_2'c_{56})]\cos\frac{n\pi}{2}(c_{66}/c_2')^{\frac{1}{2}}$$
$$+L_3\frac{\alpha}{c_3'-c_{66}}[V_{02}(c_{14}c_{66}+c_3'c_{56})-W_{02}c_{66}(c_{12}+c_3')]\cos\frac{n\pi}{2}(c_{66}/c_3')^{\frac{1}{2}}=0,$$

$$\pm L_1\alpha\left(c_{14}+\frac{c_2'B_{12}W_{02}}{c_{66}-c_2'}+\frac{c_3'B_{13}W_{03}}{c_{66}-c_3'}\right)+L_2c_2'\beta(c_{66}/c_2')^{\frac{1}{2}}W_{02}\sin\frac{n\pi}{2}(c_{66}/c_2')^{\frac{1}{2}}$$
$$+L_3c_3'\beta(c_{66}/c_3')^{\frac{1}{2}}V_{02}\sin\frac{n\pi}{2}(c_{66}/c_3')^{\frac{1}{2}}=0, \tag{50}$$

$$\pm L_1\alpha\left(c_{12}+\frac{c_2'B_{12}V_{02}}{c_{66}-c_2'}+\frac{c_3'B_{13}V_{03}}{c_{66}-c_3'}\right)+L_2c_2'\beta(c_{66}/c_2')^{\frac{1}{2}}V_{02}\sin\frac{n\pi}{2}(c_{66}/c_2')^{\frac{1}{2}}$$
$$-L_3c_3'W_{02}(c_{66}/c_3')^{\frac{1}{2}}\sin\frac{n\pi}{2}(c_{66}/c_3')^{\frac{1}{2}}=0.$$

Consequently, the determinant

$$\begin{vmatrix}
\mp c_{66}\beta\frac{n\pi}{4}(\epsilon-r^2\kappa/c_{66}) & \frac{\alpha}{c_2'-c_{66}}[V_{02}c_{66}(c_{12}+c_2') & \alpha\cos\frac{n\pi}{2}(c_{66}/c_2')^{\frac{1}{2}} \\
 & +W_{02}(c_{14}c_{66}+c_2'c_{56})]\cos\frac{n\pi}{2}(c_{66}/c_2')^{\frac{1}{2}} & \frac{}{c_3'-c_{66}}[V_{02}(c_{14}c_{66}+c_3'c_{56}) \\
 & & -W_{02}c_{66}(c_{12}+c_3')] \\
\pm\alpha\left(c_{14}+\frac{c_2'B_{12}W_{02}}{c_{66}-c_2'}\right. & c_2'\beta(c_{66}/c_2')^{\frac{1}{2}}W_{02}\sin\frac{n\pi}{2}(c_{66}/c_2')^{\frac{1}{2}} & c_3'\beta(c_{66}/c_3')^{\frac{1}{2}}V_{02}\sin\frac{n\pi}{2}(c_{66}/c_3')^{\frac{1}{2}} \\
\left.+\frac{c_3'B_{13}W_{03}}{c_{66}-c_3'}\right) & & \\
\pm\alpha\left(c_{12}+\frac{c_2'B_{12}V_{02}}{c_{66}-c_2'}\right. & c_2'\beta(c_{66}/c_2')^{\frac{1}{2}}V_{02}\sin\frac{n\pi}{2}(c_{66}/c_2')^{\frac{1}{2}} & -c_3'\beta W_{02}(c_{66}/c_3')^{\frac{1}{2}}\sin\frac{n\pi}{2}(c_{66}/c_3')^{\frac{1}{2}} \\
\left.+\frac{c_3'B_{13}V_{03}}{c_{66}-c_3'}\right) & &
\end{vmatrix} \tag{51}$$

must vanish. The determinant (51) is expanded in terms of the elements of the first row. The first co-factor is

$$\Delta_{11}=c_{66}(c_2'c_3')^{\frac{1}{2}}\beta^2\sin\frac{n\pi}{2}(c_{66}/c_2')^{\frac{1}{2}}\sin\frac{n\pi}{2}(c_{66}/c_3')^{\frac{1}{2}}(-W_{02}^2-V_{02}^2)$$
$$=-c_{66}(c_2'c_3')^{\frac{1}{2}}\beta^2\sin\frac{n\pi}{2}(c_{66}/c_2')^{\frac{1}{2}}\sin\frac{n\pi}{2}(c_{66}/c_3')^{\frac{1}{2}}, \tag{52}$$

in view of Eq. (29). The second co-factor is:

$$\Delta_{12}=\pm\alpha c_3'\beta(c_{66}/c_3')^{\frac{1}{2}}\left[\left(c_{14}+\frac{c_2'B_{12}W_{02}}{c_{66}-c_2'}+\frac{c_3'B_{13}W_{03}}{c_{66}-c_3'}\right)W_{02}\right.$$
$$\left.+\left(c_{12}+\frac{c_2'B_{12}V_{02}}{c_{66}-c_2'}+\frac{c_3'B_{13}V_{03}}{c_{66}-c_3'}\right)V_{02}\right]\sin\frac{n\pi}{2}(c_{66}/c_3')^{\frac{1}{2}}$$
$$=\pm\alpha c_3'\beta(c_{66}/c_3')^{\frac{1}{2}}\left[\frac{c_2'B_{12}}{c_{66}-c_2'}(W_{02}^2+V_{02}^2)+\frac{c_3'B_{13}}{c_{66}-c_3'}(W_{02}W_{03}+V_{02}V_{03})\right.$$
$$\left.+c_{14}W_{02}+c_{12}V_{02}\right]\sin\frac{n\pi}{2}(c_{66}/c_3')^{\frac{1}{2}}. \tag{53}$$

The second term in the bracket vanishes because the quantity in parenthesis represents the scalar product of two orthogonal eigenvectors. We substitute the value of B_{12} from Eqs. (44) into (53):

$$\Delta_{12}=\pm\alpha\beta(c_{66}c_3')^{\frac{1}{2}}\left[V_{02}\left(c_{12}+\frac{c_2'(c_{12}+c_{66})}{c_{66}-c_2'}\right)+W_{02}\left(c_{14}+\frac{c_2'(c_{14}+c_{56})}{c_{66}-c_2'}\right)\right]\sin\frac{n\pi}{2}(c_{66}/c_3')^{\frac{1}{2}}$$

$$=\pm\alpha\beta\frac{(c_{66}c_3')^{\frac{1}{2}}}{c_{66}-c_2'}[V_{02}c_{66}(c_{12}+c_2')+W_{02}(c_{14}c_{66}+c_2'c_{56})]\sin\frac{n\pi}{2}(c_{66}/c_3')^{\frac{1}{2}}. \quad (54)$$

The third co-factor is:

$$\Delta_{13}=\pm\alpha\beta c_2'(c_{66}/c_2')^{\frac{1}{2}}\left[V_{02}\left(c_{14}+\frac{c_2'B_{12}W_{02}}{c_{66}-c_2'}+\frac{c_3'B_{13}V_{02}}{c_{66}-c_3'}\right)\right.$$

$$\left.-W_{02}\left(c_{12}+\frac{c_2'B_{12}V_{02}}{c_{66}-c_2'}-\frac{c_3'B_{13}W_{02}}{c_{66}-c_3'}\right)\right]\sin\frac{n\pi}{2}(c_{66}/c_2')^{\frac{1}{2}}$$

$$=\pm\alpha\beta c_2'(c_{66}/c_2')^{\frac{1}{2}}\left[\frac{c_3'B_{13}}{c_{66}-c_3'}(V_{02}^2+W_{02}^2)+\frac{c_2'B_{12}}{c_{66}-c_2'}(W_{02}V_{02}-W_{02}V_{02})\right.$$

$$\left.+V_{02}c_{14}-W_{02}c_{12}\right]\sin\frac{n\pi}{2}(c_{66}/c_2')$$

$$=\pm\alpha\beta c_2'\frac{(c_{66}/c_2')^{\frac{1}{2}}}{c_{66}-c_3'}[V_{02}(c_3'c_{56}+c_{14}c_{66})-W_{02}c_{66}(c_{12}+c_3')]\sin\frac{n\pi}{2}(c_{66}/c_2')^{\frac{1}{2}}, \quad (55)$$

because $V_{02}=W_{03}$ and $W_{02}=-V_{03}$. The determinant Eqs. (51) can now be written in view of Eqs. (52), (54), and (55):

$$\pm c_{66}^2\beta^2\frac{\pi n}{4}(\epsilon-r^2\kappa_1/c_{66})(c_2'c_3')^{\frac{1}{2}}\sin\frac{n\pi}{2}(c_{66}/c_2')^{\frac{1}{2}}\sin\frac{n\pi}{2}(c_{66}/c_3')^{\frac{1}{2}}$$

$$\mp\frac{\alpha^2\beta}{(c_2'-c_{66})^2}(c_{66}c_3')^{\frac{1}{2}}[V_{02}c_{66}(c_{12}+c_2')+W_{02}(c_{14}c_{66}+c_2'c_{56})]^2\sin\frac{n\pi}{2}(c_{66}/c_3')^{\frac{1}{2}}\cos\frac{n\pi}{2}(c_{66}/c_3')^{\frac{1}{2}}$$

$$\mp\frac{\alpha^2\beta}{(c_3'-c_{66})^2}(c_{66}c_2')^{\frac{1}{2}}[V_{02}(c_{14}c_{66}+c_3'c_{56})-W_{02}c_{66}(c_{12}+c_3')]^2\sin\frac{n\pi}{2}(c_{66}/c_2')^{\frac{1}{2}}\cos\frac{n\pi}{2}(c_{66}/c_2')^{\frac{1}{2}}=0.$$

Solving for ϵ, we obtain $\epsilon=r^2k_n$, where

$$k_n=\frac{1}{c_{66}}\left[\kappa_1+\frac{4}{n\pi(c_{66})^{\frac{1}{2}}}\left\{\frac{\cot\frac{n\pi}{2}(c_{66}/c_2')^{\frac{1}{2}}}{(c_2')^{\frac{1}{2}}(c_{66}-c_2')^2}[V_{02}c_{66}(c_{12}+c_2')+W_{02}(c_{14}c_{66}+c_2'c_{56})]^2\right.\right.$$

$$\left.\left.+\frac{\cot\frac{n\pi}{2}(c_{66}/c_3')^{\frac{1}{2}}}{(c_3')^{\frac{1}{2}}(c_{66}-c_3')^2}[V_{02}(c_{14}c_{66}+c_3'c_{56})-W_{02}c_{66}(c_{12}+c_3')]^2\right\}\right]. \quad (56)$$

If c_{14} and c_{56} are very small:

$$k_n=\frac{1}{c_{66}}\left[c_{11}-\frac{(c_{12}+c_{66})^2(c_{44}-c_{66})}{(c_{22}-c_{66})(c_{44}-c_{66})-c_{24}^2}+\frac{c_{66}^2(c_{12}+c_2')^2}{1+\left(\frac{c_{22}-c_2'}{c_{24}}\right)^2}\frac{4}{n\pi(c_{66})^{\frac{1}{2}}}\frac{\cot\frac{\pi n}{2}(c_{66}/c_2')^{\frac{1}{2}}}{(c_2')^{\frac{1}{2}}(c_{66}-c_2')^2}\right.$$

$$\left.+\left(\frac{c_{22}-c_2'}{c_{24}}\right)^2\frac{c_{66}^2(c_{12}+c_3')^2}{1+\left(\frac{c_{22}-c_2'}{c_{24}}\right)^2}\frac{4}{n\pi(c_{66})^{\frac{1}{2}}}\frac{\cot\frac{n\pi}{2}(c_{66}/c_3')^{\frac{1}{2}}}{(c_3')^{\frac{1}{2}}(c_{66}-c_3')^2}\right]. \quad (57)$$

The fourth term vanishes with c_{24}. Indeed, by Eq. (26a), $W_{02}=0$ when $c_{24}=0$. Physically, the constant c_{24} guarantees that there shall be no purely longitudinal plane waves propagated along the y-direction, and that the displacement vectors $\mathbf{U}_{02}$ and $\mathbf{U}_{03}$ form angles with the wave vector. The fourth term in Eq. (57) is due to this fact. If c_{24} vanishes, Eq. (57) becomes

$$k_n=\frac{1}{c_{66}}\left[c_{11}-\frac{(c_{12}+c_{66})^2}{c_{22}-c_{66}}+\frac{4c_{66}^{\frac{1}{2}}(c_{12}+c_{22})^2\cot\frac{n\pi}{2}(c_{66}/c_{22})^{\frac{1}{2}}}{n\pi c_{22}^{\frac{1}{2}}(c_{66}-c_{22})^2}\right], \tag{58}$$

because then $c_2'=c_{22}$ and $V_{02}=1$. In the isotropic case,

$$c_{11}=c_{22}=2\mu+\lambda, \quad c_{12}=\lambda, \quad c_{66}=\mu,$$

while all other constants vanish, and Eq. (58) becomes

$$k_n=1+\frac{16}{n\pi}\left(\frac{\mu}{2\mu+\lambda}\right)^{\frac{1}{2}}\cot\frac{n\pi}{2}\left(\frac{\mu}{2\mu+\lambda}\right)^{\frac{1}{2}}. \tag{59}$$

We now return to the general case: The ratio $L_1:L_2:L_3$ is equal to the ratio of the corresponding co-factors:

$$\begin{aligned}L_1:L_2:L_3&=\Delta_{11}:\Delta_{12}:\Delta_{13}\\&=1:\left[\pm\frac{r}{\sin\frac{n\pi}{2}(c_{66}/c_2')^{\frac{1}{2}}}\frac{V_{02}c_{66}(c_{12}+c_2')+W_{02}(c_{14}c_{66}+c_2'c_{56})}{(c_2'-c_{66})(c_2'c_{66})^{\frac{1}{2}}}\right]\\&\quad:\left[\pm\frac{r}{\sin\frac{n\pi}{2}(c_{66}/c_3')^{\frac{1}{2}}}\frac{V_{02}(c_3'c_{56}+c_{14}c_{66})-W_{02}c_{66}(c_{12}+c_3')}{(c_3'-c_{66})(c_{66}c_3')^{\frac{1}{2}}}\right].\end{aligned} \tag{60}$$

If we substitute these values into Eq. (11A) and take into account Eqs. (32), (33), and (35), we obtain equations of the form

$$\begin{aligned}u&=\cos\alpha x\sin\beta y[1+\tfrac{1}{2}r^2(k-\kappa_1/c_{66})],\\v&=r\sin\alpha x[A_1\cos\beta y+A_2\cos\beta y(c_{66}/c_2')^{\frac{1}{2}}+A_3\cos\beta y(c_{66}/c_3')^{\frac{1}{2}}],\\w&=r\sin\alpha x[A_3\cos\beta y+A_4\cos\beta y(c_{66}/c_2')^{\frac{1}{2}}+A_5\cos\beta y(c_{66}/c_3')^{\frac{1}{2}}],\end{aligned} \tag{61}$$

where the constants $A_1\cdots A_5$ are only functions of the elastic constants. We do not need the explicit values, but it is simple to write them.

In the isotropic case, L_3, W_{01}, and W_{02} vanish. Therefore, we have

$$w=0, \quad \Delta_{11}:\Delta_{12}:\Delta_{13}=1:\left[\pm\frac{r}{\sin\frac{n\pi}{2}\left(\frac{\mu}{\lambda+2\mu}\right)^{\frac{1}{2}}}\frac{\mu(\lambda+\mu)}{(\lambda+\mu)[\mu(\lambda+2\mu)]^{\frac{1}{2}}}\right]:0,$$

$$u=\cos\alpha x\sin\beta y\left[1+r^2\frac{8}{n\pi}\left(\frac{\mu}{2\mu+\lambda}\right)^{\frac{1}{2}}\cot\frac{n\pi}{2}\left(\frac{\mu}{2\mu+\lambda}\right)^{\frac{1}{2}}\right], \tag{62}$$

$$v=r\sin\alpha x\left[-\cos\beta y\pm2\left(\frac{\mu}{\lambda+2\mu}\right)^{\frac{1}{2}}\frac{\cos\beta y\left(\frac{\mu}{\lambda+2\mu}\right)^{\frac{1}{2}}}{\sin\frac{n\pi}{2}\left(\frac{\mu}{\lambda+2\mu}\right)^{\frac{1}{2}}}\right].$$

The difference between Eqs. (61) and the solution for the infinite plate is:

(1) Instead of $u=\sin \beta y$ we have a slow variation of u with x.

(2) The derivative $\partial u/\partial y$ is not exactly zero at $y=\pm b$, because p_1 differs by a small quantity (proportional to r^2) from $\beta=n\pi/2b$.

(3) While for the infinite plate v and w vanish, we find small quantities proportional to r in the case of the finite plate. v and w do not in general vanish anywhere.

Approximate Solution for the Free Plate

The Eqs. (1) and (13A or B) are rigorously valid for sinusoidal standing waves in a plane-parallel plate. Consequently, the frequencies (56) and the modes (61) are correct solutions for this case, if higher orders of r are disregarded. For a free limited plate, however, the boundary conditions in Eqs. (2) should be satisfied on the lateral surfaces. The boundary conditions in Eqs. (2) on the faces $x=\pm a$ require that

$$\begin{aligned}
-X_x&=c_{11}\frac{\partial u}{\partial x}+c_{12}\frac{\partial v}{\partial y}+c_{14}\frac{\partial w}{\partial y}\\
&\qquad=\alpha \sin \alpha a\cdot F_1(y)=0,\\
-X_y&=c_{56}\frac{\partial w}{\partial x}+c_{66}\left(\frac{\partial u}{\partial y}+\frac{\partial v}{\partial x}\right)\\
&\qquad=\beta \cos \alpha a\cdot F_2(y)=0,\\
-X_z&=c_{55}\frac{\partial w}{\partial x}+c_{56}\left(\frac{\partial u}{\partial y}+\frac{\partial v}{\partial x}\right)\\
&\qquad=\beta \cos \alpha a\cdot F_3(y)=0,
\end{aligned}\tag{63}$$

where F_1, F_2, and F_3 are functions of y which, in general, are of order of unity. It is evident from Eqs. (63) that it is impossible to satisfy rigorously the boundary conditions by a choice of α. If the second and third Eqs. (63) are to be satisfied, $\cos \alpha a$ must vanish, but then $\sin \alpha a$ cannot vanish simultaneously, and therefore the first Eq. (63) will not be satisfied. However, if we put

$$\cos \alpha a=0;\quad \alpha=m\pi/2a\quad (m=1,3,5\cdots)\tag{64}$$

the traction X_x is proportional to $1/a$ and tends toward zero as the lateral dimensions are increased, while the other traction components vanish completely. We shall consider Eqs. (64) as the definition of α. By moving the origin of the reference system along the x-axis, we can write instead of Eqs. (61):

$$\begin{aligned}
u&=\sin \alpha x \sin y\beta\cdot[1+\tfrac{1}{2}r^2(k-\kappa/c_{66})],\\
v&=r\cos \alpha x\cdot[\cdots],\\
w&=r\cos \alpha x\cdot[\cdots].
\end{aligned}\tag{61a}$$

The boundary conditions Eqs. (2) are now:

$$\begin{aligned}
-X_x&=\alpha \cos \alpha a\cdot F_1(y)=0,\\
-X_y&=-\beta \sin \alpha a\cdot F_2(y)=0,\\
-X_z&=-\beta \sin \alpha a\cdot F_3(y)=0.
\end{aligned}\tag{63a}$$

To satisfy the second and third Eqs. (63a), we have to assume

$$\sin \alpha a=0,\quad \alpha=m\pi/2a\quad (m=2,4,6\cdots).\tag{64a}$$

Taking the even and odd modes of (64) and (64a) together, we note that m can now take on any integer value.

If the extension in the z-direction, i.e., 2c, is not infinite, the boundary conditions

$$\begin{aligned}
-Z_z&=c_{13}\frac{\partial u}{\partial x}+c_{23}\frac{\partial v}{\partial y}+c_{34}\frac{\partial w}{\partial y}=0,\\
-Y_z&=c_{14}\frac{\partial u}{\partial x}+c_{24}\frac{\partial v}{\partial y}+c_{44}\frac{\partial w}{\partial y}=0,\\
-X_z&=c_{55}\frac{\partial w}{\partial x}+c_{56}\left(\frac{\partial u}{\partial y}+\frac{\partial v}{\partial x}\right)=0.
\end{aligned}\tag{65}$$

on the faces $z=\pm c$ cannot be satisfied. However, if

$$c_{13}=c_{14}=c_{23}=c_{24}=c_{34}=c_{56}=0,$$

(e.g., in the isotropic case) w vanishes and the Eqs. (65) are satisfied exactly. Fortunately, these constants are often small so that we can expect a fair agreement between theory and experiment despite Eq. (65).

We shall consider Eq. (61) and (61a) with the definitions (64) and (64a) of α as the approximate solution of the problem for the free thin plate.

Comparison with Experiment

Combining Eqs. (37), (56), (64), and (64a), we obtain:

$$\rho\omega^2=\beta^2c_{66}(1+r^2k_n)$$

or

$$\nu=\tfrac{1}{2}(c_{66}/\rho)^{\frac{1}{2}}\left[\left(\frac{n}{2b}\right)^2+k_n\left(\frac{m}{2a}\right)^2\right]^{\frac{1}{2}}.\tag{66}$$

Observations on thin quartz plates of the so-

called Y_θ type were carried out by Sykes.[5] In this case, one major edge is parallel to the twofold x-axis, so that comparison with the present theory is possible. Sykes found an empirical formula for the shear type vibrations:

$$\nu=\tfrac{1}{2}(c_{66}/\rho)^{\frac{1}{2}}\left[\left(\frac{n}{2b}\right)^2+k\left(\frac{m}{2a}\right)^2+k'\left(\frac{p-1}{2c}\right)^2\right]^{\frac{1}{2}}. \quad (67)$$

When $p=1$, this empirical formula agrees with the theoretical Eq. (66). The numerical value of the empirical constant k is not given explicitly, but it can be calculated from Sykes' diagrams. Expansion of Eq. (66) yields, when $n=1$ and $a\gg b$:

$$\nu_m=\tfrac{1}{2}(c_{66}/\rho)^{\frac{1}{2}}\frac{1}{2b}\left(1+\frac{k}{2}m^2\frac{b^2}{a^2}\right),$$

and

$$\frac{\nu_m-\nu_1}{\nu_1}=\frac{k(b/a)^2(m^2-1)}{2[1+\frac{1}{2}k(b/a)^2]}\cong\tfrac{1}{2}k(b/a)^2(m^2-1);$$

or

$$k=\frac{2}{n^2-1}\left(\frac{a}{b}\right)^2\frac{\nu_m-\nu_1}{\nu_1}.$$

From Sykes' Fig. 6.15, we find, for $a/b=32$:

$$\nu_1=1662,\quad \nu_3=1688,\quad \nu_5=1736$$

which gives $k=4.0$ and 3.8, respectively. The average value is $k=3.9$ for the AT-cut plate. From Sykes' Fig. 6.17, we find, for $a/b=48$:

$$\nu_1=2552,\quad \nu_7=2600,\quad \nu_9=2628,\quad \nu_{11}=2658$$

which gives $k=1.8$, 1.7, and 1.6, respectively. The average value is $k=1.7$ for the BT-cut plate. With the elastic constants of quartz measured by Mason[6] and the transformation formulas listed by Sykes,[5] we obtain the following constants for the plates in units of 10^{10} dyn/cm^2 (Table I). From Eqs. (56), (39), (16), and (28), we calculate the following values for $k(n=1)$:

	AT	BT
k_{obs}	3.9	1.7
k_{calc}	3.7	1.8

The agreement is satisfactory. Theoretically, k should be independent of m, but depend on n. Sykes does not state whether this is the empirical meaning of k. However, comparison of Sykes' Figs. 6.15 and 6.16 referring to the cases $n=1$ and $n=3$ seems to show that k is definitely lower in the latter case.

TABLE I.

	AT	BT		AT	BT
c_{11}	86.05	86.05	c_{12}	−10.35	26.20
c_{22}	129.86	97.77	c_{13}	25.85	−10.70
c_{44}	39.06	40.85	c_{14}	3.55	0.13
c_{66}	29.34	68.91	c_{24}	−5.82	13.11
			c_{56}	−2.46	6.45

It appears from the empirical Eq. (67) that for the case $p=1$, the frequency is not affected by the dimension c. This confirms our assumption that for the type of vibration under consideration, the boundary conditions (65) can be disregarded.

In the lowest mode ($m=1$), where

$$\alpha=\pi/2a,$$

the displacement u is maximum in the center and decreases monotonically toward the edge $x=\pm a$. The displacement components v and w are small, but they have their maximum value at the edge. In a lycopodium powder experiment, we should expect the powder to be most vigorously moved at the center and only slightly at the edge, while no exact nodes appear. This is in agreement with experimental evidence.[7] The clamping of a crystal on the corners does not modify considerably its mode, as can be expected.

In the mode corresponding to $m=2$, i.e.,

$$\alpha=\pi/a,$$

the mode is given by Eqs. (61a). The displacement component u has the form

$$u=f(y)\sin\pi x/a,$$

which vanishes in the center while it has opposite signs in the left- and right-hand half of the plate. Observations by Sykes[6] (third figure in Fig. 6.5) are in agreement with this result.

Experiments show that a freely vibrating crystal of the kind considered here, if mounted between metal plates parallel to its major faces, excites ultrasonic vibrations of the air between the surface and the plate. This cannot be explained by the theory of the infinite plate

[5] R. A. Sykes, Bell. Sys. Tech. J. **23**, 52 (1944).
[6] W. P. Mason, Bell Sys. Tech. J. **22**, 178 (1943).
[7] G. M. Thurston, U. S. Patent 1,883,111, October 18, 1932.

because a shearing motion alone cannot cause compression or dilatation. The present theory shows that the component v is not zero and thus explains the existence of air waves.

Sykes' observations show that Eq. (67) ceases to be valid at certain ratios $a:b$ and $c:b$. With these ratios, two nearby frequencies appear, one lower and one higher than that given by Eq. (67). Sykes explains this fact qualitatively by coupling of the thickness vibration with other types of modes. We shall discuss the phenomenon of coupling from the theoretical viewpoint.

It was shown in a previous paper[8] how it is possible to represent the solution of an elastic vibration problem as a linear combination of "zero-order" or uncoupled modes. We can consider the mode given by Eq. (61) as a zero-order mode. It differs from an exact solution in that it does not exactly comply with the boundary conditions on the lateral faces. Other zero-order modes can be obtained by different solutions of Eqs. (7) and (13). We have only considered those solutions where α is small. It can be shown, however, that other types of solutions corresponding to about the same frequency

$$\nu=(c_{66}/\rho)^{\frac{1}{2}}\frac{1}{4b}$$

can be obtained when α is of the order of magnitude of p. One type corresponds to Timoshenko's flexural waves treated in Appendix I. These other modes will be equally zero-order modes because they will satisfy the boundary conditions on the lateral faces only approximately. Their frequency depends mainly on the dimensions a and c.[9] Consequently, a coupling in the sense defined in a previous paper[8] will exist between the thickness mode Eq. (61) and the "lateral" modes. As the coupling is caused by the stresses X_x (on $x=\pm a$) and Z_z, Y_z, and X_z (on $z=\pm c$), which are all small, the coupling itself will be small. As shown by the form of the secular determinant in the same paper, a weak coupling has a noticeable effect only when the frequencies of two zero-order modes are nearly equal. This explains why the exceptional regions, where the uncoupled frequency becomes incorrect, occur at the intersection of the curve representing the uncoupled thickness shear mode and one representing an uncoupled "lateral" mode.

[8] H. Ekstein, Phys. Rev. **66**, 108 (1944).
[9] The proof is omitted here.

APPENDIX I

It will be shown that Eqs. (7) and (13) include, as a special case, Timoshenko's theory of flexural waves in an isotropic plate.[10] In the isotropic case,

$$c_{11}=c_{22}=2\mu+\lambda,\quad c_{44}=c_{55}=c_{66}=\mu,\quad c_{12}=\lambda,\quad (1.1)$$

and all other constants appearing in Eqs. (7) and (13) are zero. The determinant (7) reduces to

$$\begin{vmatrix}\mu p^2+(\lambda+2\mu)\alpha^2-\rho\omega^2 & \alpha p(\lambda+\mu)\\ \alpha p(\lambda+\mu) & (\lambda+2\mu)p^2+\mu\alpha^2-\rho\omega^2\end{vmatrix}=0,\quad (1.2)$$

with $W_1=W_2=0$. The third solution:

$$\mu p^2+\mu\alpha^2-\rho\omega^2=0,$$

and

$$U_3=V_3=0,$$

can be disregarded for this discussion, as will be seen. The two solutions of (1.2) are:

$$p_1^2=\frac{\rho\omega^2}{\lambda+2\mu}-\alpha^2,\quad (1.3)$$

and

$$p_2^2=\rho\omega^2/\mu-\alpha^2.$$

If we substitute this into the first two Eqs. (6), the ratios

$$U_1:V_1=\alpha:p_1,\quad U_2:V_2=-p_2:\alpha\quad (1.4)$$

are found. We choose the case (A) corresponding to Eqs. (10A) and (13A). Equations (13A) reduce to

$$\begin{aligned}&\sum L_i[\lambda\alpha U_i+(\lambda+2\mu)p_iV_i]\sin p_ib=0,\\ &\sum L_i\mu p_iW_i\sin p_ib=0,\quad (1.5)\\ &\sum L_i\mu(p_iU_i+\alpha V_i)\cos p_ib=0.\end{aligned}$$

The second Eq. (1.5) can be satisfied identically by

$$L_3=0,$$

because $W_1=W_2=0$. We consider frequencies low enough so that:

$$\rho\omega^2/\mu<\alpha^2$$

and all the more:

$$\rho\omega^2/(\lambda+2\mu)<\alpha^2.$$

[10] S. P. Timoshenko, Phil. Mag. [6] **43**, 125 (1922).

According to (1.3), p_1 and p_2 then are both imaginary. If we put

$$m=\alpha\left[1-\frac{\rho\omega^2}{\alpha^2(\lambda+2\mu)}\right]^{\frac{1}{2}},$$
$$n=\alpha\left[1-\frac{\rho\omega^2}{\alpha^2\mu}\right]^{\frac{1}{2}}, \tag{1.6}$$

so that m and n are positive real numbers, the Eqs. (1.5) become, in view of (1.3) and (1.4):

$$\begin{aligned} &L_1[\lambda\alpha^2-m^2(\lambda+2\mu)]\sinh mb] \\ &\qquad +iL_2 2\mu n\alpha \sinh mb=0, \\ &iL_1 2m\alpha\cosh mb+L_2(n^2+\alpha^2)\cosh nb=0. \end{aligned} \tag{1.7}$$

By eliminating L_1 and L_2 from (1.7), we obtain Timoshenko's "frequency equation":

$$\begin{aligned} &4\mu\alpha^2 mn\tanh nb \\ &\quad=(\alpha^2+n^2)[(\lambda+2\mu)m^2-\lambda\alpha^2]\tanh mb. \end{aligned} \tag{1.8}$$

APPENDIX II

Instead of using Eq. (33) for the explicit value of κ_1, it is easier to find it by direct expansion of the determinant (8). If

$$p/\alpha=q. \quad (1/q\ll 1)$$

we divide the second and third rows and columns by q:

$$\begin{vmatrix} q^2(-\rho\omega^2/p^2+c_{66}+c_{11}/q^2) & c_{12}+c_{66} & c_{14}+c_{56} \\ c_{12}+c_{66} & -\rho\omega^2/p^2+c_{22}+c_{66}/q^2 & c_{24}+c_{56}/q^2 \\ c_{14}+c_{56} & c_{24}+c_{56}/q^2 & -\rho\omega^2/p^2+c_{44}+c_{55}/q^2 \end{vmatrix}=0. \tag{2.1}$$

In view of Eqs. (33) and (15):

$$\rho\omega^2/p_1^2=c_{66}+\alpha^2\kappa_1/p_{01}^2,$$

so that we can neglect the term with α^2 everywhere except in the first element of the first column of (2.1), finally omitting the terms c_{ik}/q^2 where they are in addition to c_{ik}, we obtain:

$$\begin{vmatrix} q^2(-\rho\omega^2/p_1^2+c_{66}+c_{11}/q^2) & c_{12}+c_{66} & c_{14}+c_{56} \\ c_{12}+c_{66} & c_{22}-c_{66} & c_{24} \\ c_{14}+c_{56} & c_{24} & c_{44}-c_{66} \end{vmatrix}=0. \tag{2.2}$$

We expand (2.2) and get:

$$\begin{aligned} &q^2(-\rho\omega^2/p_1^2+c_{66}+c_{11}/q^2)[(c_{22}-c_{66})(c_{44}-c_{66})-c_{24}^2]-(c_{12}+c_{66})[(c_{12}+c_{66})(c_{44}-c_{66})-c_{24}(c_{14}+c_{56})] \\ &\qquad +(c_{14}+c_{56})[(c_{12}+c_{66})c_{24}-(c_{22}-c_{66})(c_{14}+c_{56})]=0. \end{aligned} \tag{2.3}$$

Solving (2.3) for $\rho\omega^2/p_1^2$:

$$\begin{aligned} \rho\omega^2/p_1^2=c_{66}+1/q^2\Bigg[&c_{11} \\ &+\frac{(c_{14}+c_{56})\{c_{24}(c_{12}+c_{66})-(c_{22}-c_{66})(c_{14}+c_{56})\}-(c_{12}+c_{66})\{(c_{12}+c_{66})(c_{44}-c_{66})-c_{24}(c_{14}+c_{56})\}}{(c_{22}-c_{66})(c_{44}-c_{66})-c_{24}^2}\Bigg]. \end{aligned} \tag{2.4}$$

In the expression: $1/q^2=\alpha^2/p_1^2$ we can, in view of Eq. (15), substitute p_{01}^2 for p_1^2 without adding correction terms of the second order. Comparing (2.4) with (33), we find that:

$$\kappa_1=c_{11}+\frac{2c_{24}(c_{14}+c_{56})(c_{12}+c_{66})-(c_{14}+c_{56})^2(c_{22}-c_{66})-(c_{12}+c_{66})^2(c_{44}-c_{66})}{(c_{22}-c_{66})(c_{44}-c_{66})-c_{24}^2}. \tag{39}$$

Effect of Hydrogen on the X-Ray Parameter and Structure of Electrolytic Manganese[1]

E. VERNON POTTER[2] AND RALPH W. HUBER[3]
United States Department of Interior, Salt Lake City, Utah

(Received May 10, 1945)

The effect of the hydrogen content of electrolytic manganese on the average lattice parameter was determined. The parameter varies approximately linearly with the hydrogen content, the enlargement in parameter being 0.0003 percent per cc of gas per 100 grams of metal. The crystals, composing electrolytic manganese metal, are generally not uniform in parameter but show deviations up to ±0.2 or ±0.3 percent. The deviations in parameter between the unit cells of alpha-manganese in a sample of metal are not proportional to the amount of gas in the metal. The effect of various degassing treatments on the parameter and diffraction patterns was determined. The parameters are not effected unless the metal is heated over 300°C. At 500°C and over, the parameter returns to its normal value and the diffraction lines are sharp. The broadening of the diffraction lines in the patterns for the metal containing gas are attributed to non-uniform lattices in the metal due to non-uniform gas distribution, and the results indicate that manganese may be saturated with hydrogen at about 695 cc per 100 grams of metal or 0.06 percent. Manganese metal with normal lattice parameters and uniform structure may be obtained from electrolytic metal by removing the gas and heating it to 500°C for 1 hour. If the metal is heated to 500°C or more during the degassing treatment, subsequent heating is not necessary.

INTRODUCTION

DURING the rather extensive studies by the Bureau of Mines on electrolytic manganese and its alloys, a question has frequently arisen regarding the correct lattice parameter for alpha-manganese. The average parameter as determined from several samples of electrolytic manganese metal was 8.904A. Moreover, the alpha-manganese phase in the Mn-Cu alloys[4] gave a parameter of 8.906A, so it was concluded that the alpha-manganese phase in the alloys was essentially pure manganese. The published[5] parameter for alpha-manganese was only 8.894A, but since the electrolytic metal was more than 99.9 percent pure and the impurities were distributed among a large number of elements, it was unlikely that the discrepancy could be due to impurities in the metal. There was no satisfactory explanation for the discrepancy until the hydrogen content of the electrolytic manganese was investigated. In this study some vacuum-distilled metal was made, and its parameter was found to be 8.8948A. This result checked the published value quite well, and the lines in the pattern were much sharper than those obtained from electrolytic manganese metal. Obviously, some impurity in the electrolytic metal was causing the enlargement in parameter, but the amount of each of the known impurities was small when considered on a percentage basis. The hydrogen content was quite high on a volume basis, however, being 250 cc per 100 grams of metal,[6] so an investigation was made to determine what effect hydrogen might have on the parameters.

TABLE I. Variation of average parameter with gas content.

Material	Parameter in A	Hydrogen content in cc per 100 grams of Mn
Vacuum-distilled manganese	8.8948±0.001	0
Electrolytic manganese transformed from gamma-manganese to alpha-manganese	8.898 ±0.005	95±13
Regular electrolytic manganese	8.904 ±0.004	250±25
Electrolytic manganese, hydrogen content high	8.910 ±0.005	615±50

[1] Published by permission of the Director, Bureau of Mines, U. S. Department of the Interior.
[2] Physicist, Western Region, Bureau of Mines.
[3] Metallurgical Engineer, Western Region, Bureau of Mines.
[4] R. S. Dean, J. R. Long, T. R. Graham, E. V. Potter, and E. T. Hayes, "The Copper-Manganese Equilibrium System," Trans. A.S.M.E. **34**, 443 (1945).
[5] Ralph W. G. Wyckoff, *The Structure of Crystals*, second edition and second edition supplement; *Handbook of Chemistry and Physics*, twenty-seventh edition, 1943–1944.
[6] E. V. Potter, E. T. Hayes, and H. C. Lukens, "Hydrogen Content of Electrolytic Manganese and Its Removal," Am. Inst. of Mining and Metallurgical Eng.–Metals Technology (June 1945), Technical Publication 1809.

CHANGE IN AVERAGE LATTICE PARAMETER WITH HYDROGEN CONTENT

The parameters of a number of samples of regular electrolytic manganese were determined by the Debye-Scherrer method and the hydrogen content of the material was determined by the method outlined in an earlier publication.[6] Most of these samples had about the same hydrogen content; one sample was found with an unusually high hydrogen content, and some samples of manganese, deposited as flexible gamma-manganese, had unusually low hydrogen content. The gamma-manganese changed gradually at room temperature to alpha-manganese, and the parameters were obtained for the alpha-form. The results of these parameter and hydrogen-content determinations are shown in Table I along with corresponding values for vacuum-distilled manganese.

These data are plotted in Fig. 1 and show a linear relation between parameter and hydrogen content within the limits of accuracy of the parameter determinations. The lines in the pattern for vacuum-distilled manganese are quite sharp, and the *K*-alpha doublets are resolved for diffraction angles greater than 45°. The parameter could thus be determined to a greater accuracy than for the other samples, where the lines were broader and none of the doublets were resolved.

EFFECT OF DEGASSING TREATMENTS ON LATTICE PARAMETERS AND DIFFRACTION PATTERNS

Several batches of electrolytic manganese were degassed, according to the procedure suggested in a previous publication,[6] to determine the effect of degassing on the parameter. The metal was heated to temperatures from 300° to 925°C at reduced pressure until the pressure again decreased to its initial value before heating. The treatment times were about 1 hour for temperatures up to 700°C and one-half hour at 925°C. This did not remove all the gas, so samples of these batches were tested for gas content by heating them to 500°C in a hydrogen atmosphere at normal atmospheric pressure and determining the amount of gas liberated or absorbed by the sample in reaching equilibrium under these conditions. The solubility of hydrogen in manganese under these conditions is known and the amount of gas that was in the metal originally was either

TABLE II. Average parameter for various degassing treatments.

Material	Parameter
Original manganese metal	8.904
Manganese degassed at 300°C	8.902
Manganese degassed at 500°C	8.8944
Manganese degassed at 700°C	8.8948
Manganese degassed at 925°C	8.8935

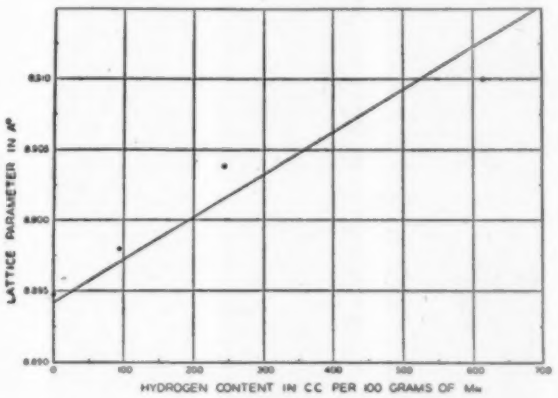

FIG. 1. Variation in average parameter with hydrogen gas content of the metal.

greater or less than this value by the volume liberated or absorbed. All the samples showed less than 10 cc of gas per 100 grams of metal or less than 4 percent of the original amount. X-ray diffraction patterns of each sample were then made, and the parameters were determined. The results are shown in Table II as compared with the parameter for the original metal.

Removing the gas from the metal has little, if any, effect on the parameter at temperatures up to 300°C. At 500°C and over, however, the parameters return nearly to normal value. The parameters listed for these three samples are essentially equal (within experimental error, which is about 0.0005A), and the average value, 8.8942A, agrees well with the published value.

A better comparison can be made from the diffraction pattern shown in Fig. 2; Figs. 2a, 2b, 2c, 2d, and 2e show the patterns for the samples treated at 925°, 700°, 500°, 300°C and the normal untreated metal, respectively. The patterns on the 500°, 700°, and 925°C samples all show sharp lines with the *K*-alpha doublets resolved. The 925°C pattern seems to be the sharpest; the

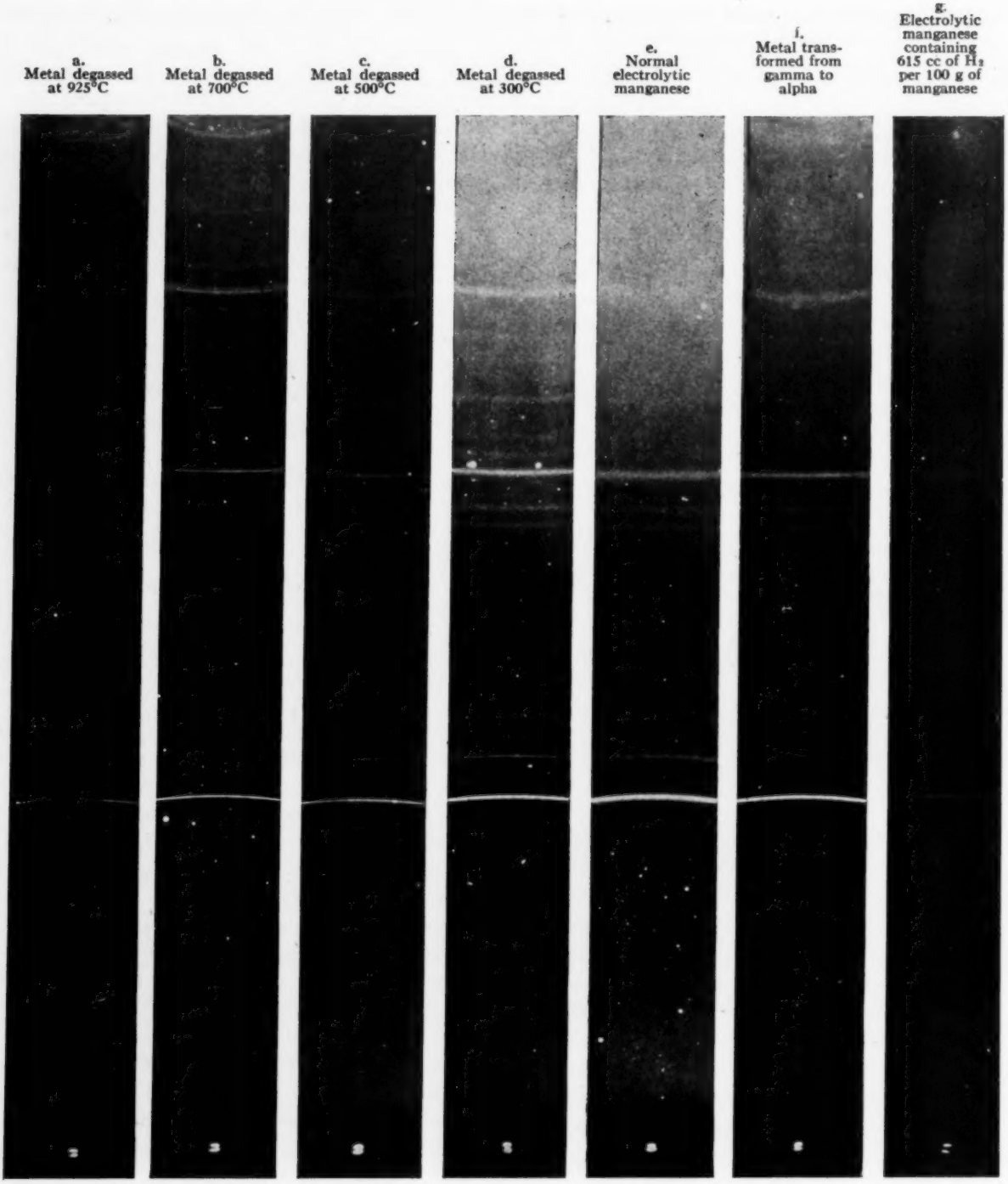

FIG. 2. X-ray diffraction patterns.

500°C pattern is definitely broader. Densitometer measurements shown in Table III show the 925° and 700°C patterns to be essentially the same, though visually the 700°C pattern would seem to be somewhat broader. The 300°C pattern cannot be distinguished from that for the untreated metal, showing that the metal is essentially the same even though the gas has been removed.

The diffraction patterns also indicate other variations in the structure aside from the differ-

ences in parameters of the various samples. The patterns shown in Figs. 2a, 2b, and 2c show sharp lines, while those in Figs. 2d and 2e show broad lines. Figure 2f shows the pattern for manganese, which was plated as flexible gamma-manganese and transformed to alpha-manganese, while Fig. 2g shows the pattern for a sample of manganese containing an unusually large amount of gas. Both of these patterns also have broad lines.

Two factors cause lines in a diffraction pattern to be broad: (1) variations in the parameters of the crystals constituting the individual sample or (2) variations in the size of the crystal aggregates in the different samples. Parameter variations in the crystals constituting the sample would obviously cause broad lines because the resulting pattern would be a composite of patterns from the individual crystals, and the lines in the individual patterns would be displaced relative to each other by amounts depending on the variations in the parameter. Measurements made at the densest portion of the lines determine the average parameter, and the width of the lines is a measure of the deviation from the average in the respective crystal units in the specimen.

Variations in the size of the crystal aggregates, which act as units to the x-ray beam, influence the width of the diffracted beam and the width of the diffraction lines. This phenomenon has been made the basis of a method for estimating the size of the crystal aggregates which act as units to the x-ray beam.[7] In the present case both of these factors may be contributing to the observed line width, so an attempt was made to determine the actual deviations in parameter. In the following discussion "deviation in parameter" will be used to mean the difference between the parameter of an individual crystal and the average parameter for a sample while "variation in parameter" will mean the difference between the average parameter of a sample and the normal parameter for manganese metal.

X-ray data alone are not sufficient to separate the two effects, so the specimens were examined microscopically to detect any variation in crystal or grain size in the different samples. No difference could be seen between the regular electrolytic manganese metal and the degassed metal for temperatures up to 700°C even though the diffraction patterns showed marked changes. In each case the grains were very small. At 925°C some evidence of larger grains was seen, but the diffraction patterns show little difference between the 925° and the 700° samples. It would seem, therefore, that crystal aggregate or grain size has little influence on the line widths and that the grains are all sufficiently large to produce sharp diffraction lines. We can then attribute the variations in the line widths to deviations of parameter only and estimate the magnitude of this deviation.

The width of the lines in six of the patterns in Fig. 2, measured with a densitometer, are shown in Table III.

The line widths were measured at an intensity equal to one-half the maximum. The sharpest lines were obtained on the samples degassed at 700° and 925°C, the widths being essentially the same. The pattern for vacuum-distilled metal is not shown because it was identical with that for the metal degassed at 900°C. These three materials should be the most uniform, in structure and, since they gave almost identical patterns and line widths, it was assumed that they most nearly represented material with a uniform parameter. The observed line width in the patterns for these samples is then due to the optical characteristics of the x-ray camera, and the size of the crystal aggregates in the specimens. These factors were assumed to be constant, and this minimum line width was used to correct the other

TABLE III. Line widths and parameter deviations in various samples.

Material	Line width in mm	Parameter deviation
Regular electrolytic manganese	0.84	±0.21 percent
Electrolytic manganese degassed		
At 300°C	0.84	±0.21 percent
At 700°C	0.52	0
At 925°C	0.55	0
Electrolytic manganese containing 615 cc per 100 grams of Mn	0.61	±0.06 percent
Electrolytic manganese transformed from gamma-Mn to alpha-Mn	0.99	±0.31 percent

[7] (a) R. Brill, "X-Ray Determination of Size and Shape of Submicroscopic X'tals," Kolloid Zeits. **55**, 164–169 (1931); (b) G. H. Cameron, and A. L. Patterson, "The X-Ray Determination of Particle Size," Symposium on Radiography and X-Ray Diffraction, A.S.M., p. 324 (1936); (c) H. Mark, "The Determination of Particle Size by the Use of X-Rays," Trans. Faraday Soc. **25** (1929).

values, the increase in width relative to this value being attributed to non-uniformity in the parameters.

The maximum parameter deviation required to explain the broadening of the lines is only 0.3 percent but, in this case, we are not justified in assuming that the crystal aggregates are the same size as in the other samples because the plating conditions required for producing gamma-manganese are different from those used for plating alpha-manganese. In the other samples a deviation of 0.2 percent in parameter value is indicated. It might be expected that the deviations would be greater with the larger amounts of gas, but this does not seem to be the case, since the samples containing the most gas show a deviation of only 0.06 percent in parameter. This observation leads to some possible conclusions regarding the solubility of hydrogen in manganese which will be discussed later.

DISCUSSION OF RESULTS

a. Variation of Average Parameter with Hydrogen Content

The data in Table I and Fig. 1 indicate that the lattices of the manganese crystals are distorted by the hydrogen present in them. This distortion produces an enlargement of the average lattice parameter roughly proportional to the amount of gas in the metal or about 0.0003 percent per cc of gas per 100 grams of metal. The lattices are not necessarily distorted uniformly; any deviations from the average parameter should cause a widening of the lines in the x-ray diffraction pattern, the widening being proportional to the amount of the deviation. The lack of resolution of the *K*-alpha doublets in the patterns obtained from the samples containing gas indicates that such deviations may exist within the lattices of those samples, but the vacuum-distilled metal seems to have rather uniform lattice dimensions.

b. Effect of Degassing Treatments on Lattice Parameters

The lattice parameters obtained for the degassed manganese metal (shown in Table II) and the x-ray diffraction patterns for these samples (shown in Fig. 2), show definitely that it is only necessary to remove the gas from the metal and heat it to 500°C or higher to produce a metal with a normal and uniform lattice parameter. Since this treatment cannot affect any of the impurities, other than the amount of hydrogen present in the metal, the enlargement of the lattice parameter in the normal electrolytic metal must be due to the presence of the hydrogen introduced into the metal as atomic hydrogen during the plating process. The amount of hydrogen is about 0.02 percent by weight; it occupies a volume at normal conditions twenty[6] times that of the metal containing it. It is not unreasonable to expect that this highly compressed gas would have some effect on the structure of the metal containing it. Degassing the metal at 300°C has virtually no effect on its lattices, probably because the mobility of the atoms at this temperature is too low to permit any appreciable readjustment of the lattice in the time required for removing the gas.

c. Significance of Broadening of Lines in the Diffraction Patterns

The line widths shown in Table III can be taken as reliable indices of the relative broadness of the lines in the various diffraction patterns, but the calculated deviations in parameter are subject to too much error to be considered as more than rough estimates. It is evident, however, that the broadening of the lines observed in the diffraction patterns might be explained by a slight non-uniformity in the lattice parameters and that the non-uniformity is not proportional to the amount of gas in the metal.

The average parameters for the regular electrolytic manganese, the manganese transformed from the gamma- to the alpha-form, and the manganese with the high hydrogen content were enlarged 0.11, 0.045, and 0.18 percent, respectively (see Table I). The deviations in parameter shown in Table III are larger than this and indicate that some of the crystals in the metal had parameters less than normal. This may be true, in which case the average enlargement must exceed the average compression of the lattice so that a net enlargement in parameter is observed. On the other hand, the calculated deviations may be too large because of improper measurement of the line width or improper cor-

rection for the width due to grain or crystal aggregate size. Possible errors from the first source cannot be discussed here because no adequate theory is available for determining the relation between grain size, parameter deviation, and line width. Errors from the second source can produce the effects noted if we assume that there is some grain growth in the manganese during the degassing treatments. The grains would be larger in the samples treated at the higher temperatures, and the lines in their diffraction patterns would be sharper. The correction for grain size, based on the line width of the 700° and 925°C samples, would be too small and we would be attributing too much of the widening effect in the other samples to parameter deviations. A more nearly correct value for the parameter deviation might then be obtained by considering that the deviation above and below the average parameter value is equal to the enlargement of the average parameter relative to that for normal alpha-manganese metal.

The parameter deviations shown in Table III do not vary with gas content in the manner that might be expected. The deviation is zero at zero gas content, high at 95 cc per 100 grams of metal, and decreases with increasing gas content up to the observed maximum gas content of 615 cc per 100 grams of metal. This behavior indicates that the deviation might again be zero at some value of gas content near 615 cc per 100 grams of manganese. In this case each crystal would be enlarged the same amount and would contain the same amount of gas. This would not be likely to occur unless the metal were saturated with gas and, in this case, there should be an integral number of atoms of gas in each unit cell of alpha-manganese. The number of unit cells of alpha-manganese in 1 gram of metal is proportional to the reciprocal of the product of the atomic weight, the number of atoms in a unit cell, and is some constant times 0.31×10^{-3}. On the same basis, 615 ± 50 cc of gas in the metal would provide $(0.55\pm.05)\times10^{-3}$ atom of hydrogen, or nearly two atoms per unit cell of alpha-manganese. If we assume that each unit cell absorbs 2 atoms of hydrogen, then it would require 695 cc of hydrogen per 100 grams of manganese to saturate the metal, and only about 90 percent of the unit cells in the sample containing 6.5 cc of gas per 100 grams of metal would be saturated. The remaining 10 percent of the unit cells would be distorted various amounts and cause the diffraction lines to be wider than if the sample were uniform. The deviation shown in Table III is consistent with this conclusion, and it would be anticipated that slightly higher gas contents would produce sharper diffraction lines.

No samples of manganese were found containing more than 615 cc of hydrogen, so we have no experimental evidence to show whether or not manganese will absorb more than 2 atoms of hydrogen. The fact that the regular electrolytic metal, containing 250 cc of gas per 100 grams, shows definitely fuzzy lines, indicates that the unit cells take 2 rather than 1 atom, however, because if the latter were true, the unit cells could be uniform with about 350 cc of gas per 100 grams of metal, and the observed diffraction patterns show no evidence to support this conclusion.

ACKNOWLEDGMENTS

The authors wish to express their indebtedness to Mr. H. C. Lukens who degassed the manganese samples and made the hydrogen-content determinations on the samples used in these tests.

PHYSICAL REVIEW VOLUME 68, NUMBERS 1 AND 2 JULY 1 AND 15, 1945

Electron Temperatures in Electrical Discharges

K. T. CHAO AND T. Y. TANG
Department of Physics, National Central University, Chungking, China
(Received October 23, 1944)

Electron temperatures in the positive column and in the Faraday dark space of a cold cathode glow discharge have been measured by the probe method when the gas pressures of dry air and carbon monoxide were varied in the range from 0.06 to 1.2 mm Hg. For the fast group, electron temperatures decrease with pressure while for the slow group they are independent of it. The electron current densities increase and the space potentials decrease when the gas pressure is increased. Different current-voltage characteristic curves have been found in the positive column and in the transition region from the negative glow to the Faraday dark space. Theoretical interpretations of these different characteristics could be obtained either from Langmuir's theory of probe or from Druyvesteyn's theory of electron energy distribution by assuming the existence in the boundary between negative glow and Faraday dark space of a drift fast electron beam superimposed upon an isotropic slow electron distribution. Spectroscopic investigations of the bands of the neutral and ionic molecules of N_2 and CO in different sections of discharges also support the supposition.

1. INTRODUCTION

OUR knowledge of the mechanism of the glow discharge has not been advanced greatly, partly because the fundamental processes are only in a small part quantitatively known, and partly because of mathematical difficulties[1–4] which arise in the description of the observed phenomena of the discharge. But it has been established that, in order to maintain a self-sustained electrical discharge, the electrons generated in the cathode region are mainly due to the γ-process, which gives electron liberation at the cathode by positive ion impact.[5–8] These electrons are accelerated in the cathode fall space and move with nearly a homogeneous velocity towards the anode.[9] Of course, most of the primary electrons are scattered in their paths and retarded by collisions with gas molecules. The light emission in the negative glow is probably due to the result of the excitation of the gas molecules by these fast electrons entering this section of discharge from the Crookes dark space.

Probe measurements[10–11] indicate that fast electrons with energies of the order of that obtained by passing through the cathode fall space are present in the Faraday dark space and sometimes in the positive column and that they are distributed according to the Maxwell-Boltzmann law. Some authors,[10,12] however, suspect that the primary electrons from the cathode dark space are able to penetrate far into the negative glow or even into the Faraday dark space, and it was suggested that these electrons are formed by some mechanism of the converse of ionization by collision, when a system of two slow electrons and one positive ion pass into a unit consisting of an excited molecule and a single fast electron. In a neon glow discharge Druyvesteyn[13] has observed spark lines with high excitation energies, which proves that electrons exist with an energy corresponding to more than 80 percent of the cathode fall. But the concentration of these electrons could not be determined. A direct determination of the energy of the electrons[14–15] showed that for a cathode fall above 400 volts, most electrons in

[1] P. M. Morse, Phys. Rev. **31**, 1003 (1928).
[2] J. J. Thomson, Phil. Mag. **8**, 393 (1929).
[3] W. Rogowski, Archiv. f. Elektrotechnik **26**, 643 (1932).
[4] W. Weizel, R. Rompe, and M. Schon, Zeits. f. Physik **112**, 339 (1939); **113**, 87 and 730 (1939).
[5] H. A. Wilson, Phys. Rev. **8**, 227 (1916).
[6] A. K. Brewer and R. R. Miller, Phys. Rev. **42**, 786 (1932).
[7] L. B. Loeb, Rev. Mod. Phys. **8**, 267 (1936).
[8] M. J. Druyvesteyn and F. M. Penning, Rev. Mod. Phys. **12**, 87 (1940); also references given there.
[9] J. J. Thomson, Phil. Mag. **48**, 4 (1924).
[10] K. G. Emeleus and W. L. Brown, Phil. Mag. **7**, 17 (1929).
[11] K. G. Emeleus, W. L. Brown, and H. M. Cowan, Phil. Mag. **17**, 146 (1934).
[12] K. G. Emeleus and O. S. Duffendack, Phys. Rev. **47**, 460 (1934).
[13] M. J. Druyvesteyn, Zeits. f. Physik **62**, 764 (1930); Physica, **1**, 427 (1934).
[14] A. K. Brewer and J. W. Westhaver, J. App. Phys. **8**, 779 (1937).
[15] J. F. Lehmann, Proc. Roy. Soc. **A115**, 624 (1927).

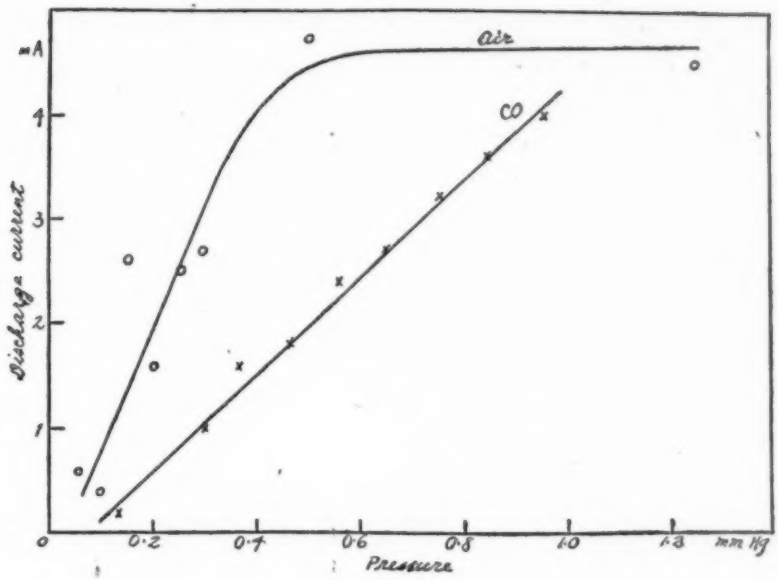

FIG. 1. Variation of tube current with gas pressure.

the negative glow had an energy which was almost equal to the cathode fall. Determinations of this kind, however, are not very reliable as a third electrode which disturbs the discharge must be brought into the negative glow. In the present investigation it is attempted to show the existence, in the transition region from negative glow to the Faraday dark space, of primary electrons coming from the cathode dark space. Probe measurements have been made in the positive column and in the Faraday dark space when the gas pressures in the discharges were varied. Different current-voltage characteristic curves in these two regions have been found. Theoretical interpretations of these different characteristics could be obtained either from Langmuir's theory[16–17] of probe or from Druyvesteyn's theory[18] of electron energy distribution by assuming the existence in the boundary between negative glow and Faraday dark space of a drift fast electron stream superimposed upon an isotropic slow electron distribution. Spectroscopic investigations of the bands of the neutral and the ionic molecules of N_2 and CO in different sections of discharges also support the supposition.

[16] I. Langmuir, Phys. Rev. **26**, 585 (1925).
[17] H. M. Mott-Smith and I. Langmuir, Phys. Rev. **28**, 727 (1926).
[18] M. J. Druyvesteyn, Zeits. f. Physik **64**, 781 (1930); Physica **10**, 69 (1930).

2. APPARATUS

The form of the discharge tube used was cylindrical, 2 cm in diameter and 10 cm in length with two aluminum disk electrodes of 1.2 cm diameter sealed through a CR lead-in wire coaxially on each end of the tube at a separation of about 7 cm. The probe was a 6-mil tungsten wire 6 mm long and spot-welded to a lead-in wire mounted in a small glass tube fused perpendicularly to the discharge tube at a distance of about 1.5 cm from one of the disk electrodes. The discharge tube was sealed by means of a side-tube on to the vacuum system made of soft glass tubings, and pumped by a Cenco steel mercury diffusion pump backed by an oil pump. The pressures in the tube were measured by two McLeod gauges for different ranges. The discharge tube and electrodes were degassed by running a discharge with an induction coil and pumping out alternatively over days.

The gases used were dry air and carbon monoxide. The latter was generated by heating oxalic acid in the presence of concentrated sulfuric acid, carbon dioxide gas and water vapor being removed by lime water and anhydrous phosphorus pentoxide, respectively. Before being employed to take readings the vacuum system and tube were flushed a few times with the gases. Because the gas pressure was not too low and the discharge temperature was not more than 35°C, it

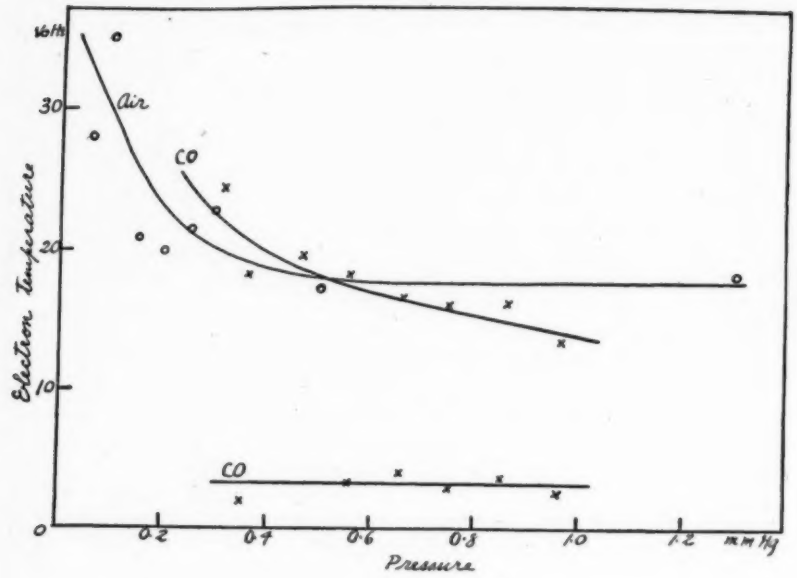

FIG. 2. Variation of electron temperature with pressure. Upper curves, fast group; bottom curves, slow group.

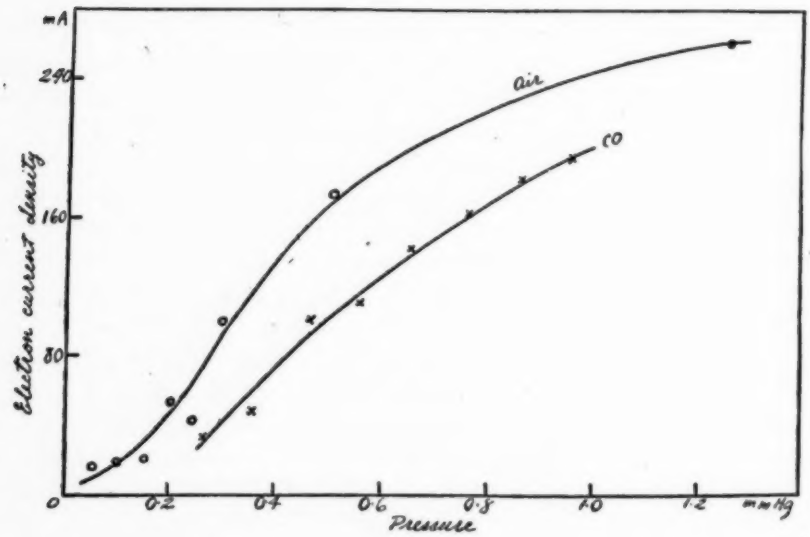

FIG. 3. Variation of electron current density with pressure.

was thought not worth while to use liquid air to remove any residual mercury vapor in the tube although traps were provided on the vacuum system.

The discharge was excited by a 500-volt rectifier stabilized by neon bulbs, with one of the electrodes grounded. The wiring in the probe circuit was arranged in the usual way. The potential of the probe was varied and the current-voltage characteristic values were obtained by means of a microammeter in combination with a universal shunt so that the current could be measured conveniently from a few microamperes to a few milliamperes.

3. EXPERIMENTAL RESULTS

In the gas pressure range between 0.06 and 1.2 mm Hg with a potential of 500 volts applied across the discharge tube, the tube current was a few milliamperes and so the discharge was probably of the normal glow type. On the anode side two or three striations could usually be observed. They were particularly sharp in the case of carbon monoxide gas. As the gas pressure was increased in the above-mentioned range, the discharge current increased linearly in the case of CO, but for air after 0.5 mm Hg the current seemed to approach a constant value as shown in Fig. 1.

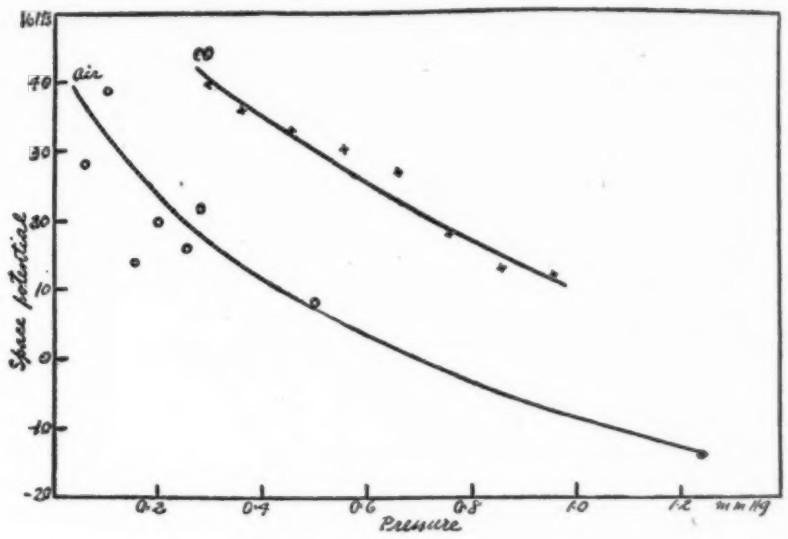

FIG. 4. Variation of space potential with pressure.

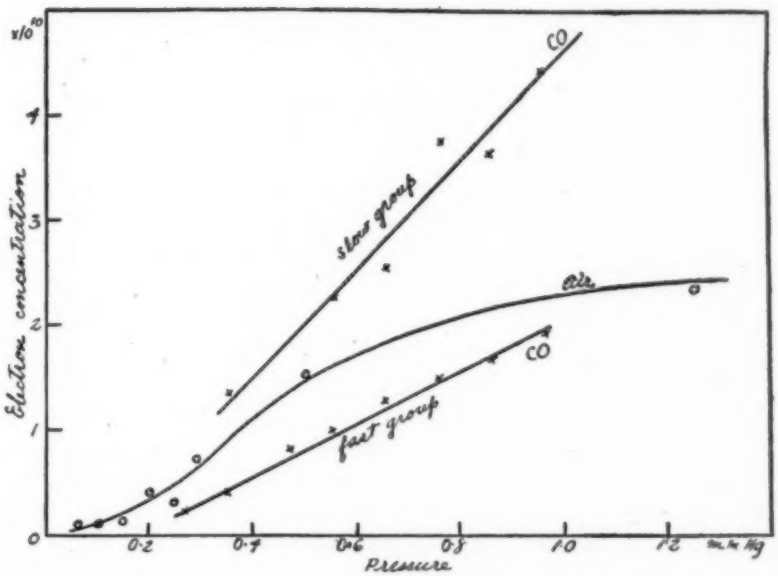

FIG. 5. Variation of electron concentration with pressure.

When the probe was at a very negative potential with respect to the anode, only a positive ion current was recorded. By decreasing the retarding potential the positive ion current at first diminished linearly and then rather rapidly, because some electrons of higher velocities were able to penetrate through the ion sheath around the probe and then were collected by the latter. As the retarding field was made still weaker, electrons of lower velocities could also be collected by the probe. Then an electron current became appreciable and continuously increased until one came to a point where the potential of the probe was the same as that of the surrounding ionized gas. In analyzing the characteristic data, a large scale plot of positive ion current *versus* probe potential was made. The extrapolation of the straight line tangent to the ion current to the smaller negative voltages gave the contribution of the positive ions to the current, and the electron current could then be obtained from the difference between this and the total observed current at that potential. In the regions of the positive column and the Faraday dark space near the anode side in the discharge, typical semi-logarithmic plots of electron current against retarding potentials are similar to the *B* curves in Figs. 6 and 7.

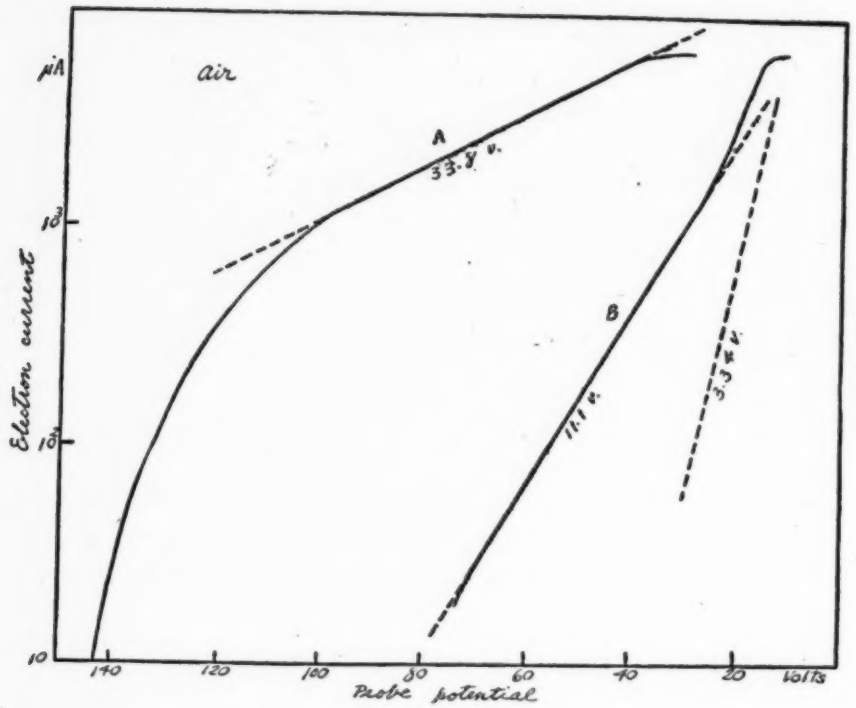

FIG. 6. Current-voltage characteristics in air discharge at a gas pressure 1.25 mm Hg, tube voltage 490 volts, tube current 4.5 ma. Curve *A* in Faraday dark space, curve *B* in positive column.

If the velocities of the electrons were described by a Maxwell-Boltzmann distribution, the semi-logarithmic plot would be, according to the probe theory of Langmuir and Mott-Smith,[19] a straight line, of which the slope determined a temperature corresponding to the electron velocities. At higher retarding potentials the observed deviation from linearity indicates that the distribution of electron velocities in the discharge must be rather complicated. However, one might assume that there existed more than one group of electrons, each of which was distributed according to Maxwell's law. The slope of the straight line drawn along the higher retarding potential characteristic curve gave the temperature of the fast electron group, and the slope of another straight line determined from the differences between the extrapolation of the first straight line and the observed values gave the temperature of the slow electron group. Sometimes a third electron group was observed. In the case of a discharge in CO, the second group came out quite definitely and was analyzed. In the case of air, the presence of the second group was revealed only at higher pressures.

[19] I. Langmuir and H. M. Mott-Smith, Gen. Elec. Rev. **27**, 449, 538, 616, 762, and 810 (1924).

Figure 2 gives the data obtained for the variation of the electron temperature with pressure. For the fast group, electron temperatures decrease strongly when the pressure was increased, while for the slow group, the electron temperature is independent of the pressure.

Figure 3 shows the data for the variation of the electron current density with pressure.

Figure 4 presents data for the change of space potentials at a point in the discharge when the pressure was increased.

Electron concentrations in the ionized gas can be calculated from the relation

$$n=(I/e)(2\pi m/kT)^{\frac{1}{2}},$$

where e and m are the charge and mass of the electron respectively, k is the Boltzmann constant, I is the electron current density, and T is the electron temperature. The results of the calculation are plotted in Fig. 5.

Figures 6 and 7 are the current-voltage characteristic curves in air and CO respectively for discharges in the Faraday dark space near the boundary with the negative glow (curves *A*) and in the positive column (curves *B*). These two regions yielded quite different characteristic curves. Near the space potential on the charac-

teristics we had a straight line portion in the Faraday dark space, which determined a temperature if the part of the characteristic at the higher retarding potentials was neglected. In the case of air at a pressure of 1.25 mm Hg this determined temperature is higher than the temperature of the fast group in the positive column, while in CO at a pressure of 0.87 mm Hg the determined temperature is lower than that in the positive column.

4. INTERPRETATION OF THE VARIATION OF ELECTRON TEMPERATURES AND SPACE POTENTIALS WITH PRESSURE

The observation of the decrease of electron temperature with pressure is quite similar to the measurements of Seelinger and Hirchert[20] in the positive column of neon and argon discharges, of Groos[21] in argon, and of Klarfeld[22] in mercury. As the pressure increases, there are more chances for the electrons to impact with gas molecules and consequently the mean kinetic energy of electrons will be diminished because of energy loss. Hence the electron temperature decreases. The slow electrons are formed from primaries after being scattered and retarded by numerous collisions with gaseous molecules. Since these ultimate electrons have already suffered many elastic impacts, further change of pressure will not probably influence their mean kinetic energy. Thus the slow electron temperature keeps constant with pressure variation.

By comparing the values given in Fig. 2 with that in Fig. 4 for any given gas pressure, one finds that the electron temperatures decrease with space potential, because in weaker fields electrons gain lower energy. This is in agreement with the observations of Duffendack and Chao[23] who found that electron temperature diminishes as one goes from cathode to anode in a nitrogen glow discharge.

5. TRANSLATIONAL AND RANDOM ELECTRON VELOCITIES

The difference of the volt-ampere characteristic curves obtained at the junction of the Faraday dark space with the negative glow and in the positive column does not seem to be explained by merely dividing electrons into isotropic Maxwellian groups, because it is not reasonable to neglect the electron current for higher retarding potentials in the characteristic curve from the dark space. These characteristics, which are concave downwards for a considerable part in higher retarding potentials, are different from the anomalous curves discussed by Emeleus and Brown,[24] and must be due to some causes other than positive space charges.

Let us assume that the resultant velocity distribution of the electrons near the Faraday dark space can be analyzed into a part with uniform translational motion and a superposed Maxwellian part with temperature motion, and that the velocities due to isotropic temperature motion are small compared to those of transla-

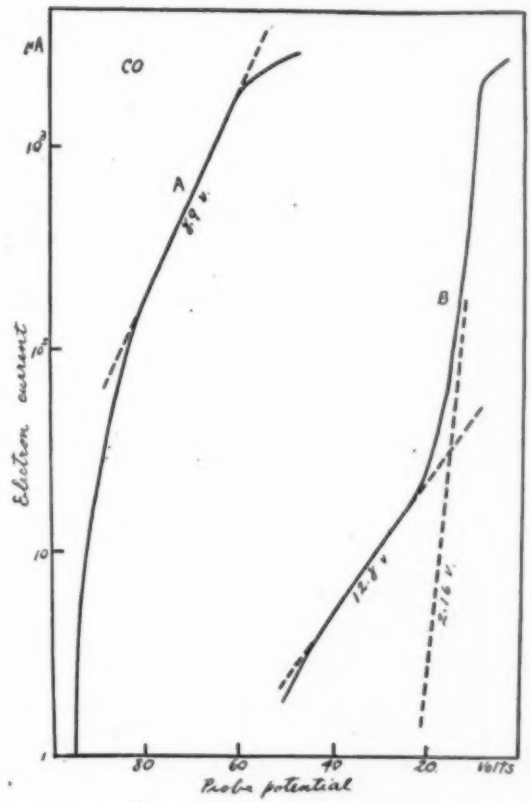

FIG. 7. Current voltage characteristics in CO discharge at a gas pressure 0.87 mm Hg, tube voltage 520 volts, tube current 3.4 ma. Curve *A* in Faraday dark space, curve *B* in positive column.

[20] R. Seelinger and R. Hirchert, Ann. d. Physik **11**, 817 (1931).
[21] O. Groos, Zeits. f. Physik **88**, 741 (1934).
[22] B. Klarfeld, Tech. Phys. USSR **4**, 44 (1937); **5**, 725 and 919 (1938).
[23] O. S. Duffendack and K. T. Chao, Phys. Rev. **56**, 176 (1939).
[24] K. G. Emeleus and W. L. Brown, Phil. Mag. **22**, 898 (1936).

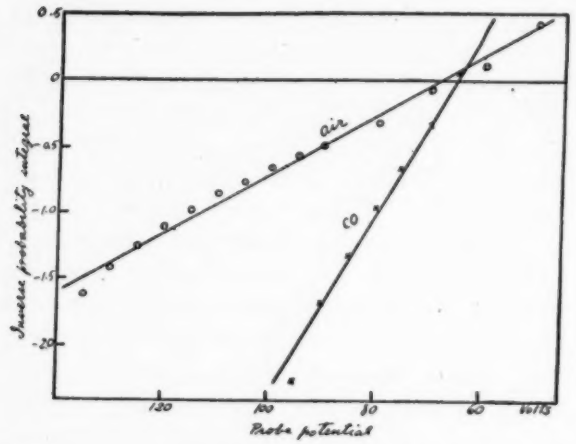

FIG. 8. Inverse probability integral against probe potential.

tion. The theory of the current to a cylindrical probe with its axis perpendicular to the direction of a stream of the drift electrons superimposed on a Maxwellian distribution has been treated by Mott-Smith and Langmuir,[17] and the result is expressed in a quite complicated series. However, in the region where the retarding potential of the probe is less than the equivalent voltage of the drift electrons, the volt-ampere characteristic of a cylindrical probe is nearly the same as that of a plane probe placed perpendicularly to the direction of the drift velocities. Langmuir[16,25] has shown that if I_0 is the current when all the electrons are collected by the probe, the electron current on the probe is given by

$$I=(I_0/2)[1+P(-\lambda)], \tag{1}$$

where $P(-\lambda)$ stands for the probability integral

$$P(-\lambda)=(2/\sqrt{\pi})\int_0^{-\lambda}\exp(-x^2)dx. \tag{2}$$

Here λ is proportional to the difference of the velocity of the electron in the mass-motion and the velocity component of any considered electron in the same direction, or defined by the relation

$$\lambda=(\sqrt{V_t}-\sqrt{V_p})/\sqrt{V_M}. \tag{3}$$

Here V_p is the retarding potential of the probe with respect to the ionized gas (or the sum of the potential of the probe with respect to the ionized gas and of the space potential), V_t is the potential corresponding to the drift velocity of the primary electrons, and V_M is the potential corresponding to the temperature motion. If V_t and V_p are not too far from each other, the geometrical mean $(V_tV_p)^{\frac{1}{2}}$ can be replaced by the arithmetical mean $\frac{1}{2}(V_t+V_p)$. Equation (3) becomes

$$\lambda=(V_t/V_M)^{\frac{1}{2}}-\left[\frac{(V_t+V_p)}{(2(V_tV_M)^{\frac{1}{2}})}\right].$$

Thus λ is a linear function of the probe potential. From Eq. (1) and Eq. (2) we have

$$P^{-1}((2I-I_0)/I_0)=\text{constant}+V_p/2(V_tV_M)^{\frac{1}{2}}. \tag{4}$$

If the plot of the inverse probability integral against the probe potential is a straight line, the supposition of the existence of the superposition of the drift electrons upon a Maxwellian group is confirmed. The intersection of the straight line with the zero line determines the average energy of the drift electrons and the slope gives that of the random electrons. Figure 8 is such a plot from Eq. (4), and the results show that the observed values fall fairly well on straight lines and thus the experiments justify our separation of the electrons into translational and random parts.

In the case of air the straight line intersects the zero line at 68 volts.[26] This is the average energy of the electron beam, while the value directly determined from the curve A in Fig. 6 is only 50.7 volts, since in the latter method of determination the higher energy electrons have been neglected. From the slope of the straight line we have

$$2(V_tV_M)^{\frac{1}{2}}=44.8. \tag{5}$$

The cathode fall potential was not measured, and the fastest electrons that were collected by the probe have an energy about 102 volts, which could not be accurately determined. If this value is taken as the energy of the electron beam, from Eq. (5) we have $V_M=4.93$ volts, which determines the temperature assigned to the random electrons. In the positive column the slow electrons have a temperature corresponding to 3.34 volts. Thus these two methods give about the same value of temperature for the slow electrons.

In the case of CO, the determined average

[25] I. Langmuir, Zeits. f. Physik **46**, 271 (1928).

[26] The value thus determined may not be very accurate because of use of the theory of current-voltage characteristics for a plane collector.

energy of the drift electrons is 65 volts and the directly measured value from curve A in Fig. 7 is only 13.4 volts. The energy of the fastest electrons that reach the probe is 35 volts, while the average energy is 65 volts, so the primary electrons can not have energies less than this. If $V_i=65$ volts and $2(V_iV_p)^{\frac{1}{2}}=15.2$, one finds $V_M=0.89$ volt. In the positive column the slow electrons have a temperature of 2.16 volts, which is a little higher.

6. ENERGY DISTRIBUTION OF ELECTRONS IN POSITIVE COLUMN AND IN FARADAY DARK SPACE

If it is assumed that an electron with a given velocity has angles of incidence upon the surface of the sheath of the probe less than a limiting value determined by the retarding potential, the energy distribution of the electrons can be derived. Druyvesteyn[18] has obtained a distribution function in the form

$$\rho\left[\frac{2e(V_g-V_p)}{m}\right]^{\frac{1}{2}}=\frac{4m}{e^2A}(V_g-V_p)\frac{d^2i}{dV_p^2},$$

where e and m are the charge and mass of the electron, A the surface area of the probe, i the electron current, and V_g and V_p are the gas and probe potentials respectively. Hence the measurement of the curvature of the current-voltage characteristics will yield the distribution function. The double differentiation from the characteristic curve, however, presents difficulties due to inevitable slight experimental errors. To simplify the operation of the double differentiation, Sloane and Emeleus,[27] by making use of a mathematical identity, have obtained a modified formula

$$\rho\left[\frac{2e(V_g-V_p)}{m}\right]^{\frac{1}{2}}=\frac{4m_i}{e^2A}(V_g-V_p)\left[\left(\frac{d\log i}{dV_p}\right)^2+\frac{d^2\log i}{dV_p^2}\right]. \quad (6)$$

In a semi-logarithmic plot the current-voltage characteristic is straightened and the determination of the second derivative is much facilitated. In the case where the semi-logarithmic plot has a linear portion, the second derivative of log i with respect to V_p vanishes, while the first derivative is a constant.

Curves B and A in Figs. 9 and 10 are the distribution functions of electrons calculated from Eq. (6) in the positive column and in the Faraday dark space respectively. In the positive column of

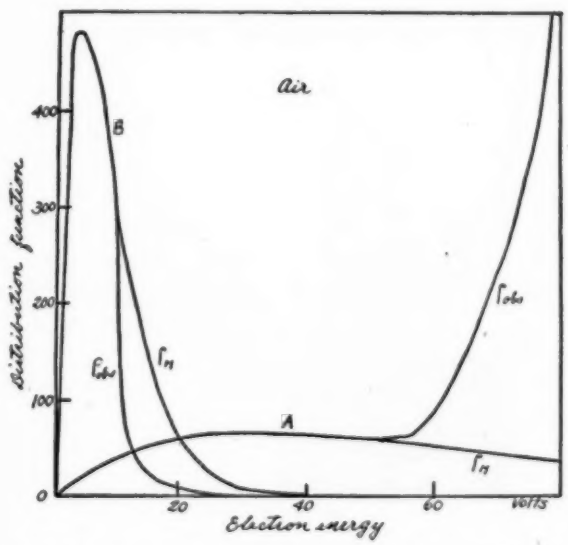

FIG. 9. Observed electron energy distributions compared with Maxwellian distributions. Curve A for Faraday dark space, curve B for positive column.

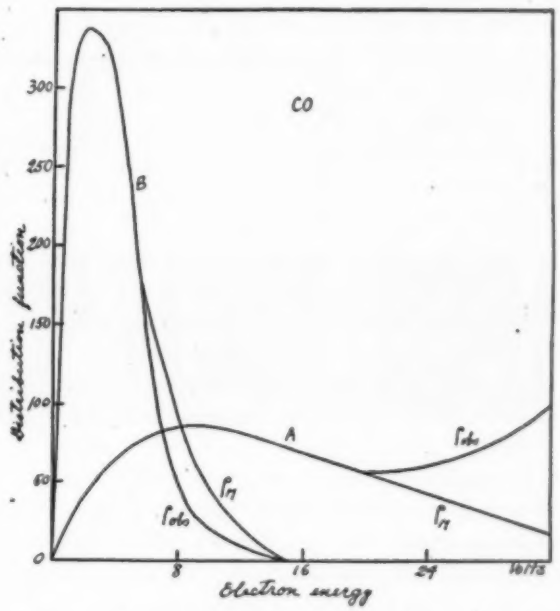

FIG. 10. Observed electron energy distributions compared with Maxwellian distributions. Curve A for Faraday dark space, Curve B for positive column.

[27] R. H. Sloane and K. G. Emeleus, Phys. Rev. **44**, 333 (1933).

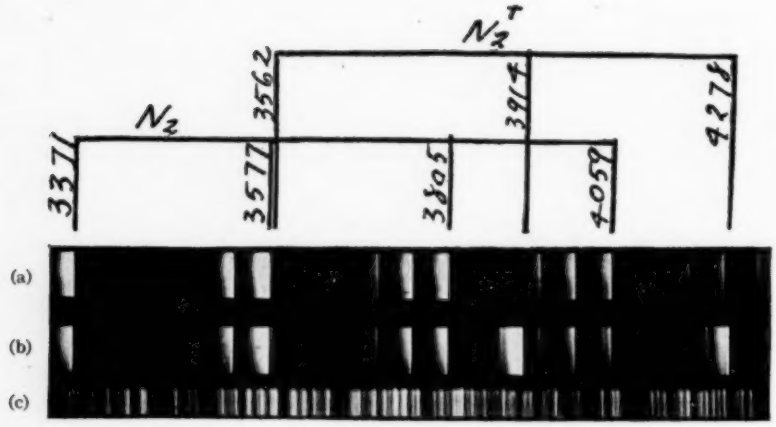

FIG. 11. Spectrogram in air discharge. (a) in positive column, (b) in negative glow, (c) Fe arc.

air discharge, the number of electrons observed with energy greater than 10 volts is less than that calculated from a Maxwellian distribution. Similarly in the CO discharge, for energies greater than 6 volts, the observed and calculated distribution functions begin to diverge. These observations are similar to those of Druyvesteyn,[18] and of Sloane and Emeleus[27] in the positive column of low voltage arcs in neon and argon. The observed number of electrons with about 14 volts in air or with about 11 volts in CO is particularly smaller probably because the energies of those electrons have been used up to excite the N_2 or CO molecules, whose observed excitation potentials[28] have values mostly less than those voltages.

In the Faraday dark space the distribution functions have a quite different form. For higher energies the number of electrons observed is so large that the Maxwellian distribution is negligible. These large values correspond to the points in the semi-logarithmic plot, where the portion of the curve has a curvature concave to the axis of voltage. The results of the distribution plot again show that in this section of discharge a fast electron stream is superimposed upon a small random electron distribution. The presence of this fast electron stream is of particular interest in the consideration of the excitation of molecular spectra in electrical discharges.

7. ELECTRON ENERGIES AND MOLECULAR SPECTRA

In order to get some information about the collisions of electrons with gas molecules, spectroscopic studies were made on the regions of the negative glow near the Faraday dark space and the positive column in air and CO discharges. An image of the positive column in air was focused by means of a condensing lens on the slit of a Hilger E-1 spectrograph. The second positive bands of N_2 are very intense on the photographs taken with Eastman Kodak plates at an exposure of about 70 minutes. When the negative glow was thrown close to the slit, the first negative bands of N_2^+ are relatively stronger than the positive bands at an exposure of about 40 minutes, both bands being on the same plate in this spectral region as shown in Fig. 11. The excitation potential for bands of the second positive system is 13 volts and the simultaneous ionization and excitation of the first negative system require 19.6 volts.[29] In the positive column the fast

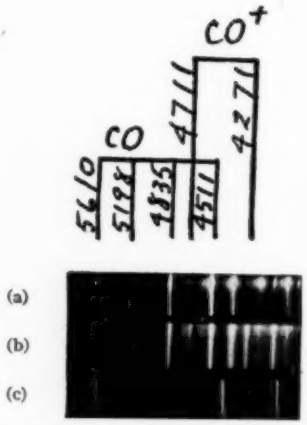

FIG. 12. Spectrogram in CO discharge (a) in positive column, (b) in negative glow, (c) Hg arc.

[28] W. Jevons, *Report on Band Spectra of Diatomic Molecules*, pp. 78–82 (1932).

[29] Recent studies of the excitation of N_2 and N_2^+ bands have been published in two papers by R. Bernard and R. C. Pankhurst, Science Abstracts **43**, 917 (1941). These papers, however, are not available here.

electron group has an average energy of 16.6 volts which is sufficient to excite the positive bands but not the negative ones. The negative bands can be easily excited in the negative glow by the fast electrons whose average energy measured is 68 volts. This seems to explain the different appearence of the spectra in these two regions.

In case of CO a Hilger E-2 spectrograph happened to be employed to take pictures of the emission from the positive column and the negative glow. The spectrograms also show some difference in these two regions as seen in Fig. 12. The Angstrom bands of CO on both spectrograms are strong, but few of the comet-tail bands[30–31] of CO^+ come to appear in the negative glow. Probably some of the Baldet-Johnson bands are also present. The excitation potential of the Angstrom bands is 10.7 volts, while that for the comet-tail bands is 16.7 volts. In the positive column the fast electrons have an energy of 19.2 volts, but in the region of transition from negative glow to Faraday dark space they have 65 volts. It is obvious that the molecular ions are easily excited in the negative glow. That much higher energies are used to excite the bands of the molecular ions than that needed for the simultaneous ionization and excitation, is because of the probability of excitation. Experimental investigations of the electron-impact excitation function of the negative bands of N_2^+ and the comet-tail bands of CO^+ have been reported by many people.[32–34] The conclusion is that the excitation functions for N_2^+ and CO^+ molecules behave in a quite similar manner and both functions have a maximum at a potential about 2.5 times the value of the excitation potential. The fact could be explained that though the excitation potential of CO^+ bands (16.7 volts) is less than that of N_2^+ bands (19.6 volts), about the same amount of the electron energies is required to excite these bands.

The authors wish to thank Mr. C. C. Yang who built a part of the vacuum system and Messrs L. Yang and F. S. Li of the Chemistry Department who helped to produce the carbon monoxide gas.

[30] T. R. Merton and R. C. Johnson, Proc. Roy. Soc. **A103**, 383 (1923).
[31] R. C. Johnson, Proc. Roy. Soc. **A108**, 355 (1925).
[32] A. E. Lindh, Zeits. f. Physik **67**, 67 (1931).
[33] R. Bernard, Comptes rendus **204**, 488 (1937).
[34] F. P. Bundy, Phys. Rev. **52**, 698 (1937).

PHYSICAL REVIEW VOLUME 68, NUMBERS 1 AND 2 JULY 1 AND 15, 1945

Correction of G-M Counter Data

J. D. KURBATOV AND H. B. MANN
The Ohio State University, Columbus, Ohio

(Received June 4, 1945)

It has been shown that the mean number $B(T)$ of discharges during any time T is given by

$$B(T)=\int_0^T[1-p(t)]a(t)dt,$$

where $a(t)$ is the total density of radiation penetrating the tube at the time t and $p(t)$ is the solution of the integral equation:

$$p(t)=\int_{t-\tau}^{t}[1-p(x)]a(x)d(x)$$

for $t>\tau$ and $p(t)=1-e^{-at}$ for $0\leqslant t\leqslant\tau$. $B(t)$ is explicitly obtained for the case that $a(t)$ is constant. In this case it is also shown that

$$aT=\frac{B(T)-\eta}{1-[B(T)-\eta]\frac{\tau}{T}},\quad |\eta|\leqslant\frac{(a\tau)^2}{1-(a\tau)^2}\quad\text{for}\quad a\tau<1.$$

INTRODUCTION

THE errors in data obtained with G-M counter tubes, due to their finite resolving time have been subjected to mathematical analysis by several authors.

In the past the expression $n=n_0\exp[-n_0\tau/T]$ has been derived for correction of the number of discharges "n" obtained in time T with regard to the total number of particles n_0 penetrating a G-M counter tube and capable of producing discharges.[1]

For this derivation it was assumed that in order for a counter to register a particle, that particle should be preceded by a certain small time interval τ during which no particle arrives at the counter.

Most recently this simplified model was refined. It was assumed that a particle would produce a discharge at time $(t+dt)$ even if any number of particles arrived in the G-M counter tube during the time $(t-\tau, t)$ provided, however, that these particles did not produce a discharge.

The complete expression derived according to the second model for the number of particles missed is too complicated for practical use, especially if T is very large compared with τ, as it usually is. Consequently an asymptotic expression for the evaluation of particles missed was proposed by the same author.[2]

$$A(t)\cong n_0-n\cong n_0^2\tau/(t+n_0\tau).$$

In addition the probability that m discharges will be produced in the G-M tube during the time T was derived on the basis that the probability of an electron passing through the tube in the time $(t, t+dt)$ is given by $a(t)dt$. The mean value and the variance of this probability distribution likewise were given.

In the present paper it will be shown, with the second model, that the mean number of discharges, during the time T, can be obtained from the solution of an integral equation. The special case when $a(t)$ is constant is treated, and an expression for the expected number of discharges is obtained for this case, which is somewhat simpler than the one previously derived.[2]

COMPUTATION OF THE EXPECTED NUMBER OF DISCHARGES

Let $p(t)$ be the probability that a discharge will take place in the interval $(t-\tau, t)$. Let $a(t)dt$ be the probability that an electron passes through the tube during the interval $(t, t+dt)$. The fact that $p(t)$ is a continous function of t is used here but its proof is postponed. In order that a discharge take place, it is necessary and sufficient that:

[1] L. I. Schiff, Phys. Rev. **50**, 88 (1936).

[2] B. V. Gnedenko, J. Exper. Theor. Phys. U.S.S.R. **11**, 101 (1941).

1. An electron passes through the tube in the time interval $(t, t+dt)$.

2. No discharge takes place in the time interval $(t-\tau, t)$.

Since 1 and 2 are independent events, the probability of one discharge in the time dt becomes $[1-p(t)]a(t)dt$.

Then, since only one discharge can occur in the interval $(t-\tau, t)$, the probability of one discharge in that interval is

$$\int_{t-\tau}^{t}[1-p(x)]a(x)dx.$$

But this is just $p(t)$.

Hence we obtain the integral equation

$$p(t)=\int_{t-\tau}^{t}[1-p(x)]a(x)dx. \tag{1}$$

Putting

$$1-p(x)=q(x),$$

we then obtain

$$q(t)=1-\int_{t-\tau}^{t}q(x)a(x)dx. \tag{2}$$

For $0\leqslant t\leqslant\tau$;

$$q(t)=\exp\left[-\int_{0}^{t}a(x)dx\right].$$

Equation (2) may also be written in the form

$$q'(t)=q(t-\tau)a(t-\tau)-q(t)a(t). \tag{3}$$

Let $p(t)=1-q(t)$ be a solution of (1). The expected number $B(t)$ of discharges in the time t is then given by

$$B(t)=\int_{0}^{t}[1-p(x)]a(x)dx. \tag{4}$$

If $t=s\tau+\tau'$ with $\tau'<\tau$, we may on account of 1 write

$$B(t)=\sum_{\alpha=1}^{\alpha=s}p(\alpha\tau)+\int_{s\tau}^{s\tau+\tau'}[1-p(x)]a(x)dx. \tag{5}$$

This reduces the problem to the solution of the integral Eq. (1).

If $a(t)=a$ independent of t, then Eq. (3) reads

$$q'(t)=aq(t-\tau)-aq(t). \tag{3'}$$

It is easy to see that Eq. (3') together with the initial condition $q(t)=e^{-at}$ for $0\leqslant t\leqslant\tau$ determine completely the solution of Eq. (3'). This solution is easily found as

$$q(t)=\sum_{i=0}^{i=\alpha}\frac{a^i(t-i\tau)^i}{i!}e^{-a(t-i\tau)}$$

$$\text{for } \alpha\tau\leqslant t\leqslant(\alpha+1)\tau. \tag{6}$$

Hence, if s is the largest integer smaller then t/τ,

$$p(t)=1-\sum_{i=0}^{i=\alpha}\frac{a^i(t-i\tau)^i}{i!}e^{-a(t-i\tau)} \text{ for } \alpha\tau\leqslant t\leqslant(\alpha+1)\tau,$$

$$\begin{aligned}B(t)&=\sum_{\alpha=1}^{\alpha=s}p(\alpha\tau)+a\int_{s\tau}^{t}[1-p(x)]dx\\&=s-\sum_{\alpha=1}^{\alpha=s}\sum_{i=0}^{i=\alpha-1}\frac{a^i\tau^i(\alpha-i)^i}{i!}e^{-a\tau(\alpha-i)}\\&\quad+a\int_{s\tau}^{t}\sum_{i=0}^{i=s}\frac{a^i(x-i\tau)^i}{i!}e^{-a(x-i\tau)}dx\\&=s-\sum_{i=0}^{i=s-1}\frac{a^i\tau^i}{i!}\sum_{\beta=1}^{\beta=s-i}\beta^ie^{-a\beta\tau}\\&\quad+a\int_{s\tau}^{t}\sum_{i=0}^{i=s}\frac{a^i(x-i\tau)^i}{i!}e^{-a(x-i\tau)}dx.\end{aligned} \tag{7}$$

The number $A(t)$ of particles which fail to produce discharges has previously been computed.[2] Clearly $A(t)+B(t)=at$. It was found that

$$\begin{aligned}A(t)&=a\tau\sum_{k=1}^{k=s}\frac{a^k(t-k\tau)^k}{(k-1)!}e^{-a(t-k\tau)}\\&\quad+\sum_{k=1}^{k=s}a^{k+1}\int_{t-\tau}^{t}\left[t\frac{[t_k-(k-1)\tau]^{k-1}}{(k-1)!}\right.\\&\quad\left.-\frac{[t_k-(k-1)\tau]^k}{(k-1)!}\right]\\&\quad\times\exp\left(-a[t_k-(k-1)\tau]\right)dt_k\\&\quad+a^{s+2}\int_{s\tau}^{t}t\frac{(t_k-s\tau)^{s+1}}{s!}\exp\left[-a(t_k-s\tau)\right]dt_k.\end{aligned}$$

In using the value $B(t)$ which has been obtained in the present paper and the value for $A(t)$ above, one obtains as a side result an interesting identity from the relation $B(t)+A(t)=at$.

To justify the above solution, it is necessary to show that $p(t)$ is a continuous function of t. Now $p(t+\Delta t)-p(t)$ is certainly smaller in absolute value than the probability of a discharge taking place during $(t, t+\Delta t)$ plus the probability of a discharge taking place in the time $(t-\tau, t-\tau+\Delta t)$. The probability of a discharge taking place during any time is smaller than the probability of an electron passing through the tube during this time. Hence

$$|p(t+\Delta t)-pt| \leqslant \int_{t-\tau}^{t-\tau+\Delta t} a(x)dx+\int_{t}^{t+\Delta t} a(x)dx.$$

Hence $p(t)$ is continuous if

$$\int_{t}^{t+\Delta t} a(x)dx$$

exists for all t.

Formula 7 is hard to evaluate if S is large, as is usually the case in practical applications. For this case the asymptotic formula

$$n_0=n/(1-n\tau/t), \tag{8}$$

has been derived, where n_0 is the number of electrons passing through the counter and n the number of discharges during the time t. In this derivation it was assumed without proof that $p(t)$ converges to a constant.[2]

In the following a proof will be given for Eq. (8), for the case $a\tau<1$, and also an estimate for the error committed in using Eq. (8) for finite t. In the following, it will therefore be assumed that $a\tau<1$. The inequality $a\tau<1$ holds true in almost all practical applications, since τ is of the order 10^{-4}, and $a\tau$ is the mean value of the number of particles in the time interval τ.[3,4]

Putting

$$p(t)=\frac{a\tau}{1+a\tau}+\epsilon(t),$$

then on account of (1) we have

$$\epsilon(t)=-a\int_{t-\tau}^{t}\epsilon(x)dx \qquad \text{for } t\geqslant\tau,$$
$$\epsilon(t)=1-e^{-at}-\frac{a\tau}{1+a\tau} \quad \text{for } 0\leqslant t\leqslant\tau; \tag{9}$$

and

$$|\epsilon(t)|\leqslant\frac{a\tau}{1+a\tau} \quad \text{for } 0\leqslant t\leqslant\tau,$$
$$|\epsilon(t)|\leqslant 1 \qquad \text{for all } t. \tag{10}$$

Applying the mean value theorem repeatedly, we have from Eq. (9)

$$\epsilon(t)=-a\tau\epsilon(t-\theta\tau)=\cdots$$
$$=(-a\tau)^{\alpha}\epsilon(t-\alpha\theta'\tau), \quad 0\leqslant\theta\leqslant 1, \quad 0\leqslant\theta'\leqslant 1; \tag{11}$$

for

$$\alpha\tau\leqslant t\leqslant(\alpha+1)\tau.$$

If $t-\alpha\theta'\tau$ is not yet in the first τ interval, the process may be continued. If $\epsilon(t)$ is different from 0, we must on account of $|\epsilon(t)|\leqslant 1$, $a\tau<1$ finally obtain an equation of the form

$$\epsilon(t)=(-a\tau)^{h}\epsilon(t') \quad \text{with } 0\leqslant t'\leqslant\tau,\ h\geqslant\alpha.$$

Hence on account of the relations (10)

$$|\epsilon(t)|\leqslant\frac{(a\tau)^{\alpha+1}}{1+a\tau} \quad \text{for } \alpha\tau\leqslant t\leqslant(\alpha+1)\tau. \tag{12}$$

For the integral in Eq. (7) we have

$$a\int_{s\tau}^{t}[1-p(t)]dt=\frac{a(t-s\tau)}{1+a\tau}+\delta \tag{13}$$

where

$$|\delta|\leqslant\frac{(a\tau)^{s+2}}{1+a\tau}.$$

From Eqs. (7), (12), and (13) we have

$$B(t)=\frac{at}{1+a\tau}+\eta,$$
$$|\eta|\leqslant\frac{(a\tau)^2}{1-(a\tau)^2}[1-(a\tau)^{s+1}]. \tag{14}$$

The term η is very small even if $a\tau$ is close to 1. Thus, for instance, if $a\tau=0.95$ from (14), $|\eta|\leqslant 10$. Considering even that τ is in the neighborhood of 10^{-3} then a should be in the neighborhood of 10^3, and η is quite negligible indeed.[3,4]

If the intensity of radiation is increased indefinitely, then n must approach t/τ. Hence, τ may be found by increasing the intensity of radiation until n remains constant. If $\bar{n}$ is this limit value

[2] C. G. Montgomery and D. D. Montgomery, Phys. Rev. **57**, 1030 (1940); J. Frank. Inst. **231**, 447, 509 (1941).
[4] W. E. Ramsey, Phys. Rev. **57**, 1022 (1940).

of n, then

$$\tau = t/n. \tag{15}$$

Since for all practical purposes $B(t)=n$, $at=n_0$ there is obtained from Eq. (14)

$$n_0 = \frac{n-\eta}{1-(n-\eta)(\tau/t)}. \tag{16}$$

This is for all practical purposes equivalent to Eq. (8) as long as $a\tau$ is not very close to 1.

ACKNOWLEDGMENT

The grant of the Research Foundation of the Ohio State University and the support given by The Ohio State University Development Fund are greatly appreciated by the authors.

PHYSICAL REVIEW VOLUME 68, NUMBERS 1 AND 2 JULY 1 AND 15, 1945

Theory of Photoelectric Emission from Metals

H. Y. FAN
Radio Research Institute, National Tsing Hua University, Kumming, China

(Received May 18, 1945)

The theory of volume effect in photoelectric emission is developed. Formulae are derived for the rate of electron excitation and for the photoelectric yield. The calculated threshold frequencies for volume effect are 5.91×10^{14} and 5.69×10^{14} for sodium and potassium respectively. The estimated photoelectric yields for these metals are of the same order of magnitude as those calculated for surface effect and are comparable with those observed experimentally. The volume effect should not, therefore, be neglected except in the immediate neighborhood of the threshold frequency. Approxmate estimation indicates that light absorption of sodium and potassium in the visible and ultraviolet regions should be largely due to quantum excitation of electrons. Accurate calculation of electron excitation and absorption requires detailed knowledge of electron wave functions.

INTRODUCTION

THE theory of photoelectric emission from metals is usually based on Sommerfeld's model of free electrons for metals. Since a free electron cannot absorb the whole energy of a light quantum (the kind of absorption for photoelectric emission), it has been suggested that light absorption takes place only at the surface of the metal where the electrons are subject to the surface potential field. The phenomenon is then a surface effect.

Wentzel[1] takes into account the damping of the light wave and accredits it with enabling the free electrons in the metal to absorb the energies of the light quanta. In this picture light absorption takes place inside the metal and is a volume effect. It has, however, been shown by Bethe[2] that the order of magnitude of emission given by this picture is too small.

The free electron model is too crude. Actually the electrons in a solid are in a periodic potential field. They can therefore absorb energies of light quanta independent of the damping of the light wave. Tamm and Schubin[3] made a rough estimation of the frequency, at which emission due to such absorption should begin, showing that it is much higher than the ordinary threshold frequency. Thereupon volume effect is neglected in the subsequent developments of the theory of photoelectric emission. It is our purpose to investigate this volume effect due to the periodic potential field inside the metal.

DEVELOPMENT OF THE THEORY

The potential energy of an electron in the crystal lattice of a solid is periodic

$$V=\sum_g V_g e^{-2\pi i g\cdot r}. \tag{1}$$

The electron wave function is then of the form

$$\psi_k = e^{ik\cdot r}u_k(r),$$

[1] G. Wentzel, *Probleme der Modernen Physik* (Sommerfeld Festschrift), p. 79.
[2] H. Bethe, *Handbuch der Physik* 24/2, p. 472.
[3] I. Tamm and S. Schubin, Zeits. f. Physik 68, 97 (1931).

where $u_k(r)$ is a function having the same periodicity as the potential. Optical phenomena with such electrons have been discussed in many places.[4] Let the vector potential of the light wave in the metal be

$$A=A_\xi\cos 2\pi\nu\left(t-\frac{n\eta}{c}\right)=\tfrac{1}{2}[A_\xi\epsilon^{-2\pi i n\eta/c}\epsilon^{2\pi i\nu t}+A_\xi\epsilon^{2\pi i n\eta/c}\epsilon^{-2\pi i\nu t}].$$

The damping can be neglected, since within the thickness in which we are interested, the wave is not appreciably damped. The perturbation due to this light wave is $(eh/2\pi imc)A\cdot\nabla\Psi$. By using the method of variation of constants we get for an electron originally in the state k

$$a_{k,k'}=-\frac{eh}{4\pi imc}\left[\frac{\exp\frac{2\pi i}{h}(E_{k'}-E_k-h\nu)t-1}{E_{k'}-E_k-h\nu}C^+_{k,k'}+\frac{\exp\frac{2\pi i}{h}(E_{k'}-E_k+h\nu)t-1}{E_{k'}-E_k+h\nu}C^-_{k,k'}\right] \quad (2)$$

where

$$C^+_{k,k'}=\int\psi^*_{k'}A_\xi\epsilon^{2\pi i n\eta/c}\cdot\nabla\psi_k d\tau;$$

$$C^-_{k,k'}=\int\psi^*_{k'}A_\xi\epsilon^{-2\pi i n\eta/c}\cdot\nabla\psi_k d\tau.$$

As the wave-length of the light wave is much longer than that of the electron waves, we can neglect $2\pi n\eta/c$ compared with k and k', then

$$C^+_{k,k'}=C^-_{k,k'}=\alpha_\xi\int\psi^*_{k'}\frac{\partial\psi_k}{\partial\xi}d\tau$$

$$=\alpha_\xi\int\epsilon^{-i(k'-k)\cdot r}u^*_{k'}\frac{\partial u_k}{\partial\xi}d\tau=\alpha_\xi C_{k,k'}. \quad (3)$$

It has been pointed out by Kronig[5] that because of the periodic nature of the functions $u(r)$, this integral is zero unless

$$k'-k=2\pi g.$$

This gives definite relations between the original state and the excited states; the electron cannot be excited from one state into any arbitrary state.

[4] A. H. Wilson, *The Theory of Metals*, see references on p. 127.
[5] R. de L. Kronig, Proc. Roy. Soc. **A124**, 409 (1929).

The probability of excitation of an electron in state k is

$$\sum_g\frac{d}{dt}|a_{k,k+2\pi g}|^2$$

per unit time. The total rate of excitation, i.e., the total number of excited electrons per unit time, is

$$N=2\frac{\Omega}{8\pi^3}\sum_g\frac{d}{dt}\int\int\int|a_{k,k+2\pi g}|^2dk_xdk_ydk_z \quad (4)$$

where Ω is the volume of the metal. The integration is over all occupied states. At $T=0°$K the limits of integration are given by the surface of Fermi distribution. By changing coordinates, the integral can be written

$$\int\int\int|a_{k,k+2\pi g}|^2dudvdw,$$

where u and v are coordinates in the surface of constant energy difference

$$H=E_{k+2\pi g}-E_k-h\nu=0 \quad (5)$$

in the k space, and w is the coordinate perpendicular to this surface. Since $a_{k,k+2\pi g}$ has a strong maximum at $w=0$ due to the factor

$$\frac{\exp(2\pi i/h)(E_{k+2\pi g}-E_k-h\nu)t-1}{E_{k+2\pi g}-E_k-h\nu},$$

we may put the slowly varying factor

$$C_{k,k+2\pi g}=C_{k,k+2\pi g\,w=0}$$

in the integration with respect to w, and neglect the second term in $a_{k,k+2\pi g}$. We then get

$$\int|a_{k,k+2\pi g}|^2dw=\left(\frac{eh}{4\pi mc}\right)^2|\alpha_\xi|^2|C_{k,k+2\pi g}|^2_{w=0}\times\int\left|\frac{\exp(2\pi i/h)(E_{k+2\pi g}-E_k-h\nu)t-1}{E_{k+2\pi g}-E_k-h\nu}\right|^2dw.$$

The main contribution to this integral comes from near $w=0$. We may therefore extend the limits to $-\infty$ and $+\infty$ and put

$$E_{k+2\pi g}-E_k-h\nu=\nabla H_{w=0}w. \quad (6)$$

Carrying out the integration we get

$$\int|a_{k,k+2\pi g}|^2dw=\left(\frac{e}{2mc}\right)^2ht|\alpha_\xi|^2\frac{|C_{k,k+2\pi g}|^2_{w=0}}{|\nabla H|_{w=0}}.$$

Substituting this expression into (4) we get[6]

$$N=2h\frac{\Omega}{8\pi^3}\left(\frac{e}{2mc}\right)^2|\mathfrak{a}_\xi|^2\sum_g\int\int\frac{|C_{k,k+2\pi g}|^2}{|\nabla H|}dudv. \quad (7)$$

The integration is over the portion of surface $H=0$ bounded by the intersection of this surface with the surface of Fermi distribution.

Not all excited electrons can be emitted. As the tangential components of k are continuous at the surface, on account of the continuity of wave function, the condition for an excited electron to be emitted is

$$E(k_x+2\pi g_x, k_y+2\pi g_y, k_z+2\pi g_z) \geqq W+\frac{h^2}{8\pi^2 m}[(k_y+2\pi g_y)^2+(k_z+2\pi g_z)^2], \quad (8)$$

where W is the potential energy of an electron outside the metal. The volume of the metal Ω being the product of the surface area and the thickness l, the emission current per unit surface area is

$$J=2eh\left(\frac{e}{2mc}\right)^2\frac{l}{8\pi^3}|\mathfrak{a}_\xi|^2 \times\sum_g\int\int\frac{|C_{k,k+2\pi g}|^2}{|\nabla H|}dudv, \quad (9)$$

where the integration is over that part of the surface $H=0$, which is bounded by the intersections of this surface with the surface of Fermi distribution and the surface (8).

Effect of Surface Reflection

The above equation gives the emission current in terms of the vector potential of the light wave inside the metal. To obtain the emission in terms of the incident light energy, we must find the relation between this vector potential and that of the incident wave. We can find this relation from the classical electromagnetic theory by using optical constants of the metal: n and k. The quantum theory of reflection developed by Schiff and Thomas[7] shows that the classical relations hold true for the tangential components. For the normal components the relation differs from the classical theory only in the immediate neighborhood of the surface within a thickness of the order of 10^{-8} cm. This is important for the surface effect. For the volume effect we are considering it of no importance. Let the incident wave be plane polarized, and let the subscripts i, r, and t refer to the incident, reflected, and transmitted (refracted) waves respectively.

(1) Electric vector of the incident wave parallel to the plane of incidence (x axis normal to the surface in the outward direction):

$$A_i=(\mathfrak{a}_{ix}, -\mathfrak{a}_{ix}\cot\theta_i, 0) \times\exp\frac{2\pi i\nu}{c}(x\cos\theta_i+y\sin\theta_i+ct),$$

$$A_r=(\mathfrak{a}_{rx}, \mathfrak{a}_{rx}\cot\theta_i, 0) \times\exp\frac{2\pi i\nu}{c}(-x\cos\theta_i+y\sin\theta_i+ct),$$

$$A_t=(\mathfrak{a}_{tx}, -\mathfrak{a}_{tx}\cot\theta_t, 0) \times\exp\frac{2\pi i\nu}{c}[(n-ik)(x\cos\theta_t+y\sin\theta_t)+ct].$$

The relation between θ_i and θ_t is given by

$$(n-ik)\sin\theta_t=\sin\theta_i.$$

Therefore

$$\sin\theta_t=\frac{\sin\theta_i}{n-ik}; \quad \cos\theta_t=\frac{1}{n-ik}[(n-ik)^2-\sin^2\theta_i]^{\frac{1}{2}}.$$

Now curl $A=H$ and $-(1/c)(\partial A/\partial t)=E$. From the conditions of continuity for the tangential components H_z and ϵ_y, we get

$$\mathfrak{a}_{tz}=\mathfrak{a}_i\frac{2\sin\theta_i}{(n-ik)^2+[(n-ik)^2-\sin^2\theta_i]^{\frac{1}{2}}/\cos\theta_i}=\mathfrak{a}_iK_{\parallel z},$$
$$\mathfrak{a}_{ty}=-\mathfrak{a}_{tx}\cot\theta_t=-\mathfrak{a}_i\frac{2[(n-ik)^2-\sin^2\theta_i]^{\frac{1}{2}}}{(n-ik)^2+[(n-ik)^2-\sin^2\theta_i]^{\frac{1}{2}}/\cos\theta_i}=\mathfrak{a}_iK_{\parallel y}. \quad (10)$$

[6] This is substantially the same as Eq. (22.17), p. 457, *Handbuch der Physik*, 24/2.

[7] L. I. Schiff and L. H. Thomas, Phys. Rev. **47**, 860 (1935).

The transmitted wave in the metal is elliptically polarized since α_{tx} and α_{ty} are complex with different arguments. For the special case of normal incidence

$$K_{IIx}=0; \quad K_{IIy}=-2/(1+n-ik). \tag{11}$$

(2) Electric vector of the incident wave perpendicular to the plane of incidence:

$$A_i=(0, 0, \alpha_{iz}) \exp \frac{2\pi i\nu}{c}(x \cos\theta_i+y \sin\theta_i+ct),$$

$$A_r=(0, 0, \alpha_{rz}) \exp \frac{2\pi i\nu}{c}(-x \cos\theta_i+y \sin\theta_i+ct),$$

$$A_t=(0, 0, \alpha_{tz}) \exp \frac{2\pi i\nu}{c} \times[(n-ik)(x \cos\theta_t+y \sin\theta_t)+ct].$$

By the same procedure we get

$$\alpha_t=\alpha_{tz}=\alpha_i \frac{2}{1+[(n-ik)^2-\sin^2\theta_i]^{\frac{1}{2}}/\cos\theta_i} = \alpha_i K_\perp. \tag{12}$$

For the case of normal incidence

$$K_\perp=2/(1+n-ik). \tag{13}$$

The incident light energy per unit area of the surface per unit time is

$$(\pi\nu^2/2c) \cos\theta_i |\alpha_i|^2. \tag{14}$$

Substituting (10) or (12) into (9) and dividing by (14), we get the photoelectric yield, i.e., the charge emitted per unit area per unit incident energy

$$q=\frac{4ceh}{\pi\nu^2}\left(\frac{e}{2mc}\right)^2 \frac{l}{8\pi^3} \frac{1}{\cos\theta_i} \sum_g \int\int \times \frac{|K_{IIx}C^x_{k,k+2\pi g}+K_{IIy}C^y_{k,k+2\pi g}|^2}{|\nabla H|} dudv,$$

$$q=\frac{4ceh}{\pi\nu^2}\left(\frac{e}{2mc}\right)^2 \frac{l}{8\pi^3} \frac{|K_\perp|^2}{\cos\theta_i} \times \sum_g \int\int \frac{|C^z_{k,k+2\pi g}|^2}{|\nabla H|} dudv, \tag{15}$$

for the two cases of electric vector parallel and perpendicular to the plane of incidence, respectively. Since the electrons excited deep inside the metal cannot be emitted because of the loss of energy by collisions with other electrons, l in these equations is an effective thickness within which excited electrons reach the surface without much loss of energy. It depends, therefore, on the collision process between electrons which is very difficult to calculate. Bethe[2] estimates the effective thickness to be of the order of 10^{-7} cm. Rudberg's experiments[8] on inelastic scattering of electrons from solids shows that electrons of 100- to 200-volts energy can penetrate several atomic layers. Compton and Rose,[9] and Goldschmidt and Dember[10] by experiments on photoelectric emission by light irradiating the back side of a thin layer, conclude that the electron mean free path in platinum is 1.08 to 2.67×10^{-7} cm. It seems then reasonable to assume that l is of the order of 10^{-7} cm.

To determine the photoelectric yield, we must know the electron energy levels for the calculation of H and the electron wave functions for the calculation of $C_{k,k+2\pi g}$. Such data have been obtained for a number of metals by the cellular method of Wigner and Seitz,[11] and Slater.[12] But the data have not been published in full. However, for the determination of low frequency limits for light absorption and electron emission, we need to know only electron energy levels. Knowing the energy as a function of k, we shall have the equations of the three surfaces: (5), (8), and the surface of Fermi distribution with $h\nu$ and g as parameters. The area, over which each of the integrals in the sums of (7) and (9) is to be integrated, can then be determined. For each integral (each value of g) there is a frequency below which the area and consequently the integral itself become zero. The frequency below which all integrals in (7) become zero is the long wave-length limit of light absorption; the corresponding frequency for (9) is the threshold frequency of emission. It has been shown by Wigner and Seitz,[13] and Slater[14] that except at energy discontinuities, the energy

[8] E. Rudberg, Phys. Rev. **50**, 138 (1936).
[9] K. T. Compton and L. W. Ross, Phys. Rev. **13**, 295 (1919).
[10] H. Goldschmidt and H. Dember, Zeits. f. tech. Physik **7**, 137 (1926).
[11] E. Wigner and F. Seitz, Phys. Rev. **43**, 804 (1933).
[12] J. C. Slater, Phys. Rev. **45**, 794 (1934).
[13] E. Wigner and F. Seitz, Phys. Rev. **46**, 515 (Fig. 3), (1934).
[14] See reference 12 (Fig. 3).

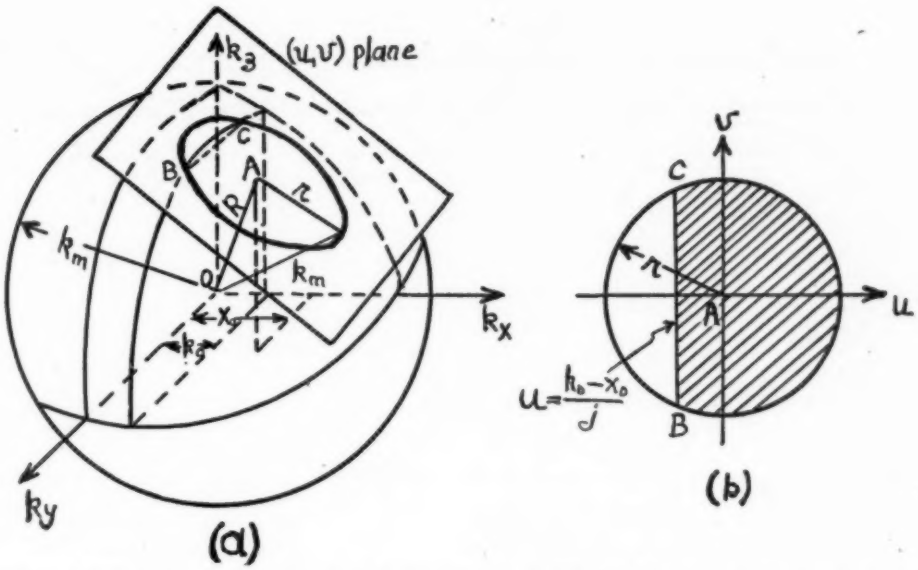

FIG. 1 (a) Geometric representation of Eqs. (17) and (18). (b) Portion of the (u, v)-plane over which the integral of Eq. (9) is to be taken.

levels of sodium are given very closely by the expression for free electrons

$$E_k=(h^2/8\pi^2m)k^2. \tag{16}$$

We shall use this approximation for the determination of threshold frequencies for sodium and potassium.

THRESHOLD FREQUENCY

Using the approximation (16) we find that Eq. (5) of the (u, v) surface becomes

$$(h^2/8\pi^2m)(\pi g^2+g\cdot k)=h\nu, \tag{17}$$

which is the equation of a plane in k-space. The surface of Fermi distribution becomes a sphere

$$k_x^2+k_y^2+k_z^2=k_m^2. \tag{18}$$

The area over which we have to integrate for (7) is the portion of (17) bounded by its intersection with (18). This is a circle with radius (Fig. 1a)

$$r=\left[k_m^2-\left(\frac{(2\pi m/h^2)h\nu-\pi g^2}{g}\right)^2\right]^{\frac{1}{2}}=(k_m^2-R^2)^{\frac{1}{2}}. \tag{19}$$

The area πr^2 is zero unless $|R|\leqslant k_m$ or

$$\pi g^2-gk_m\leqslant\frac{2\pi m}{h^2}h\nu\leqslant\pi g^2+gk_m. \tag{20}$$

This relation gives the low frequency and high frequency limits of absorption of light for the given g. The lowest of the low frequency limits for all possible values of g is the absorption limit of the metal.

For electron emission the condition (8) must be satisfied, which by the approximation (16) becomes

$$\frac{h^2}{8\pi^2m}(k_x+2\pi g_x)^2\geqslant W=E_\varphi+E_m=\frac{h^2}{8\pi^2m}(k_\varphi^2+k_m^2), \tag{21}$$

where E_φ is the work function of the metal. This can be written

$$k_x\geqslant(k_\varphi^2+k_m^2)^{\frac{1}{2}}-2\pi g_x=k_0.$$

Let point A (Fig. 1a) be the origin of coordinates in the (u, v)-plane and let the axis v be parallel to the (k_y, k_z)-plane. Then we have

$$k_x=ju+x_0,$$

where x_0 is the k_x-coordinate of point A. From (17) we have

$$x_0=Rg_x/g.$$

j is cosine of the angle between axes u and k_x

$$j=[\cos^2(0A, k_y)+\cos^2(0A, k_z)]^{\frac{1}{2}}=[(g_y/g)^2+(g_z/g)^2]^{\frac{1}{2}}.$$

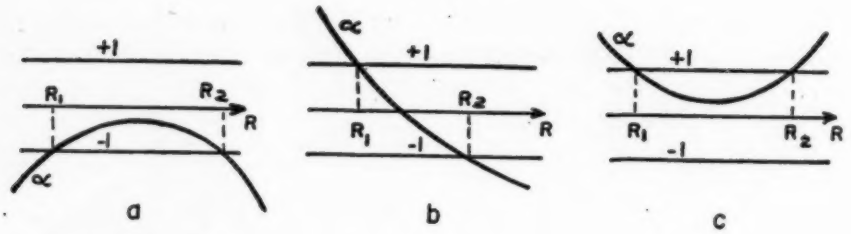

FIG. 2. Values of α:

(a) $jk_0+\frac{g_z}{g}(k_m^2-k_0^2)^{\frac{1}{2}}<0$

(b) $jk_0+\frac{g_z}{g}(k_m^2-k_0^2)^{\frac{1}{2}}>0$ and $jk_0-\frac{g_z}{g}(k_m^2-k_0^2)^{\frac{1}{2}}<0$

(c) $jk_0-\frac{g_z}{g}(k_m^2-k_0^2)^{\frac{1}{2}}>0.$

The area $\int\int dudv$ over which the integrals in (9) are to be integrated is the part of (u, v)-plane (Eq. (17)) bounded by the circle πr^2 (see (19)) and the line

$$u=(k_0-x_0)/j$$

shown by the shaded area in Fig. 1b. It is easily shown

$$\int\int dudv=\pi r^2, \quad \text{if } \alpha\leqslant -1;$$

$$\int\int dudv=r^2\{\cos^{-1}\alpha-\alpha(1-\alpha^2)^{\frac{1}{2}}\},$$

$$\text{if } -1<\alpha<+1; \quad (22)$$

$$\int\int dudv=0, \quad \text{if } \alpha\geqslant +1;$$

$$\alpha=\frac{k_0-x_0}{jr}=\frac{k_0-Rg_z/g}{j(k_m^2-R^2)^{\frac{1}{2}}}.$$

We see that α is a function of g and ν, R being a function of ν. For each value of g we can determine the limiting frequency ν_g below which $\alpha>+1$ and $\int\int dudv=0$. The lowest of these for all possible values of g is then the threshold frequency.

To determine ν_g we shall solve the equation

$$\alpha=1, \quad \text{or} \quad (k_0-Rg_z/g)^2=j^2(k_m^2-R^2).$$

The two roots are

$$R=(k_0g_z/g)\pm j(k_m^2-k_0^2)^{\frac{1}{2}}.$$

We note that g_z must be positive since $g_z<0$ means decrease in the outward momentum, which certainly cannot give emission. There are then three possible cases

(A) $jk_0+\frac{g_z}{g}(k_m^2-k_0^2)^{\frac{1}{2}}<0,$

(B) $jk_0+\frac{g_z}{g}(k_m^2-k_0^2)^{\frac{1}{2}}>0$

and

$$jk_0-\frac{g_z}{g}(k_m^2-k_0^2)^{\frac{1}{2}}<0,$$

(C) $jk_0-\frac{g_z}{g}(k_m^2-k_0^2)^{\frac{1}{2}}>0.$

It can be easily shown that the curves of α *versus* R for the three cases are as shown in Fig. 2. To have $\alpha<+1$, R must observe the following conditions

For case A: no limitations on R,

For case B: $R>\frac{g_z}{g}k_0-j(k_m^2-k_0^2)^{\frac{1}{2}}$,

For case C:

$$\frac{g_z}{g}k_0-j(k_m^2-k_0^2)^{\frac{1}{2}}<R<\frac{g_z}{g}k_0+j(k_m^2-k_0^2)^{\frac{1}{2}}.$$

Furthermore, if $k_0^2>k_m^2$ we have two possible cases

D: $k_0<-k_m$,

E: $k_0>k_m$.

We deduce from Fig. 2a and Fig. 2c:

For case D: α always smaller than $+1$, therefore no limitations on R.

For case E: α always larger than $+1$, therefore no emission.

TABLE I. Low frequency limit of light absorption and the threshold frequency.

Na	Emission surface	1, 0, 0	Threshold frequency	12.6×10^{14}		9.0×10^{14}	
			n_1, n_2, n_3	+1, 0, 0	+1, +1, 0	+1, −1, 0	+1, 0, +1	+1, 0, −1
		1, 1, 0	Threshold frequency	5.91×10^{14}			
			n_1, n_2, n_3	+1, +1, 0			
		1, 1, 1	Threshold frequency			7.34×10^{14}	
			n_1, n_2, n_3	+1, +1, 0	+1, 0, +1	0, +1, +1	
	Absorption limit				3.14×10^{14}		
	n_1, n_2, n_3			±1, ±1, 0	±1, 0, ±1	0, ±1, ±1	
K	Emission surface	1, 0, 0	Threshold frequency	9.57×10^{14}		6.82×10^{14}	
			n_1, n_2, n_3	+1, 0, 0	+1, +1, 0	+1, −1, 0	+1, 0, +1	+1, 0, −1
		1, 1, 0	Threshold frequency	6.21×10^{14}			
			n_1, n_2, n_3	+1, +1, 0			
		1, 1, 1	Threshold frequency		5.69×10^{14}		
			n_1, n_2, n_3	+1, +1, 0	+1, 0, +1	0, +1, +1	
	Absorption limit				4.96×10^{14}		
	n_1, n_2, n_3			±1, ±1, 0	±1, 0, ±1	0, ±1, ±1	

Case E gives a limit for g_z, for it shows that a necessary condition for emission is $k_0<k_m$

$$(k_m^2+k_\varphi^2)^{\frac{1}{2}}-2\pi g_z<k_m, \quad g_z>\frac{(k_m^2+k_\varphi^2)^{\frac{1}{2}}-k_m}{2\pi}.$$

This condition can also be directly deduced from (21). It gives the lower limit for g_z and confirms our previous statement that g_z must be positive. In addition to the limitations on R obtained for these different cases, we must also have $|R|<k_m$, otherwise r in (22) will be imaginary. It can be shown by combining the limitations on R that to have $\alpha<+1$ we must have

$$h\nu>\frac{h^2}{2\pi m}(\pi g^2-gk_m) \quad \text{if} \quad jk_0+\frac{g_z}{g}(k_m^2-k_0^2)^{\frac{1}{2}}<0,$$
$$h\nu>\frac{h^2}{2\pi m}[\pi g^2+g_zk_0-((g^2-g_z^2)(k_m^2-k_0^2))^{\frac{1}{2}}] \quad \text{if} \quad jk_0+\frac{g_z}{g}(k_m^2-k_0^2)^{\frac{1}{2}}>0. \tag{23}$$

These relations give us the limiting frequency ν_g. The threshold frequency is the lowest of ν_g for all possible values of g. It can be shown that if g and g_z were continuous variables, then the minimum $h\nu_g$ is

$$(h^2/8\pi^2m)k_\varphi^2=E_\varphi,$$

which is the ordinary expression for threshold frequency. The emission due to surface effect begins at this frequency. As g and g_z can take only discrete values, the minimum ν_g will be higher than this value. This confirms the general impression that emission due to volume effect begins at a higher threshold. In general ν_g increases with g, but the lowest ν_g does not necessarily correspond to the lowest value of g. Tamm and Schubin derived by simple reasoning an expression for $\nu_{[(1/a),0,0]}$ and assumed this to be the threshold frequency for volume effect. Actually, as shown later, for body-centered cubic lattices g does not have the value $[(1/a), 0, 0]$. But even if g has such a value, the

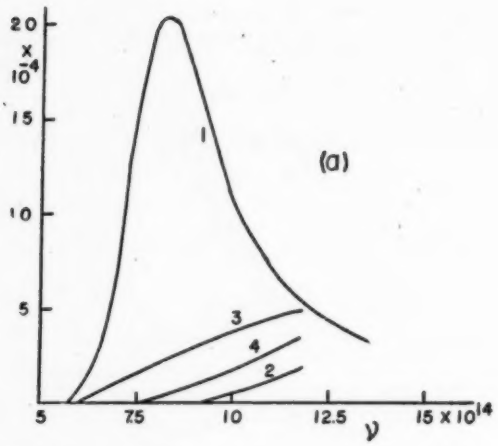

FIG. 3a. Sodium:
Curve 1. Experimental spectral distribution of photoelectric yield in coulomb/calorie.
Curve 2. $K_\nu \times 10^7$, plane (1, 0, 0).
Curve 3. $K_\nu \times 10^7$, plane (1, 1, 0).
Curve 4. $K_\nu \times 10^7$, plane (1, 1, 1).

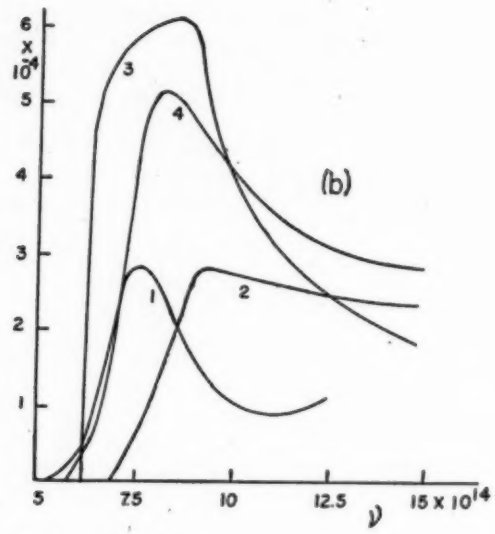

FIG. 3b. Potassium:
Curve 1. Experimental spectral distribution of photoelectric yield in coulomb-calorie.
Curve 2. $K_\nu \times 10^7$, plane (1, 0, 0).
Curve 3. $K_\nu \times 10^7$, plane (1, 1, 0).
Curve 4. $K_\nu \times 10^7$, plane (1, 1, 1).

corresponding ν_g is not the lowest both for sodium and potassium as shown in Table I; the lowest ν_g corresponds to $g=[(1/a), \pm(1/a), 0]$ and $g=[(1/a), 0, \pm(1/a)]$ which have a larger value of g.

The factor g comes from (1). For cubic lattices

$$g=\frac{1}{a}(n_1, n_2, n_3)=\frac{n}{a},$$

where n_1, n_2, and n_3 are integers, and a is the lattice constant. For body-centered and face-centered cubic lattices, the Fourier coefficients V_g can be written: $V_n=A_nS_n$, where S_n is the structure factor. Sodium and potassium have body-centered lattices for which[15]

$$S_n=1+\cos\pi(n_1+n_2+n_3).$$

Thus $S_n=0$ if $(n_1+n_2+n_3)$ is odd, and $S_n=2$ if $(n_1+n_2+n_3)$ is even. Therefore for such lattices $V_{(1,0,0)}$, $V_{(1,1,1)}$, etc., are zero, and g does not have the values $[(1/a), 0, 0]$, $[(1/a), (1/a), (1/a)]$, etc.

The maximum k of the occupied states is given by

$$k_m=(3\pi^2)^{\frac{1}{3}}(n_0/v_0)^{\frac{1}{3}}$$

where n_0 is the number of electrons per atom, and v_0 is atomic volume. For metals with one conduction electron per atom ($n_0=1$) and for body-centered cubic lattices ($v_0=a^3/2$)

$$k_m=(6\pi^2)^{\frac{1}{3}}/a.$$

The lattice constant $a=4.24\times10^{-8}$ cm for sodium and $a=5.33\times10^{-8}$ cm for potassium. For the work function we take $E_\varphi=2.29$ ev for sodium[16] and $E_\varphi=2.01$ ev for potassium.[17] From these data the low frequency limit of light absorption and the threshold frequency can be calculated from (20) and (23). These and the corresponding values of $n=g/a$ are given in Table I. The values of ν_g for the non-existent $g=[(1/a), 0, 0]$ is also given. The threshold frequency depends upon what lattice plane is the surface of emission, since the value of g_x depends upon the direction of x (direction normal to the surface of emission). The table gives threshold frequency for three different lattice planes. For sodium the plane (1, 1, 0) gives the lowest threshold 5.91×10^{14}; whereas for potassium, the plane (1, 1, 1) gives the lowest threshold. 5.69×10^{14}. These are higher than the corresponding ordinary thresholds of emission E_φ/h (5.53×10^{14} for sodium and 4.84×10^{14} for potassium). The low frequency limit of light

[15] N. F. Mott and H. Jones, *The Theory of the Properties of Metals and Alloys*, p. 158.

[16] M. W. Mann, Jr. and L. A. DuBridge, Phys. Rev. **51**, 120 (1937).

[17] R. Suhrmann and H. Theissing, Zeits. f. Physik **52**, 453 (1928).

absorption is 3.14×10^{14} for sodium and 4.96×10^{14} for potassium. Although experiments do not show strong absorption for these metals in the visible and ultraviolet regions, but, as pointed out by Kronig,[18] the "conductivity" $(nk\nu)$, characterizing the absorption, computed from experimental data is 10 times larger than the value calculated theoretically without taking into account the photoelectric absorption. So, although light is weakly absorbed in these regions, it should be almost entirely due to such absorption.

APPROXIMATE ESTIMATION OF THE PHOTOELECTRIC YIELD

Without data on electron wave function, the photoelectric yield cannot be calculated. We shall attempt to estimate approximately its order of magnitude. Using (16) we get from (5)

$$\nabla H=\nabla\left[\frac{h^2}{2\pi m}(\pi g^2+g\cdot k)-h\nu\right]$$
$$=\frac{h^2}{2\pi m}\nabla(g\cdot k)=\frac{h^2}{2\pi m}g.$$

Substituting this into (15) and writing $\langle|C_{k,k+2\pi g}|^2\rangle_{Av}$ for the average value, we get for normal incidence

$$q=1.395\times10^{-2}\left\{\frac{4ceh}{\pi\nu^2}\left(\frac{e}{2mc}\right)^2\frac{1}{8\pi^3}\frac{2\pi m}{h^2}\times\left|\frac{2}{1+n-ik}\right|^2\sum_g\frac{1}{g}\int\int dudv\right\}\times l\langle|C_{k,k+2\pi g}|^2\rangle_{Av}\frac{\text{coulomb}}{\text{calorie}}$$
$$=K_\nu l\langle|C_{k,k+2\pi g}|^2\rangle_{Av}\frac{\text{coulomb}}{\text{calorie}}\qquad(24)$$

all factors being in e.s.u. The integrals $\int\int dudv$ can be calculated from Eq. (22). From the data of Ives and Briggs[19] for n and k, the factor K_ν is calculated and shown in Fig. 3. The value of $\int\int dudv$ depends upon what lattice plane is the emission surface; K_ν is calculated for three different planes, i.e., (1, 0, 0), (1, 1, 0), and (1, 1, 1).

TABLE II.

Sodium								
ν	10^{14}	4.96	6.0	7.0	9.0	11.0	13.0	15.0
R_ν	10^{-14}	0	0.666	0.889	1.583	1.597	1.081	0.881
Potassium								
ν	10^{14}	3.14	5.2	6.0	7.0	8.0	9.0	11.0	11.82
R_ν	10^{-14}	0	0.083	0.274	0.417	0.624	0.842	1.80	2.61

[18] R. de L. Kronig, Nature **133**, 211 (1934).

The rate of consumption of energy per unit volume by the excitation of electrons is

$$P_e=(N/\Omega)h\nu.$$

The number of excited electrons per unit time

TABLE III.

r_s	3.21	3.33	3.62	3.88
$E_{2\pi g}-E_0$	0.64	0.60	0.50	0.43
$C_{0,2\pi g}$	0.2402	0.2214	0.1720	0.1407
$E_{2\pi g}-E_0$	2.27	2.10	1.79	1.54
$C_{0,2\pi g}$	0.2718	0.2565	0.2317	0.2142
$E_{2\pi g}-E_0$	4.84	4.55	3.95	3.47
$C_{0,2\pi g}$	0.2045	0.1822	0.1568	0.1513

N is given by (7)

$$P_e=\left\{h\nu\frac{2h}{8\pi^3}\left(\frac{e}{2mc}\right)^2\frac{2\pi m}{h^2}\sum_g\frac{1}{g}\int\int dudv\right\}\times\langle|C_{k,k+2\pi g}|^2\rangle_{Av}|\mathfrak{A}|^2.\qquad(25)$$

The rate of loss of energy per unit volume by the light wave is

$$P_l=\tfrac{1}{2}nk\nu|\epsilon|^2=\frac{2\pi^2}{c^2}nk\nu^3|\mathfrak{A}|^2.\qquad(26)$$

The ratio is

$$\frac{P_e}{P_l}=\left[\frac{c^2}{2\pi^2}\frac{2h^2}{8\pi^3}\left(\frac{e}{2mc}\right)^2\frac{2\pi m}{h^2}\sum_g\frac{1}{g}\int\int dudv\right]\frac{1}{nk\nu^2}\times\langle|C_{k,k+2\pi g}|^2\rangle_{Av}=R_\nu\langle|C_{k,k+2\pi g}|^2\rangle_{Av}.\qquad(27)$$

The integrals $\int\int dudv$ can be calculated by using (19). As pointed out above, the energy loss of the light wave is almost entirely due to photoelectric absorption, so the ratio P_e/P_l should be nearly equal to one. Table II gives calculated values of R_ν. We see that to make $P_e/P_l\approx1$ the factor $\langle|C_{k,k+2\pi g}|^2\rangle_{Av}$ should be $\sim10^{14}$.

Although the factor $\langle|C_{k,k+2\pi g}|^2\rangle_{Av}$ is not the same in (27) and (24), as it is not averaged over the same area in the two cases, its magnitude

[19] H. E. Ives and H. B. Briggs, J. Opt. Soc. Am. **26**, 238 (1936); **27**, 181 (1937).

will not be very different. We have stated that l should be $\sim 10^{-7}$ cm, so the product $l\langle|C_{k,k+2\pi g}|^2\rangle_{h\nu}\sim 10^7$. From curves K_r in Fig. 3, we see that the photoelectric yield will be between 10^{-4} to 10^{-3} coulomb/calorie. The experimental values of absolute photoelectric yield for these metals are not very reliable because of the difficulty of obtaining perfectly clean surfaces for these very active metals. In Fig. 3 the curves of Hill[20] (computed from data of Mann and DuBridge[16]) for sodium, and Suhrmann and Theissing[17] for potassium are reproduced. It is seen that our estimated photoelectric yield is comparable with the experimental values in order of magnitude. It may perhaps be too small for sodium and too large for potassium. Anyway, for both metals the photoelectric yield calculated from surface effect is the same in order of magnitude as our estimated values.[21] As to the shape of spectral distribution curves, it cannot be predicted in our case without detailed knowledge of electron wave functions, since $\langle|C_{k,k+2\pi g}|^2\rangle_{h\nu}$ is a function of frequency and the curves K_r do not, therefore, represent the shapes of the distribution curves. Furthermore, the metal is usually not a single crystal, and the surface is not a single plane; therefore the spectral distribution curve should be a combination of those for different planes.

Seitz gives for lithium the values of

$$C_{0,2\pi g}=\int\psi^*_{2\pi g}\frac{\partial\psi_0}{\partial x}d\tau$$

for several values of g. In Hartree's units the results are[22] those shown in Table III. We see that the larger the radius of atomic spheres r_s, or rather the larger the part of the atomic volume in which ψ is constant, the smaller becomes $C_{0,2\pi g}$. The radius of atomic spheres for sodium is 3.9 (Hartree's unit), and the region around the nucleus, within which the wave function is not constant, is about the same as for lithium.[23] Therefore $C_{0,2\pi g}$ should be 0.1 to 0.2 in Hartree's units. The same is probably true also for potassium which has still larger radius of atomic spheres, $r_s=4.93$. We have estimated

$$\langle|C_{k,k+2\pi g}|^2\rangle_{h\nu}\sim 10^{14}\text{ absolute units}$$
$$=0.0073\text{ Hartree's units}$$
$$(\langle|C_{k,k+2\pi g}|^2\rangle_{h\nu})^{\frac{1}{2}}\sim 0.085\text{ Hartree's units.}$$

Although $C_{0,2\pi g}$ and $(\langle|C_{k,k+2\pi g}|^2\rangle_{h\nu})^{\frac{1}{2}}$ are not the same, we may judge from this that our estimated value is quite reasonable. It is satisfying that our equation of absorption (25) with a reasonable value for $\langle|C_{k,k+2\pi g}|^2\rangle_{h\nu}$ should agree with the absorption given by experimental values of n and k $[(P_e/P_l)\gtrsim 1]$.

CONCLUSION

Although emission due to volume effect does begin at a higher frequency, at least for sodium and potassium it comes in over most of the region for which spectral distribution has been investigated experimentally, long before the maximum in the distribution curve is reached. The estimated order of magnitude of photoelectric yield is the same as that calculated from surface effect and is comparable with that observed experimentally. Therefore the volume effect cannot justifiably be neglected in the theory of photoelectric emission except for the immediate neighborhood of the threshold frequency. It is then worth the labor to calculate accurately the spectral distribution curve by use of the electron wave functions. It would also be interesting to calculate accurately the energy loss due to photoelectric absorption to compare with the light absorption computed from experimental values of n and k.

Recently Cashman and Bassoe[24] working with barium, which has more stable surface than the alkali metals, have observed an abrupt second rise in the spectral distribution curve which they attribute to the onset of the volume effect. Unfortunately, the free electron approximation for energy cannot be applied to this metal with justification, and we cannot calculate the threshold frequency by the same method used here for sodium and potassium. We have to wait for the solution of electron energy levels for this metal.

[20] A. G. Hill, Phys. Rev. **53**, 184 (Fig. 8), (1938).
[21] R. E. B. Makinson, Proc. Roy. Soc. **A162**, 367 (1937); R. J. Maurer, Phys. Rev. **57**, 653 (1940).
[22] F. Seitz, Phys. Rev. **47**, 404 (1935), Table III.
[23] Cf. reference 13, Fig. 1, and reference 22, Fig. 3.
[24] J. Cashman and E. Bassoe, Phys. Rev. **55**, 63 (1939).

Letters to the Editor

PROMPT publication of brief reports of important discoveries in physics may be secured by addressing them to this department. The closing date for this department is the third of the month. Because of the late closing date for the section no proof can be shown to authors. The Board of Editors does not hold itself responsible for the opinions expressed by the correspondents. Communications should not in general exceed 600 words in length.

Experiments on Counters with Grids

SERGE A. KORFF
New York University, New York, New York
June 25, 1945

CONTINUING the investigation of triode counters originally undertaken in collaboration with W. E. Ramsey,[1] some further tests have been carried out. In the present experiments, several Geiger counters with grids of different dimensions were studied. A resistance serving as a voltage divider was connected across the high voltage source, and the lead from the grid ran to an adjustable point on the voltage-divider. In this manner, the field between the grid and cathode could be controlled. A Lucite window was provided so that a stream of beta particles could be projected into the counter. A glass bead, 3 mm in radius, was located at the middle of the central wire in order to render the device capable of coincidence counting. The pulses were examined on an oscilloscope. (See Fig. 1.) Voltage pulses corresponding to a simultaneous discharge of both halves of the counter were about twice the amplitude of those corresponding to a discharge of either section by itself. An identical counter, with bead but no grid, was attached to the same gas-distributing system so that the kind and pressure of gas in the two would be identical, and the effects produced by the grid could be studied.

It will be recalled that the effect of the grid is to alter the potential distribution inside the counter. The cumulative ionization (Townsend avalanche) process in the Geiger counter discharge takes place in the immediate vicinity of the central wire. The rest of the counter serves as a volume in which the primary ionization may be produced. The customary high counter voltage is necessary to produce the requisite high field near the wire, but the electrons can be accelerated toward the high field region by a comparatively low field in the outer portions of the counter between the grid and the cathode. Thus the grid permits a substantial reduction in the over-all voltage.

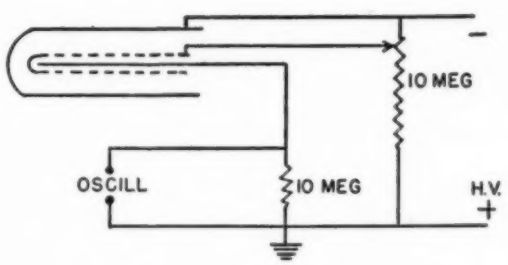

FIG. 1. Connections for triode counter.

One counter was 31 cm long and 7.5 cm in diameter, with a 3-mil tungsten central wire and a grid 7.5 mm in diameter made of bronze screening. It was filled to a pressure of 2 cm of alcohol plus 8 cm argon. It operated as a Geiger counter at voltages between 900 and 970. The similar counter without a grid and attached to the same vacuum system, required 1370 to 1500 volts. Thus, while operating voltages are reduced, the width of the plateau is also somewhat reduced, but represents approximately the same percentage of the total voltage. In an attempt to get still lower voltages, a grid 2 mm in radius was tried. The counter with this grid, operated at 550 volts when filled with a mixture of 1.5 cm of alcohol plus 7 cm of argon. Of this 550 volts, 20 volts was the potential difference between grid and cylinder.

Preliminary experiments indicate that the resolving time of the counter employing the grid is somewhat less than that of the identical one without the grid. The reason for this presumably is that the positive ions need to move only the small distance to the grid before the field between grid and central wire returns to normal. The studies are being continued.

[1] S. A. Korff and W. E. Ramsey, Rev. Sci. Inst. 11, 267–269 (1940).

A Theorem on Functional Determinants

BENJAMIN LIEBOWITZ
350 Fifth Avenue, New York, New York
June 25, 1945

IN my paper on "A Calculus of Finite Precision"[1] I gave, without proof, the following theorem:

$$-(1/Q)(dQ/ds)=\nabla\cdot\mathbf{t}. \tag{1.6}$$

Here Q is given by the functional determinant

$$\frac{1}{Q}=\begin{vmatrix} t_1 & t_2 & \cdots & t_n \\ \dfrac{\partial x_1}{\partial a_1} & \dfrac{\partial x_2}{\partial a_1} & \cdots & \dfrac{\partial x_n}{\partial a_1} \\ \cdot & \cdot & \cdot & \cdot \\ \dfrac{\partial x_1}{\partial a_{n-1}} & \dfrac{\partial x_2}{\partial a_{n-1}} & \cdots & \dfrac{\partial x_n}{\partial a_{n-1}} \end{vmatrix}.$$

The x_i $(i=1, 2\cdots n)$ are functions of $n-1$ parameters a_j and of the variable s which measures the distance along a curve represented by the x_i in the n-dimensional space. The vector with components $t_k=dx_k/ds$ is the unit tangent to the curve. By differentiation, the a_j may be eliminated so that the t_k may be expressed as functions of the x_i alone.

The proof of Eq. (1.6) for three dimensions or less is simple and straightforward; for more dimensions, my original (unpublished) proof was also straightforward but laborious. I have since found a very simple proof which, it is felt, should be published for the sake of completeness.

To prove Eq. (1.6), rewrite the determinant in the form

$$1/Q=|a_k{}^j|,$$

where

$$a_k^1 = t_k \quad a_k^l = \partial x_k/\partial a_{l-1} \quad (l \neq 1).$$

By the formula for differentiating determinants

$$(d/ds)(1/Q) = \sum_{jk} A_j^k (d/ds) a_k^j$$

where A_j^k is the co-factor of a_k^j. Now

$$\frac{d}{ds} a_k^1 = \frac{dt_k}{ds} = \sum_m \frac{\partial t_k}{\partial x_m} \frac{dx_m}{ds} = \sum_m \frac{\partial a_k^1}{\partial x_m} a_m^1.$$

Also, for $l \neq 1$,

$$\frac{d}{ds} a_k^l = \frac{d}{ds} \frac{\partial x_k}{\partial a_{l-1}} = \frac{\partial}{\partial a_{l-1}} \frac{dx_k}{ds} = \sum_m \frac{\partial t_k}{\partial x_m} \frac{\partial x_m}{\partial a_{l-1}} = \sum_m \frac{\partial a_k^1}{\partial x_m} a_m^l,$$

provided that the x_i are uniformly continuous in s and the a_j. Hence, for all values of j,

$$\frac{d}{ds} a_k^j = \sum_m \frac{\partial a_k^1}{\partial x_m} a_m^j$$

$$\therefore \quad \frac{d}{ds} \frac{1}{Q} = \sum_{jkm} A_j^k a_m^j \frac{\partial a_k^1}{\partial x_m} = \sum_{km} \frac{1}{Q} \delta_m^k \frac{\partial a_k^1}{\partial x_m}$$

$$= \frac{1}{Q} \sum \frac{\partial a_k^1}{\partial x_k} = \frac{1}{Q} \Delta \cdot \mathbf{t}.$$

[1] B. Liebowitz, Phys. Rev. 66, 343 (1944).

Detection of Metastable Ions with the Mass Spectrometer

J. A. Hipple and E. U. Condon
Westinghouse Research Laboratories, East Pittsburgh, Pennsylvania
June 4, 1945

It has usually been customary to operate mass spectrometers with the filament and electron gun at a positive potential with respect to the analyzer section which is grounded. Under these conditions the ions pass through the exit slit and strike the ion-collector plate with the full energy acquired in the ion gun since this plate is at ground potential. Recently with an instrument of the sector type employing a magnetic deflection of 90°, the first slit in the ion gun was connected to ground while the analyzer section was made negative with respect to ground. Since the ions are formed in a region one or two volts above ground, they reach the collector plate in this arrangement with an energy of only a few electron volts.

This change has had a very interesting effect on the spectra of hydrocarbons. In Fig. 1 a portion of the spectrum of normal butane is shown. The lower curve shows the baseline with the conventional arrangement, and the upper curve shows the improved baseline when the ion source is grounded. These curves were obtained with an automatic recorder employing a non-linear scale with provision for recording large peaks (such as mass 43 which was allowed to go off scale since it is of no concern at the moment). The "hump" on the side of the peak at mass 39 has not previously been investigated carefully but was usually attributed to the formation of $C_3H_3^+$ with kinetic energy. However, it should still be present in the upper curve of Fig. 1 if this explanation is correct. Its disappearance means it must be associated with a loss in energy. Similarly, the disappearance of the diffuse peaks around 30.5 and 32 requires a loss in energy.

The experimental results may be explained by supposing that some of the ions dissociate after acquiring energy in the ion gun, i.e., if metastable ions are formed in the ion source. If this dissociation occurs in the region of the instrument between the ion source and the magnet, the ion will have an apparent mass m^* which has the following relation to m_0, the mass of metastable ion, and m_1, the mass of the ion to which the metastable dissociates,

$$m^* = m_1^2/m_0.$$

This simple relation assumes that the metastable ion dissociates into two fragments with negligible release of internal kinetic energy. In general, of course, there may be some energy release. Also the dissociation processes in general will follow an exponential decay distribution in time, and so some will occur in the magnetic analyzer and other parts of the instrument giving rise to the observed unsharpness of the peaks. On dissociation the ion has therefore only that fraction of the kinetic energy represented by its fraction of the original mass and is therefore unable to reach the collector when there is a full retarding field between the main analyzer tube and the collector.

The peak around mass 32 can be explained by the dissociation

$$C_4H_{10}^+ \rightarrow C_3H_7^+ + CH_3,$$

giving

$$m^* = (43)^2/58 = 31.9.$$

In this case the parent ion dissociates, and one fragment is the most abundant ion in the n-butane spectrum.

Similarly the ionization around mass 30.5 in the spectrum can be explained by the dissociation

$$C_4H_{10}^+ \rightarrow C_3H_6^+ + CH_4,$$

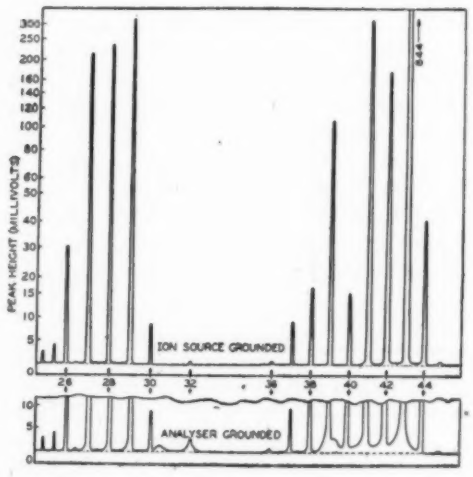

FIG. 1. Portion of the spectrum of normal butane obtained on an automatic recorder employing a non-linear scale. The two curves show the effect on the spectrum of operation of the mass spectrometer with and without the ion source grounded. The disappearance of the diffuse peak at mass 32, for instance, is attributed to the presence of metastable ions in the mass spectrometer. The small residual peak at mass 32 is caused by O_2-impurity in the tube. The original charts have been retouched for reproduction.

giving

$$m^* = (42)^2/58 = 30.4.$$

The hump on the side of mass 39 might be explained by

$$m^* = (40)^2/41 = 39,$$

or

$$m^* = (41)^2/43 = 39.2.$$

Similar peaks have been noticed in the spectra of a great many hydrocarbons, and in all cases the explanation appears to fit into the pattern outlined above. Some other observations on mass spectra of hydrocarbons, such as variation of relative peak heights from one instrument to another, and with initial temperature of the gas, find plausible interpretation as effects due to dissociation of metastable ions.

We wish to thank H. A. Thomas and R. E. Fox for their assistance in this experiment. A more complete report on metastable ions in the mass spectrometer is in preparation.

Further Work on the Artificial Production of Mesotrons

GERHART GROETZINGER AND LLOYD SMITH
University of Illinois, Urbana, Illinois
July 3, 1945

AS reported in an earlier publication, one of us observed a new penetrating radiation in the neighborhood of a cyclotron a few years ago.[1] A detailed investigation showed that this neutral radiation definitely had properties different from those of neutrons and gamma rays.[1,2] The suggestion was made that the radiation consisted of low mass uncharged mesotrons, a hypothesis which was strengthened by the reported occurrence of charged mesotrons of from 10 to 20 electron masses in cosmic radiation.[3] Recently, cloud chamber pictures have been reported[4] which are claimed to confirm the existence of low mass neutral mesotrons. These pictures show electron pairs of high energy emerging in opposite directions from an aluminum plate placed in a cloud chamber situated some distance from the cyclotron and in line with the beam striking the target.

In our earlier publication,[1] it was stated that the electrons which caused the coincidences were of energy greater than 5 Mev. With the arrangement described at that time, experiments have been made to investigate the properties of these electrons by interposing slabs of aluminum between the two coincidence counters. Figure 1 shows the dependence of the coincidence counting rate upon thickness of aluminum (including the equivalent thickness of the two counter walls), when a Mn target is bombarded by the cyclotron. It is seen that the counting rate decreases gradually at first and then quickly drops to zero at a thickness of about 12 mm.

If this behavior is interpreted in terms of a process which leads to the production of single electrons only, then these electrons must be nearly all of the same energy. The second scale of abscissae represents the energy of an electron which is just able to penetrate the corresponding thickness of aluminum, showing that the energy of this homogeneous group would be approximately 6.5 Mev.

If, on the other hand, the much more probable process of the decay of the neutral mesotron into a pair of electrons is assumed, some of the coincidences are caused by one of the pair electrons penetrating both counters and the rest by pairs created between the counters, one electron tripping each counter. From a certain thickness of aluminum on, all the counts will be due to mesotrons decaying between the counters. The third energy scale gives the energy of one of a pair of electrons which could just penetrate half of the corresponding thickness of aluminum having been created in the center of the slab. If this second interpretation is correct, the rest energy of the mesotrons is $2(3.5+.5) = 8$ Mev $= 16\ mc^2$.

An estimate of the cross section for the production of neutral mesotrons is now possible, since the energy of the electrons determines the thickness of lead near the counters which is effective as an electron producing layer and thus determines the effective solid angle subtended by the counter arrangement at the target. If we assume that all counts recorded behind 19 cm of lead[1] are due to the decay of neutral mesotrons which have been slowed down or stopped in the lead, the counting rate behind 28.5 cm of lead gives a measure of the rate of absorption of the mesotrons and enables one to calculate the number of mesotrons leaving the target. Because of the small mass of the particle, the forward direction is probably preferred in the emission process; if we estimate that mesotrons leave the target in the forward direction ten times more often than the number per unit solid angle averaged over all directions, the total cross section for production is found to be 10^{-30} cm^2. The mechanism by which the particles are created is probably similar to the "bremsstrahlung" process postulated in the case of cosmic ray mesotrons.

We have also performed an experiment on the production of charged mesotrons by 11-Mev deuterons using a method of delayed coincidences. For this work, a portion of the deuteron beam was deflected in a magnetic analyzer and piped through the water tanks which surround the cyclotron.[5] The beam was made to strike foils of Al, Ni, Cu, and Pb just thick enough to stop the deuterons. In line

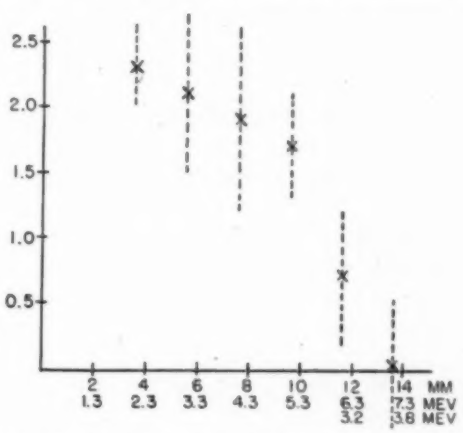

FIG. 1. Coincidences per 10^{17} deuterons striking the target as a function of thickness of aluminum between the counters.

with the incident beam and separated from the target by a 15-cm long channel formed by lead blocks was placed a counter telescope consisting of two thin-walled counters. Behind the telescope was an aluminum plate inclined at an angle of 45 degrees to the direction of the telescope. Beside this plate, out of line with the target and telescope, was placed a third thin-walled counter. The purpose of the arrangement was to detect charged mesotrons which were created in the target and stopped in the aluminum plate after traversing the telescope, the decay electrons tripping the third counter. The circuits were adjusted so that processes were recorded in which the third counter was set off 1.0 to 1.4 microseconds later than the two counters of the telescope. With a beam of 10^{-9} ampere at the target, real delayed coincidences occurred at a rate of two per minute.

However, the counting rate was not changed appreciably by removing the aluminum plate or by interposing several millimeters of lead between the telescope and the delay counter to shield the latter completely from the expected decay electrons. Therefore, the observed counts can not be attributed to charged mesotrons decaying into electrons.

If charged mesotrons of low mass are actually created when the deuterons strike the target, the failure of this experiment may be laid to a combination of three causes:

(1) Production cross section too small. If the lifetime of these particles is of the order of 10^{-6} second, a cross section for production greater than 10^{-31} cm^2 would be sufficient for their detection in this experiment.

(2) Lifetime too long or too short. If the cross section for production is 10^{-30} cm^2, as for the uncharged mesotrons, then particles of a lifetime longer than 10^{-5} second or shorter than 5×10^{-7} second would pass unnoticed.

(3) Kinetic energy acquired by the mesotron at the moment of creation too small for it to penetrate the target material and the counter walls. A charged particle of rest energy 20 mc^2 and a kinetic energy of 1 Mev or less would easily be stopped before reaching the aluminum plate.

[1] G. K. Groetzinger, P. G. Kruger, and L. Smith, Phys. Rev. **67**, 52 (1945).
[2] G. K. Groetzinger and L. Smith, Phys. Rev. **67**, 53 (1945).
[3] M. Schein (private communication).
[4] P. G. Kruger and L. W. Smith, abstract presented before the Stanford meeting of the American Physical Society, July 14, 1945.
[5] P. G. Kruger, G. K. Groetzinger, *et al.*, Rev. Sci. Inst. **15**, 333 (1944).

Refraction Effects in Electron Diffraction

LORENZO STURKEY AND LUDO K. FREVEL
The Dow Chemical Company, Midland, Michigan
July 3, 1945

IN an attempt to use MgO smoke as a calibration specimen for electron diffraction patterns in a camera with a 72.3-cm specimen-to-plate distance, rather unexpected diffraction patterns were obtained:

(a) The (hhh) reflections appeared as resolved doublets.
(b) The (h00) reflections were very sharp.
(c) Other reflections were considerably broadened.

(This phenomenon for MgO has also been observed by J. Hillier and reported without explanation in a contributed paper at the American Physical Society meeting at Ohio State, June, 1945. Hillier used a camera with a 20-cm specimen-to-plate distance.)

Since x-ray back reflection patterns taken with Cu$K\alpha$-radiation of MgO smoke deposited on a glass microscope slide showed no signs of deviation from the usual cubic structure, it must be concluded that the broadening and doubling of reflections other than (h00) are characteristic of electron diffraction. It is well known that electron diffraction patterns are very sensitive to the shape of the diffracting particles. The observed splitting of the non-pinacoid reflections is attributable to the uniform cubic habit of MgO smoke. Electron rays reflected from the (h00) planes pass through the crystal as through a parallel plate and suffer no appreciable change in direction other than the change by diffraction; but rays reflected from prism planes often pass through an effective prism and suffer an additional change in direction due to refraction at the crystal faces. To check this deduction, the following observations were made:

(1) CdO smoke, which also shows a pronounced cubic habit, gives electron diffraction patterns exhibiting the same peculiarities as MgO smoke.

(2) MgO was prepared in irregularly shaped particles ranging in size from 200A to 500A as observed in the electron microscope. Electron diffraction patterns of this material showed no anomalies, and all diffraction rings are essentially equally sharp, though not so sharp as for MgO smoke.

(3) Diffraction patterns of MgO smoke were taken at various electron accelerating voltages. It was frequently observed that, at lower voltages, the center of the broadened (220) reflection decreased in intensity. Since this central part is due to diffraction through a consistently thicker portion of the crystal than the side parts, absorption tends to decrease the intensity at lower voltages.

(4) ZnO smoke patterns show broadening of the (100) and (101) reflections. This material has a spike-like habit instead of cubic.

For a cube-shaped crystal, the deviation of the electron rays in the diffracted direction—the only direction affecting ring broadening—may be approximately calculated by finding an "effective refracting triangle" for the ray. This effective triangle is found by passing a plane through the cube perpendicular to the diffracting plane and including the incident and reflected rays from this diffracting plane. The intersection of this plane with the diffracting plane is the base of the effective triangle, and the intersections with the faces of the cube on the "reflecting" side of the diffracting plane form the other two sides. The deviation δ in radians from the Bragg angle is given approximately by the following expression:

$$\delta=(\pm[\tan^2 r_1+\sin r_1\cos r_1]\pm[\tan^2 r_2+\sin r_2\cos r_2](P/2E),$$

where

r_1 and r_2 are the angles of refraction at sides of triangle, sign of brackets being *negative* if face normal is between ray and diffracting plane, and *positive* otherwise

P = inner potential of crystal
E = accelerating potential of electrons.

A calculation of the inner potential of MgO from the doublet spacing of the (111) reflection gives a value of 12 ± 4 volts, which agrees in order of magnitude with measurements, etc., of inner potentials for other ionic crystals.[1]

A more detailed analysis of the effect of refraction on electron diffraction patterns will be published later.

[1] (See Thomson and Cochrane, *Theory and Practice of Electron Diffraction*, Chap. X.)

K-Capture and e^+-Emission of 6.7-hr. Cd: An Experimental Verification of the Fermi Theory of β-Decay

H. Bradt, P. C. Gugelot, O. Huber, H. Medicus, P. Preiswerk, and P. Scherrer
Physikalisches Institut der Eidgenössischen Technischen Hochschule, Zurich
July 3, 1945

IT may be possible to discriminate between different theories of β-decay by the determination of the relative probabilities of K-capture and e^+-emission. The experimental difficulties of an exact determination of this kind are evident; until now, no exact value of the quotient $Q=p_K/p_+$ for an allowed transition was known.

We found, that the 6.7-hr. $Cd^{107/109}$ which is mostly decaying by K-capture, emits also positive electrons. The e^+-spectrum was measured with the magnetic spectrometer and the upper limit of the spectrum found to be $E=(320\pm10)$ kev. The corresponding annihilation-radiation was detected by $(\gamma\text{-}\gamma)$-coincidences, following the 6.7-hr. period.

Both disintegrations, K-capture and e^+-emission, lead to a metastable $Ag^{107/109}$-nucleus which goes over to the stable Ag with a half-period of (44.3 ± 0.2) sec. Only 1 percent of this transition is connected with the emission of a 93.5-kev γ-ray; in 99 percent, according to the high internal conversion coefficient, a K, L, or M electron is ejected. Therefore, the number of conversion-electrons of the 93-kev radiation, emitted by the 44-sec. $Ag^{107/109}$ in equilibrium with the 6.7-hr. Cd, is practically equal to the total number of the Cd-disintegration-processes. The relative probabilities of K-capture and e^+-emission are therefore in this special case easily determined, being the proportion of the total number of conversion-electrons to the total number of positrons from the same source of 6.7-hr. Cd.

The experimental value, determined with the magnetic spectrometer is found to be

$$Q_{exp}=p_K/p_+=320\pm20$$

in excellent agreement with the theoretical value calculated according to the Fermi theory of β-decay.

$$Q_{theor\ Fermi}=342.$$

The Konopinski-Uhlenbeck modification leads to a value 60 times greater than the one actually found:

$$Q_{KU}=19800.$$

With $\lambda_+=8.97\times10^{-8}$ sec.$^{-1}$ and $W_+/mc^2=1.62$ the matrix element of the Fermi theory turns out to be $M=0.125$, the e^+-decay therefore corresponding to an allowed transition.

Besides the radiation of 0.51 Mev resulting from annihilation of the e^+, we were able to measure the energy and intensity of the weak nuclear γ-radiation of the 6.7-hr. Cd. The energy of this γ-radiation is 0.842 Mev and the absolute intensity is 0.042 quanta per disintegration. The K-capture leading to the excited level of Ag with 0.842 Mev energy is, therefore, at once forbidden. A detailed report will be published in the *Helvetica Physica Acta*.

Proceedings of the Metropolitan Section of the American Physical Society

Meeting of June 2, 1945

A meeting of the Metropolitan Section of the American Physical Society was held on Saturday, June 2, 1945, at the Polytechnic Institute of Brooklyn, 85 Livingston Street, Brooklyn, New York, as a joint local symposium with the Polytechnic Institute and the Society of Rheology on the Ultracentrifuge in Polymer Research. The program was as follows:

10:00 a.m.

Introductory Remarks, J. B. Nichols, *Chairman of the Symposium* (E. I. duPont deNemours & Company, Wilmington, Delaware).

10:30 a.m.

Special Problems in Ultracentrifuge Research on High Polymers, C. O. Beckmann (Columbia University, New York City).

1:00 p.m.

Business Meeting of the Metropolitan Section of the American Physical Society.

1:30 p.m.

The Size Distribution of Gelatin, George Scatchard (Massachusetts Institute of Technology), J. L. Oncley (Harvard University), and J. W. Williams (University of Wisconsin).

3:00 p.m.

Studies on the Molecular Weight and Shape of Linear Polymers, Paul Doty, Seymour Singer and Kurt G. Stern (Highpolymer Research Bureau, Polytechnic Institute of Brooklyn).

4:00 p.m.

General Discussion.

At the business meeting of the Metropolitan Section the following officers were elected for the season 1945–1946:

Chairman, H. Mark
Brooklyn Polytechnic Institute
Vice Chairman, H. A. Barton
American Institute of Physics
Secretary-Treasurer, W. H. Crew
National Defense Research Committee

Elected Members of the Executive Committee:

Edith Quimby, Dept. of Radiology, Columbia University
J. B. Fisk, Bell Telephone Laboratories

A vote of thanks was tendered to W. S. Gorton for his service of twelve years as Secretary-Treasurer of the Metropolitan Section.

W. S. Gorton, *Secretary-Treasurer*